Mid-Permian cyclothem development in the onshore Canning Basin, Western Australia

Volume I

Thesis submitted by

Rhonda Michelle Adkins (M.S. Virginia Tech)

in May 2003

for the degree of Doctor of Philosophy

in the School of Earth Sciences

James Cook University of North Queensland, Australia

Statement of Access

I, the undersigned author of this thesis, understand that James Cook University will make this thesis available for use within the University Library and, by microfilm or other means, allow access to other users in other approved libraries.

All users consulting this thesis will have to sign the following statement:

> *In consulting this thesis I agree not to copy closely or paraphrase it in whole or in part without the written consent of the author; and to make proper public written acknowledgment for any assistance that I have obtained from it.*

Beyond this, I do not wish to place any restrictions on access to this thesis.

Rhonda M. Adkins May 2003

Thesis Abstract

Earth's climate during the latter part of the Permian has long been the subject of speculation and debate. Some studies suggest that Permo-Carboniferous glaciation persisted on parts of Gondwana up to at least the Permo-Triassic boundary. Other studies argue that deglaciation occurred as early as the late Sakmarian (lower Early Permian). Many such investigations have been based upon the sometimes ambiguous occurrence of direct glacial deposits (e.g. striated clasts, tillites). In contrast, this study evaluates the likelihood of post-Sakmarian glaciation by testing high-frequency, sedimentary cycles for a glacio-eustatic driving mechanism.

The focus of this thesis is the Artinskian (upper Early Permian) Tuckfield Member of the Poole Sandstone. The Tuckfield Member is exposed around the periphery of the St George, Poole, and Grant Ranges of the Fitzroy Trough (onshore Canning Basin, Western Australia). In the St George and Poole Ranges, the Tuckfield Member outcrops as a 50 to 100 m thick package of vertically stacked, laterally continuous, coarsening- and thickening-upward cycles. In contrast, the Tuckfield Member outcrops in the Grant Range as a less than 50 m thick package of vertically stacked, laterally discontinuous, fining- and thinning-upward cycles. Primary sedimentary structures, trace fossils, and the vertical succession of facies suggest that the Tuckfield Member records shallow-marine, shorezone deposition in the St. George and Poole Ranges and non-marine, coastal plain deposition in the Grant Range.

Gamma-ray and grainsize data, collected from 17 measured outcrops (11 in the St George Ranges; 4 in the Poole Range; 2 in the Grant Range), were analyzed for cyclicity. Spectral analyses identified several orders of meter- to decameter-scale cycles in both the shallow-marine and non-marine facies. The average periodicities of the identified cycles occur in the ratio of ~36:10:4:2 m. This ratio correlates strongly with the known mid-Permian orbital periodicities of elongated eccentricity, eccentricity, obliquity, and precession (~410:100:40:20 thousand years).

Additionally, the Tuckfield Member is herein traced throughout the northern Fitzroy Trough and onto the adjacent Lennard Shelf via sub-surface data. Similar to outcrop, subsurface gamma-ray logs display several orders of meter- to decameter-scale cycles that correlate strongly with the orbital periodicities. This cyclicity is manifested

by the systematic bundling of smaller-scale cycles into larger-scale cycles that can be traced laterally for more than 200 km.

For comparison, correlative shallow-marine cycles from the Artinskian to Ufimian Pebbley Beach Formation (Sydney Basin, New South Wales) were also studied. Four outcrop sections were measured and correlated, giving a total stratigraphic column of approximately 45 m. Spectral analysis of gamma-ray data identified several orders of meter- to decameter-scale cycles. These cycles correlate strongly with the mid-Permian orbital periodicities and the identified Tuckfield Member cycles.

The favorable comparison between the Tuckfield Member cycles and the orbital parameters indicates that Milankovitch-forcing of climate influenced the formation of depositional cyclicity. Furthermore, it is highly probable that these cycles are glacio-eustatic in origin due to their laterally extensive nature and positive correlation with identified cyclicity in New South Wales. This suggests that Permo-Carboniferous glaciation must have persisted into at least the Ufimian stage of the Late Permian.

Acknowledgments

This project benefited from the assistance and support of many people and professional organizations. The research was funded by the Australian Research Council, the American Association of Petroleum Geologists, and the Society of Professional Well Log Analysts. Additional support was provided by James Cook University in the form of an International Postgraduate Research Scholarship and a School of Earth Sciences Scholarship. The Petroleum Exploration Society of Australia, the Geological Society of Australia, and the Australasian Sedimentologists Group (all of whom provided grants to attend professional conferences) are gratefully acknowledged for their support.

The Geological Survey of Western Australia is also thanked for its advice and assistance. At the survey, Neil Apak and Rosie Emms provided much appreciated geological and logistical help. At James Cook University, the Advanced Analytical Center assisted with the collection of geochemical data. Additionally, Graham Weedon is thanked for providing a copy of his spectral analysis program to our research group. Thanks are also given to Phil Playford and Albert Brakel who reviewed the manuscript associated with Chapter 1. The entire thesis was much improved by their constructive comments. In the Canning Basin, the Kimberley Land Council, local aboriginal communities, and local station owners/managers are gratefully acknowledged for land access and assistance in the field.

I would also like to acknowledge many people in the School of Earth Sciences at James Cook University. I greatly appreciate the assistance that I received from departmental staff members (especially Melissa Thomson, Rachel Mahon, Kevin Hooper, and Paul Givney). As a post-doc, Steve Abbott inspired this project before moving on to bigger and better things. Helen Lever assisted with fieldwork in New South Wales and generally acted as an empathetic sounding board for this work. Members of the Marine Group and Samri provided much appreciated advice, support, and companionship. Keith Crook and Peter Crosdale are especially noted for their geological help. People in my office block (particularly Mike Page), Cameron Huddlestone-Holmes (and Laurene), Tom Evans (and Rachel), and Katharine Grant are especially noted for their friendship and general support.

Of course, my biggest thanks go to my advisor, Bob Carter. In addition to providing geological/professional guidance, Bob also supplied financial and (sometimes much needed) emotional support. During the past three years, I have come to realize that Bob is not only a superb geologist but also a fair, forward-thinking, and extremely generous man. I consider myself fortunate to have had the opportunity to study under his tutelage.

Finally, I would like to thank my friends and family in the USA. There are no words to describe how much I appreciated their support and encouragement during my time in Australia. I also give a huge, heart-felt thanks to Peter Welch: my field assistant, computer technician, personal chef, dear friend, and most cherished love. He has been my source of sanity throughout everything, and none of this would have been possible without his unending support.

Table of Contents

Volume I

Chapter 2

Chapter 3

Chapter 4

Chapter 5

Chapter 5 continued

Volume II

List of Figures

List of Tables

Statement of Sources

Declaration

I declare that this thesis is my own work and has not been submitted in any form for another degree or diploma at any university or other institute of tertiary education. Information derived from the published or unpublished work of others has been acknowledged in the text and a list of references is given.

___________ ______

Rhonda M. Adkins May 2003

Preface

Mid-Permian cyclothem development in the onshore Canning Basin, Western Australia: project overview and thesis details

INTRODUCTION

The Permian was a period of significant climatic change. During that time, the late Paleozoic ice age reached its climax, waned, and eventually gave way to global greenhouse conditions (Crowell, 1978). Similar to the Permo-Carboniferous, Earth's climate during the past 35 million years has been characterized by alternating glacial (colder) and interglacial (warmer) phases (e.g. Dickens, 1996; Zachos et al., 2001). As occurred during the late Paleozoic, it can be expected that today's glaciers will eventually retreat and again give way to global greenhouse conditions. For this reason, it is important for us to gain a better understanding of Earth's climatic evolution during the Permian. By doing so, we may obtain valuable insight into Earth's present climatic systems and be able to better predict future climatic variations.

Today, it is widely accepted that the earliest Permian was marked by widespread glaciation. Likewise, it is equally accepted that, by the earliest Triassic, global greenhouse conditions prevailed. However, Earth's climate during the transitional period between the earliest Permian and the earliest Triassic remains the subject of much speculation. Evidence suggests that glacial retreat began during the Sakmarian stage of the Early Permian (Dickens, 1996), but exactly how long glaciation continued past this point is debatable. Some believe that there is strong evidence in Australia that glaciation may have persisted up to the Triassic boundary (Veevers, 2000a). However, others suggest that Gondwanan deglaciation and the onset of global greenhouse conditions occurred by the end of the Early Permian (Visser, 1993a; von Brun, 1996). Some have even argued that Gondwanan deglaciation occurred as early as the late Sakmarian (Dickens, 1985; 1996; Scotese et al., 1999). Historically, many of these investigations have been based upon the sometimes ambiguous occurrence of direct glacial deposits (e.g. striated pavements, tillites, and outwash deposits). This study has evaluated the likelihood of the occurrence of mid- to Late Permian (post-Sakmarian) glaciation by testing high-frequency sedimentary cycles for a glacio-eustatic driving mechanism.

PROJECT DETAILS

This thesis is part of a larger Australia-wide study (initiated by Dr. Steve Abbott) testing for post-Sakmarian glacio-eustatic cyclothem development. Australia is an ideal place in which to test for post-Sakmarian glacio-eustacy because thick packages of Permian deposits occur in sedimentary basins throughout the continent

(Figure A). This particular thesis concentrates on the late Sakmarian to Artinskian Poole Sandstone of the onshore Canning Basin, Western Australia. Similar work has been conducted in the Carnarvon Basin (H. Lever), Tasmanian Basin (S. Abbott and J. Brooker), and southern Sydney Basin (R. Adkins and H. Lever). Figure B summarizes the stratigraphic intervals studied in this large-scale project. When combined, these four successions provide a reasonable spatial and temporal distribution of mid- to Late Permian (post-Sakmarian) sediments within Australia.

THESIS FORMAT AND CHAPTER SUMMARIES

This thesis consists of five chapters, each written as stand-alone bodies of work. Volume I contains all text, figures, and references. Volume II contains all appendices. Each chapter is intended for publication in a scientific journal and has been structured accordingly. The thesis is organized with the intention of providing a logical progression of thought between the sections. Although each section was written as an independent study, the five chapters when taken together comprise a detailed account of mid-Permian cyclothem development in the onshore Canning Basin.

Chapter 1 presents the first detailed description of the Artinskian Tuckfield Member of the Poole Sandstone. This chapter concentrates on the sedimentology and stratigraphy of shallow-marine sedimentary cycles preserved in the St George and Poole Ranges of the Fitzroy Trough (onshore Canning Basin). This work has been accepted for publication by the *Australian Journal of Earth Sciences.* In this document, the manuscript appears in its published form with only minor alterations to accommodate thesis format.

Chapter 2 considers the potential mechanism(s) of formation responsible for the shallow-marine cyclicity described in Chapter 1. Spectral analysis is used to identify average cycle periods recorded in these deposits. Identified cycles are compared with the known mid-Permian orbital periodicities to determine the role that Milankovitch-forcing and glacio-eustacy played in the formation of depositional cyclicity.

Chapter 3 describes the cyclic development of a non-marine, sand-dominated coastal plain in the Fitzroy Trough. The Tuckfield Member outcrops in the Grant Range as a stacked series of non-marine cycles. This chapter describes the sedimentology and stratigraphy of those deposits. It then discusses the potential mechanism(s) of formation for the non-marine cyclicity preserved in this area.

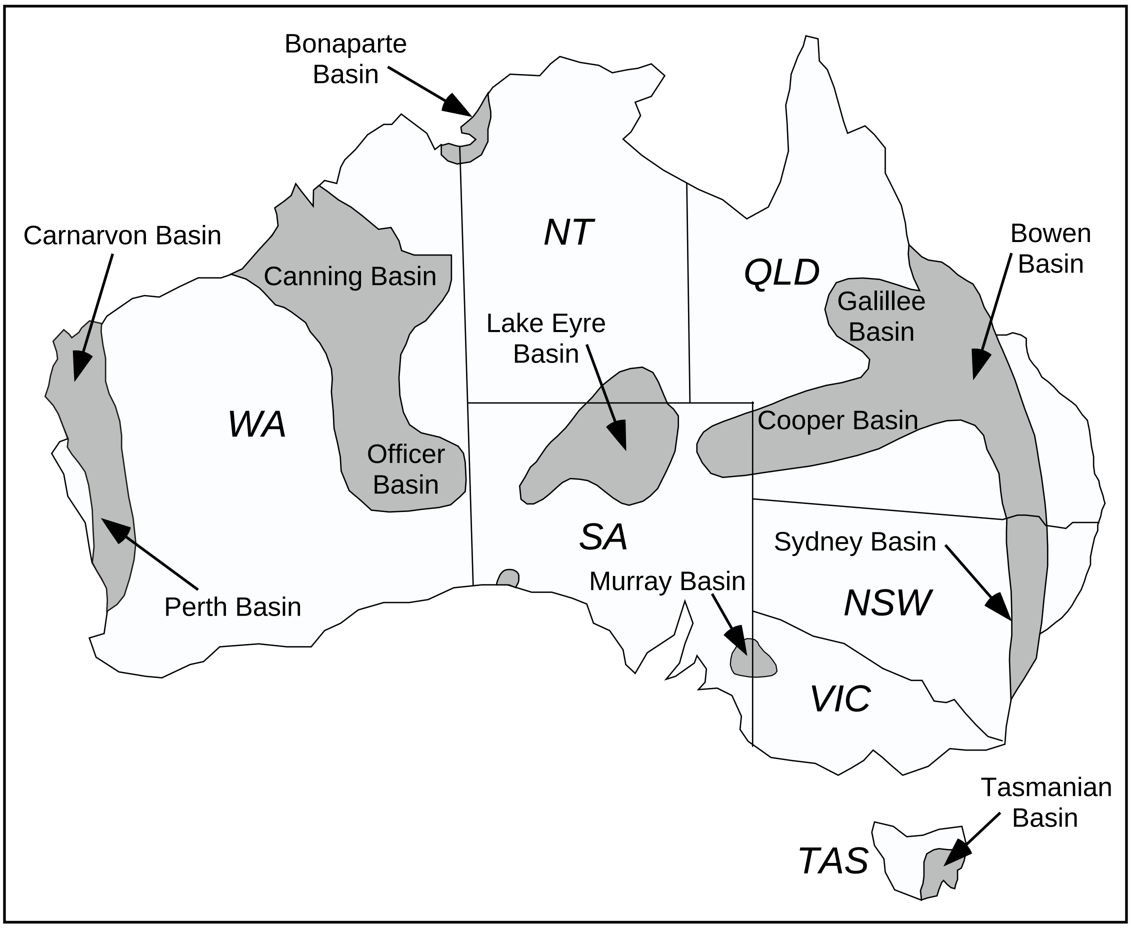

Figure A: Simplified map showing the Permian basins of Australia (adapted from Brown et al., 1968). In this project, the following basins were studied: Canning Basin (R. Adkins); Carnarvon Basin (H. Lever); Sydney Basin (R. Adkins and H. Lever); Tasmanian Basin (S. Abbott and J. Brooker).

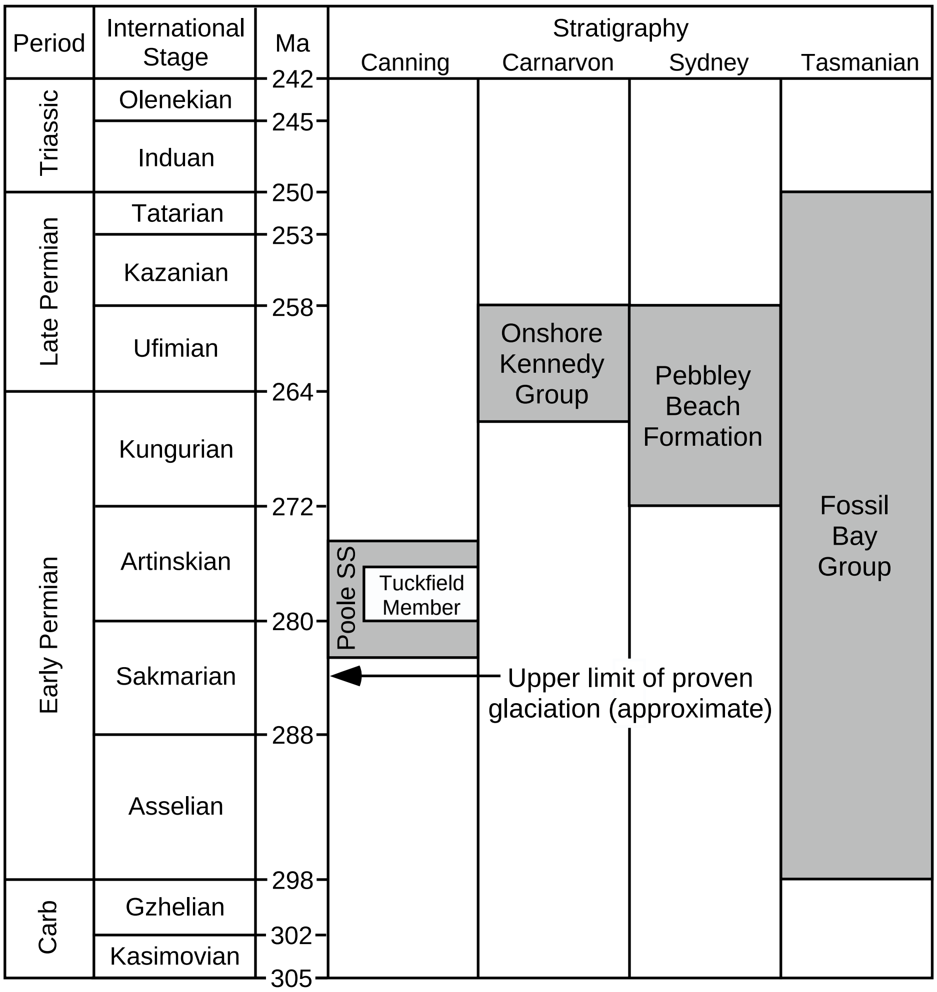

Figure B: Permian stratigraphy included in Australia-wide study. Dates from Veevers, 2000b.

Chapter 4 considers the development of the Poole Sandstone (Nura Nura and Tuckfield Members) on a regional scale. Thirty subsurface gamma-ray logs are used to map the Poole Sandstone and trace cyclothem development throughout the northern Fitzroy Trough and onto the adjacent Lennard Shelf (covering an area of approximately 15,000 km^2).

For comparison, Chapter 5 addresses cyclothem development in the Pebbley Beach Formation of the Shoalhaven Group (southern Sydney Basin, New South Wales). If cycles identified in the Canning Basin are indeed glacio-eustatic in origin, comparable cyclicity should be preserved in analogous environments worldwide. This study utilizes the techniques developed in Western Australia to assess cyclicity recorded in mid-Permian shallow-marine deposits in eastern Australia.

Chapter 1

Regressive systems tract cyclicity in shorezone deposits: the sedimentology and stratigraphy of the Early Permian Tuckfield Member (Poole Sandstone), onshore Canning Basin, Western Australia

ABSTRACT

The Early Permian Tuckfield Member of the Poole Sandstone is exposed around the periphery of the St George and Poole Ranges of the Fitzroy Trough (onshore Canning Basin, Western Australia). It outcrops as a 50 to 100 m thick package of vertically stacked, coarsening- and thickening-upward cycles. These cycles consist upwards of siltstone, sandstone, and mud-pellet conglomerate, with minor amounts of silty mudstone at the base of some cycles. At the outcrop scale, cycles range in thickness from less than 5 m up to approximately 12 m and dictate the geomorphological features of the area, with benches occurring at cycle tops. Primary sedimentary structures, trace fossils, and the vertical succession of facies suggest that each cycle records an episode of shorezone progradation. The Tuckfield Member in the St George and Poole Ranges is here interpreted to consist predominantly of a stacked series of regressive systems tract cycles.

Key Words: Canning Basin, cyclicity, Permian, Poole Sandstone, regressive systems tract, Tuckfield Member

INTRODUCTION

The onshore segment of the Phanerozoic Canning Basin is the largest onshore sedimentary basin in Western Australia (Figure 1.1). During the twentieth century, exploration in the basin produced an immense amount of geological data. Many journal articles, government reports, and industry symposiums (e.g. Purcell, 1984; Purcell and Purcell, 1994) have been dedicated to the understanding of this vast area. Previous research has concentrated on the basin's tectonic evolution and depositional history (e.g. Brown et al., 1984; Goldstein, 1989), petroleum and mineral systems (e.g. Botten, 1984; Ellyard, 1984; Eyles et al., 2001), and biota (e.g. Nicoll, 1984). Much of this research has focused on the Devonian reef complex that outcrops in the northern Canning Basin (e.g. Playford, 1984; Wood, 2000), and recently several studies have been published on the widespread Carboniferous Reeves Formation (e.g. Apak and Backhouse, 1998) and Permian Grant Group (e.g. Redfern and Millward, 1994; Eyles and Eyles, 2000). Although the amount of existing data appears to be quite large, portions of the basin remain relatively unexplored. Covering an area approximately equal to Victoria and with a basin fill of over 15 km (Figure 1.2) (Yeates et al., 1984), extensive regions and

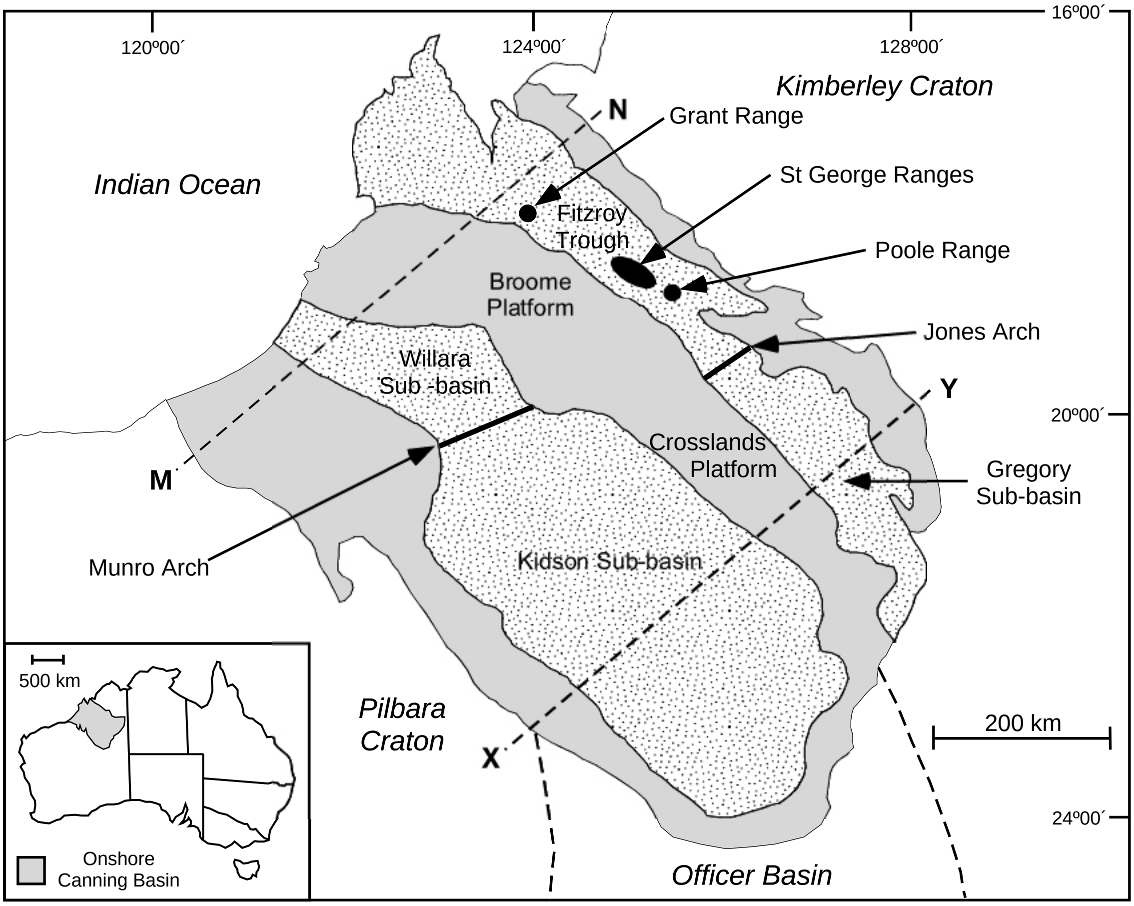

Figure 1.1: Simplified map of the onshore Canning Basin showing locations of the Grant, St George and Poole Ranges (adapted from Kennard et al., 1994). Lines M-N and X-Y are shown in Figure 1.2.

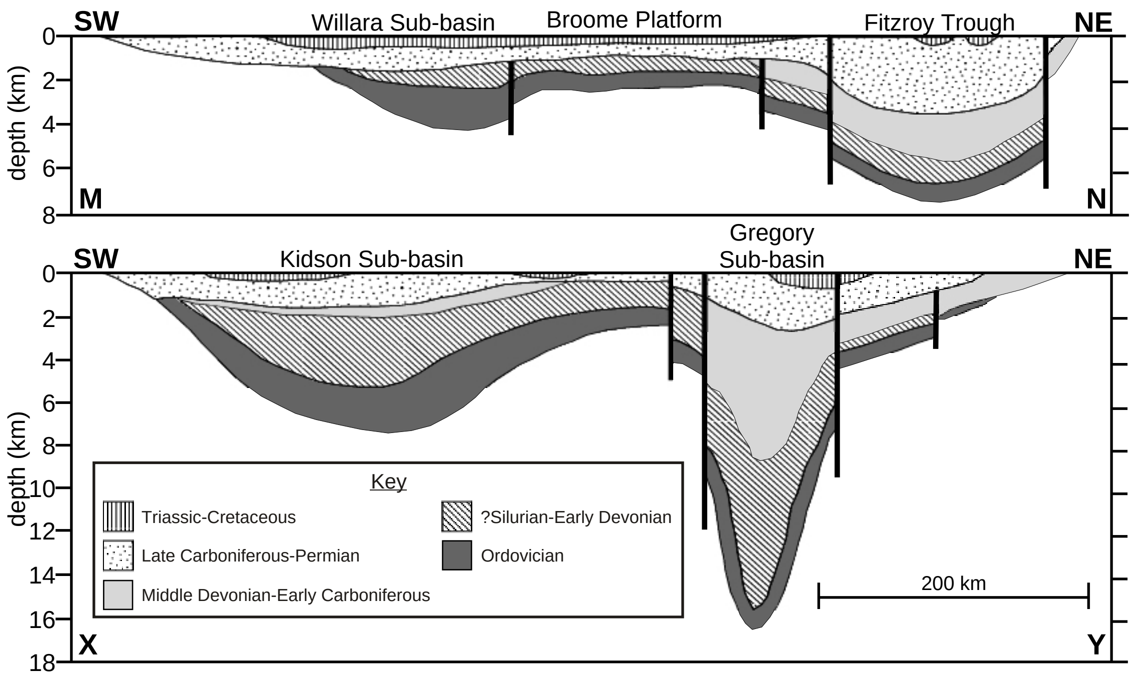

Figure 1.2: Schematic cross-section of the Canning Basin (adapted from Yeates et al., 1984). Location of section lines is shown in Figure 1.1.

many depositional units in the onshore Canning Basin have yet to be studied in any detail.

The Early Permian Poole Sandstone (defined by Guppy et al., 1952, 1958) has been considered as a potential petroleum reservoir (Jackson et al., 1994; Apak and Carlsen, 1996), a source rock (Horstman, 1984; Kennard et al., 1994), and an important aquifer (Yeates et al., 1984). Although it may thereby be economically important, the Poole Sandstone remains poorly understood because few sedimentological and/or stratigraphic analyses have been performed on this unit. In 1976, Crowe and Towner published two brief reports on the Poole Sandstone: the first report introduced the uppermost Christmas Creek Member (Crowe and Towner, 1976a), whereas the second discussed the depositional environment of the lowermost Nura Nura Member (Crowe and Towner, 1976b) (Figure 1.3). Since 1976, the Geological Survey of Western Australia and the Bureau of Mineral Resources (now Geoscience Australia) have published general descriptions of the unit with geological maps (e.g. Crowe and Towner, 1981; Gibson and Crowe, 1982) and in reports on Permo-Carboniferous hydrocarbon prospectivity (Apak, 1996; Havord et al., 1997). Other than these few government reports, only brief descriptions of the Poole Sandstone can be found in a few large-scale overview papers (e.g. Yeates et al., 1984).

This article describes in detail the sedimentology and stratigraphy of the middle Tuckfield Member of the Poole Sandstone (Figure 1.3). This work has practical applications because it is the first in-depth study of the Tuckfield Member, thereby providing a sedimentological and stratigraphic framework for this prospective unit. Additionally, this paper lays the foundation for subsequent work addressing Milankovitch-band cyclicity that is preserved in the Tuckfield Member.

METHODS

This research is based upon field investigations of the Tuckfield Member, where it is exposed around the periphery of the St George and Poole Ranges of the Fitzroy Trough (Figure 1.4; Appendix 1). Fifteen outcrop sections of the Tuckfield Member were evaluated on a bed-by-bed basis for lithology, fossils, and sedimentary structures, including bed thickness variations and vertical stacking of facies (Appendix 2). Measured sections, ranging from 30 to 110 m thick, focus on the documentation of repetitive, meter-scale cycles recorded within the succession. Based upon these observations, an idealized cycle model has been developed for the Tuckfield Member.

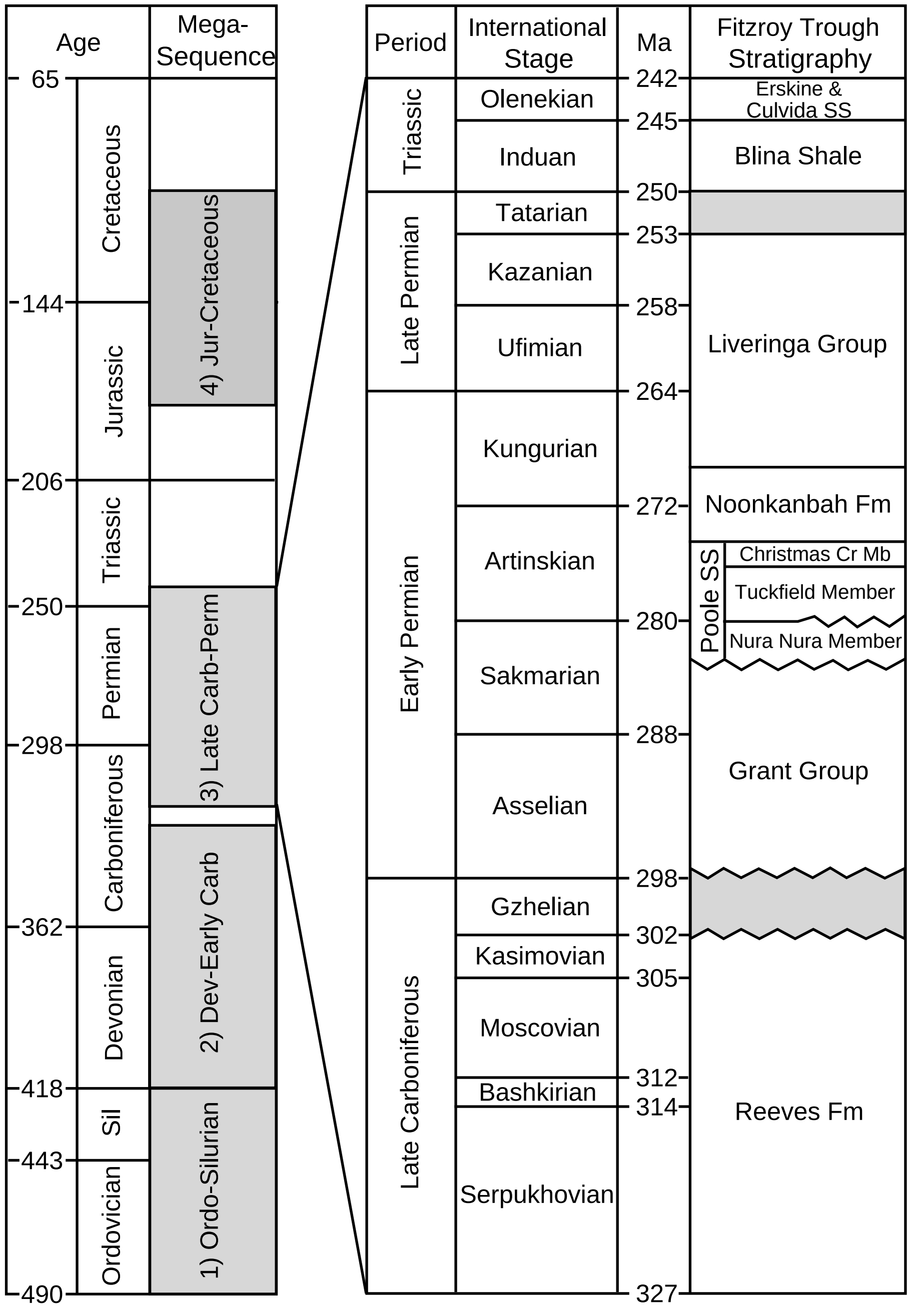

Figure 1.3: Canning Basin stratigraphic column summarizing the basin's four tectono-stratigraphic megasequences (adapted from Kennard et al., 1994). Detailed lithostratigraphy is presented for the Late Carboniferous-Permian megasequence. Period and stage dates from Veevers, 2000b.

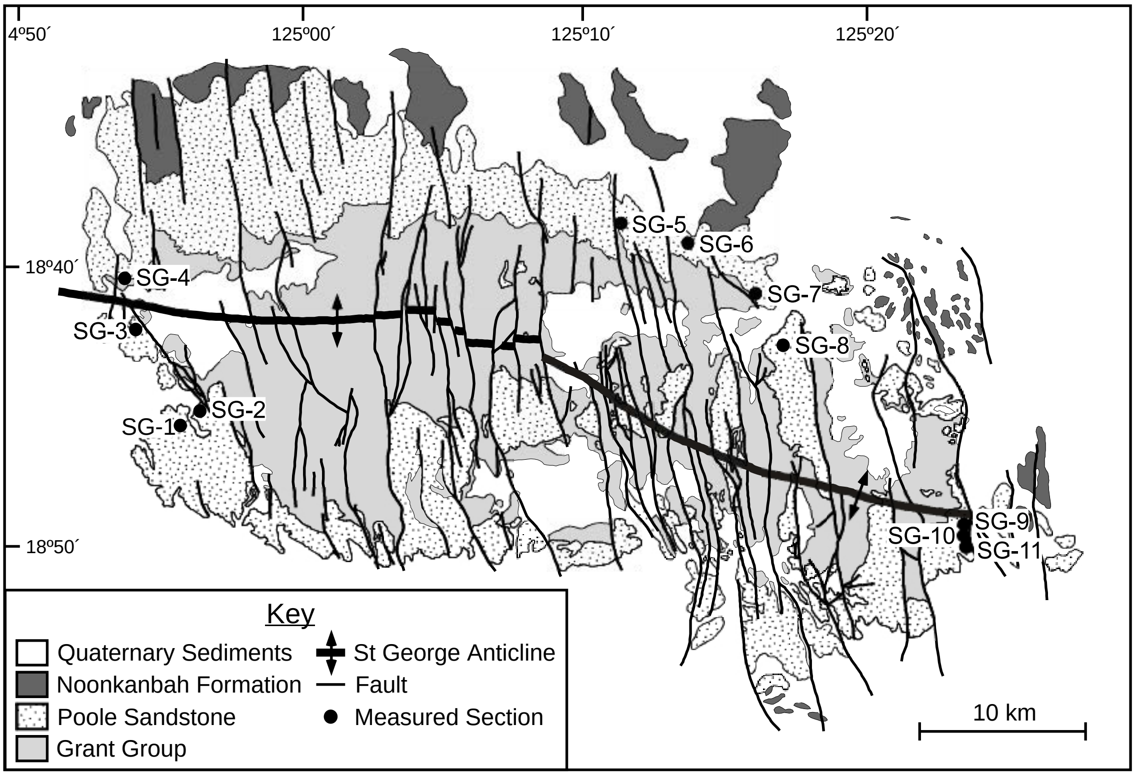

Figure 1.4a: Simplified geological map of the St George Ranges (adapted from Crowe and Towner, 1981) showing the location of the measured sections.

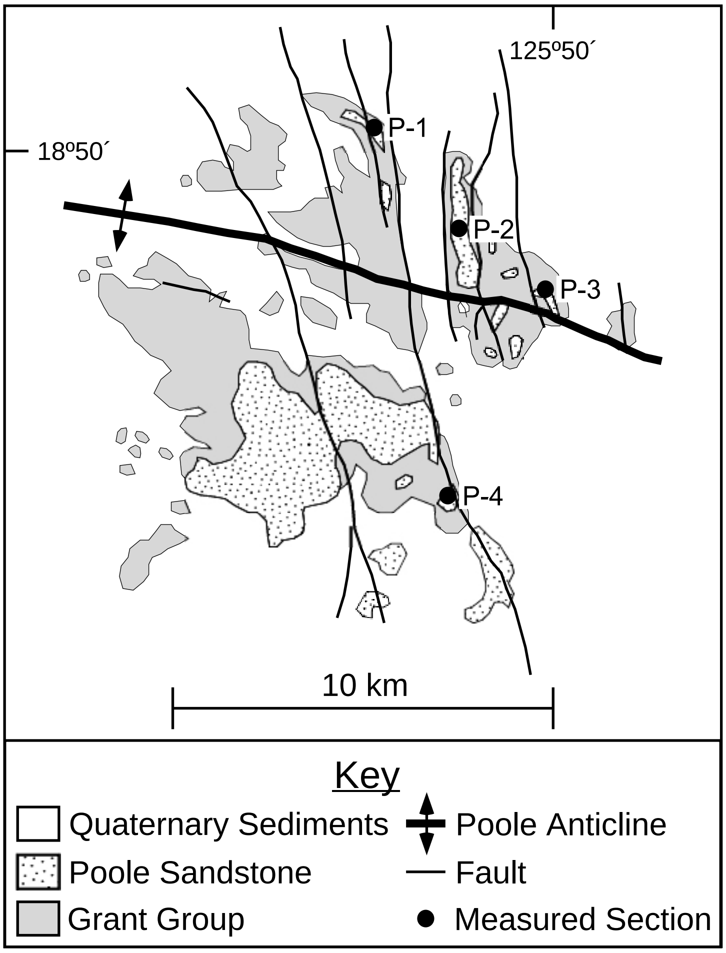

Figure 1.4b: Simplified geological map of the Poole Range (adapted from Crowe and Towner, 1981) showing the location of the measured sections.

Gamma-ray measurements were collected from each outcrop at a 0.5 m spacing and plotted against the corresponding lithological log (Appendices 2 and 3). Gamma-ray emissions are related to the content of radiogenic isotopes of potassium, uranium, and thorium. These elements (particularly potassium) are common in clay minerals (Cant, 1992) and hence, the gamma-ray log from each measured section should reflect the amount of clay present and quantitatively detect changes in lithology.

To better understand the nature of the Tuckfield Member, one typical cycle was analyzed in detail. Ten hand-sized samples were collected from a 3.5 m section of outcrop (one cycle) located on the eastern side of the St George Ranges. Thin-sections were prepared for each sample and analyzed for cycle trends. Petrographic data, including mineralogy, grainsize, roundness, sorting, and porosity, were recorded from each thin-section. Porosities were calculated using the following method. Rock chips were impregnated with dyed epoxy before being made into thin-sections. Digital photographs were taken of the thin-sections and set to a scale of 256 greys (Appendix 4). In the grey-scale photographs, epoxy-filled pore spaces are easily differentiated from the samples' mineralogy. For each thin-section, the computer program NIH was used to create a density slice corresponding to pore space. The area of each density slice was then calculated and used as a proxy for the rock's porosity (Appendix 5). XRF and quantitative XRD data (Appendix 6) were also collected from each hand-sample to better constrain compositional and mineralogical trends in the cycle.

REGIONAL SETTING AND DEPOSITIONAL HISTORY

The onshore Canning Basin is a broad, intracratonic rift basin located between the Proterozoic Kimberley Craton to the northeast and the Archean Pilbara Craton to the southwest (Figure 1.1) (Purcell, 1984). Cretaceous sediments in the basin extend southward, connecting the Canning Basin to the Phanerozoic Officer Basin (Yeates et al., 1984).

Although the onshore Canning Basin is now quite stable, it had a complex tectonic evolution that lasted from the Early Ordovician to the Tertiary. At *ca* 500 Ma, thrust-related shearing in basement rock to the north (Shaw et al., 1992a) resulted in extension, rapid subsidence, and the formation of the basin. Successive episodes of crustal stretching followed by tectonic quiescence resulted in the deposition of four tectono-stratigraphic megasequences: (i) Ordovician-Silurian; (ii) Devonian-Early

Carboniferous; (iii) Late Carboniferous-Permian; and (iv) Jurassic-Cretaceous (Kennard et al., 1994) (Figure 1.3).

This paper focuses on deposits of the Late Carboniferous-Permian megasequence (Figure 1.3). The deposition of this megasequence was initiated by compression and inversion of pre-existing Devonian faults (Meda Transpressional Movement) during the mid-Carboniferous. This movement probably coincided with the peak of the Alice Springs Orogeny, when Laurasia and Gondwana collided, subjecting much of western and central Australia to compression and uplift (Shaw et al., 1992b). In the Canning Basin, this time is marked by the deposition of syntectonic fluvial, glaciofluvial, and glaciomarine deposits (Kennard et al., 1994; Redfern and Millward, 1994) of the Reeves Formation (formerly the Lower Grant Group: Apak and Backhouse, 1998) (Figure 1.3). By the earliest Permian, renewed extension and rapid subsidence (Point Moody Extensional Movement) corresponded with continued glacial conditions (Kennard et al., 1994) and deposition of the Grant Group (formerly the Upper Grant Group: Apak and Backhouse, 1998). Following the Point Moody Extensional Movement, the basin entered an extended period of tectonic quiescence that was interrupted by short pulses of regional tectonism. This period was also marked by the widespread deposition of a transgressive, shallow-marine sand sheet (Poole Sandstone) that coincided with the termination of glacial conditions throughout the basin. From the mid-Permian to the Early Triassic, two successive third-order transgressive-regressive cycles (Poole-Noonkanbah-Liveringa and Blina-Erskine), consisting of marine shale and siltstone overlain by shallow shelf and fluvial sandstone, were deposited in the Canning Basin (Kennard et al., 1994).

Today, regionally-extensive, northwest-trending extensional faults define the predominant structure of the basin (Kennard et al., 1994). Two major northwest-trending depositional troughs are separated by an uplifted mid-basin arch (Figures 1.1 and 1.2). This arch dips gently to the southeast and is capped by a thin succession (1-2 km) of predominantly Ordovician, Devonian and Permian rocks (Bentley, 1984). The elongated northern trough contains up to 18 km of predominantly Devonian and younger sediments. It is further divided by a basement high (the Jones Arch) into the asymmetrical Fitzroy Trough to the northwest and the Gregory Sub-basin to the southeast. The southern trough contains a 4 to 5 km thick succession of Ordovician to Silurian rocks with a thin cap (approximately 1-2 km) of Devonian and younger sediments (Kennard et al., 1994). The southern trough is divided by a basement high (the Munro Arch) into the Willara Sub-basin to the northwest and the broad Kidson Sub-basin to the southeast.

THE TUCKFIELD MEMBER OF THE POOLE SANDSTONE

The Tuckfield Member is one of three distinct depositional units that together comprise the Poole Sandstone. The Poole Sandstone is a laterally extensive package of shallow-marine and non-marine sediments. It consists of the lower Nura Nura Member, the middle Tuckfield Member, and the upper Christmas Creek Member (Figure 1.3). Today, the Poole Sandstone is predominantly encountered in the sub-surface. However, dextral wrench faulting in the Late Triassic to Early Jurassic (Fitzroy Transpressional Movement) uplifted and exposed thick outcrop sections of the Poole Sandstone in a few locations throughout the basin (Kennard et al., 1994).

The best exposures of the Tuckfield Member are found in the Grant, St George, and Poole Ranges of the Fitzroy Trough (Figure 1.1; Appendix 1). This study concentrates on outcrops around the periphery of the St George and Poole Ranges. In these areas, the Tuckfield Member conformably to disconformably overlies the Nura Nura Member and conformably underlies the Christmas Creek Member. In the Fitzroy Trough, no age-diagnostic fossils occur in the Tuckfield Member. However, palynomorphs from elsewhere in the basin indicate an early to late Artinskian age for this unit (Figure 1.3) (Yeates et al., 1975).

In the St George and Poole Ranges, the Tuckfield Member outcrops as a series of small (up to approximately 150 m high), rounded hills (Figure 1.5). Each hill comprises multiple, vertically stacked, flat-lying benches that can be traced laterally for several kilometers. Most benches correspond with the tops of coarsening- and thickening-upward cycles (Figures 1.6 and 1.7; Appendix 2 where heavy horizontal lines mark the tops of these cycles). At the outcrop scale, cycles range in thickness from less than 5 m up to approximately 12 m. The transition from the top of an underlying cycle to the base of an overlying cycle often corresponds to an abrupt increase in gamma-ray values (Appendices 2 and 3), indicating a larger proportion of clay minerals at cycle bases than at cycle tops.

Cycle Model

In the St George and Poole Ranges, most Tuckfield Member cycles follow a similar progression of sediment facies. Because the Tuckfield Member consists of a

Figure 1.5: Outcrop of the Tuckfield Member (Poole Sandstone), eastern St George Ranges. Note the flat-lying, laterally continuous benches that mark the tops of coarsening- and thickening-upward cycles. Photograph taken at 51K 0752494/UTM 7917909 (using the Australian Geodetic Datum 1966 coordinates), facing west. Field of view is approximately 1 km wide.

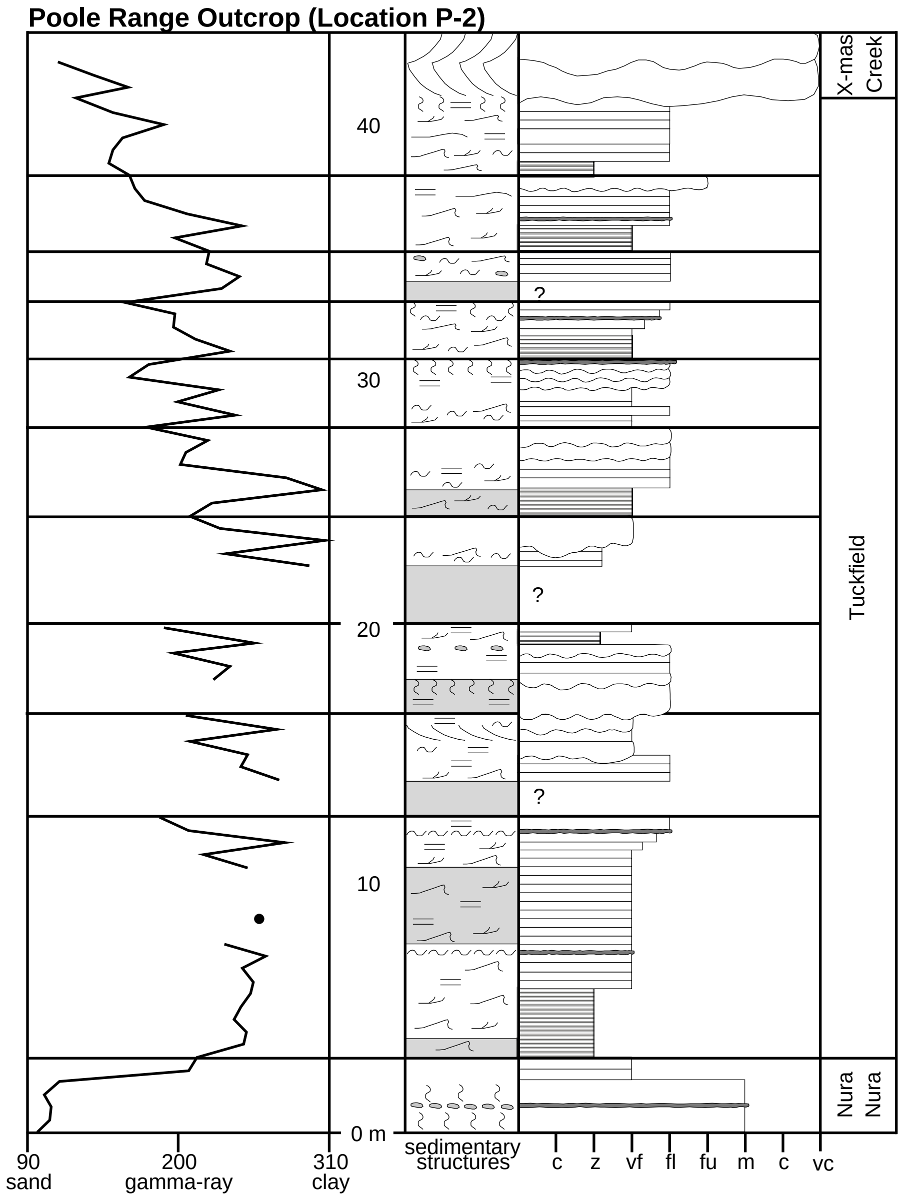

Figure 1.6a: Lithology log with associated gamma-ray data from the Poole Range. The base of the measured section is located at 51K 0795598/UTM 7913141 (using the Australian Geodetic Datum 1966 coordinates). Heavy horizontal lines mark the tops of coarsening- and thickening-upward cycles. These lines generally correspond to the benches shown in Figure 1.5. Grainsize increments from left to right on x-axis are as follows: c (clay/mud); z (silt); vf (very fine sand); fl (lower half of fine sand); fu (upper half of fine sand); m (medium sand); c (coarse sand); vc (very coarse sand). Fine sand was divided into lower and upper halves to better depict variations in grainsize. Member names are given in the right-hand column. See Figure 1.6b for key.

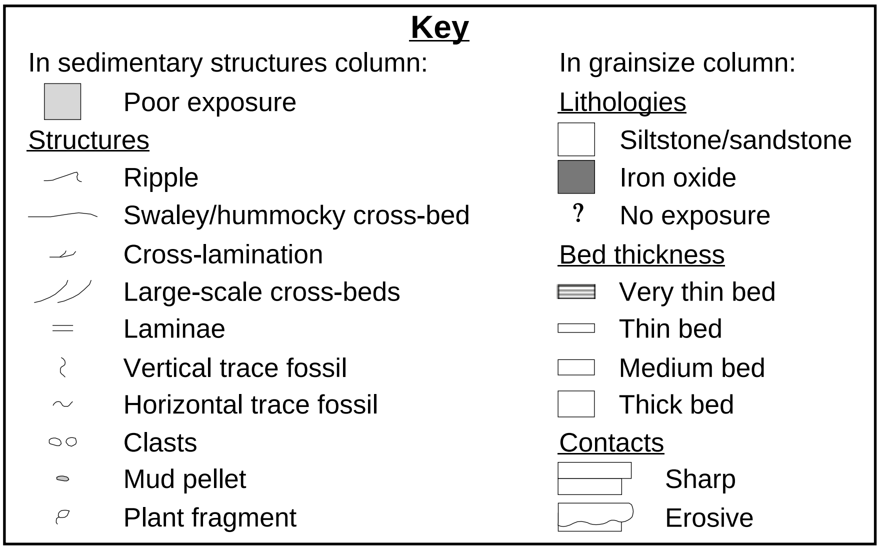

Figure 1.6b: Key for Figures 1.6a and 1.7.

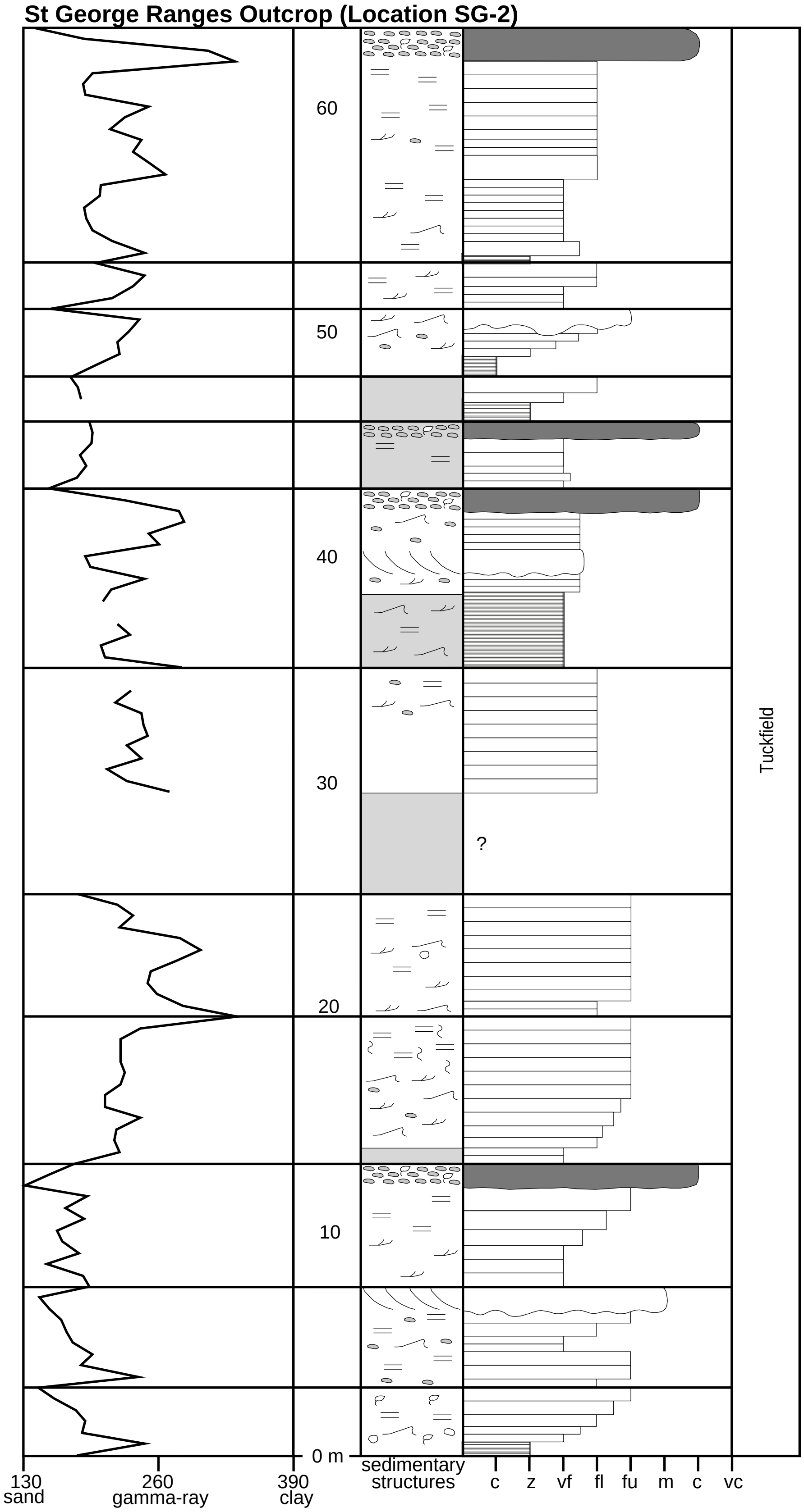

Figure 1.7: Lithology log with associated gamma-ray data from the St George Ranges. The base of the measured section is located at 51K 0702875/UTM 7925682 (using the Australian Geodetic Datum 1966 coordinates). Heavy horizontal lines mark the tops of coarsening- and thickening-upward cycles. These lines generally correspond to the benches shown in Figure 1.5. Key as in Figure 1.6b.

repetitive, vertically stacked series of cycles, a generalized cycle model can be used to describe the basic sedimentology of the Tuckfield Member in this area (Figure 1.8).

A scree-covered, gentle slope often occurs at the base of cycles. This area of poor exposure usually grades upward from silty mudstone to very thin-bedded, rippled siltstone with asymmetrical cross-lamination (Figure 1.9a). These deposits gradually coarsen and thicken upward to medium-bedded, fine-grained sandstone. Within this coarsening- and thickening-upward package, ripple cross-laminated beds are gradually replaced by beds with flat-lying, internal laminae. Symmetrical ripple marks occur throughout the cycle, but are more prevalent near the base, whereas non-rippled beds are more prevalent near the top of the cycle. Ripple marks record a variety of bi-directional currents with a dominant paleo-flow to the northwest/southeast (Appendix 7). Beds tend to be laterally continuous with non-erosive to slightly erosive bases. Detrital muscovite flakes often occur on bedding planes. Thin beds of iron oxide and surficial ferruginization are common throughout this package. Abundant horizontal trace fossils, typical of a *Cruziana* ichnofacies, often occur on bedding planes and are preferentially preserved in the ferruginous zones (Figure 1.9b).

Overlying this gradually coarsening- and thickening-upward succession is medium- to thick-bedded, medium-grained sandstone. These thicker sands can be: (i) massive; (ii) have large-scale, trough- to planar-cross beds; or (iii) consist of a series of extremely faint, thin to medium beds with planar laminations. These coarser sand bodies usually have erosive bases and often contain abundant vertical burrows, typical of a *Skolithos* ichnofacies (Figure 1.9c). Rare root beds are also present.

Iron-rich, silty mud-pellet and plant-fragment conglomerates occasionally cap these cycles (Figure 1.9d). The silty mud pellets tend to be elongated and bedding-parallel, with a muddy center and a thick (up to 1 cm) iron-oxide outer shell. The conglomerates have an iron-rich sandy matrix. They occur in the western part of the area. They range in thickness from a few centimeters up to approximately 1 m. The thinner beds typically occur in the central part of the St George Ranges, whereas the thicker beds typically occur in the western part of these ranges.

Detailed Cycle Analyses

One cycle was studied in detail to gain a better understanding of cycle development in the Tuckfield Member. A particular cycle was chosen based upon its representative nature and total thickness. Ten hand-sized samples were analyzed for

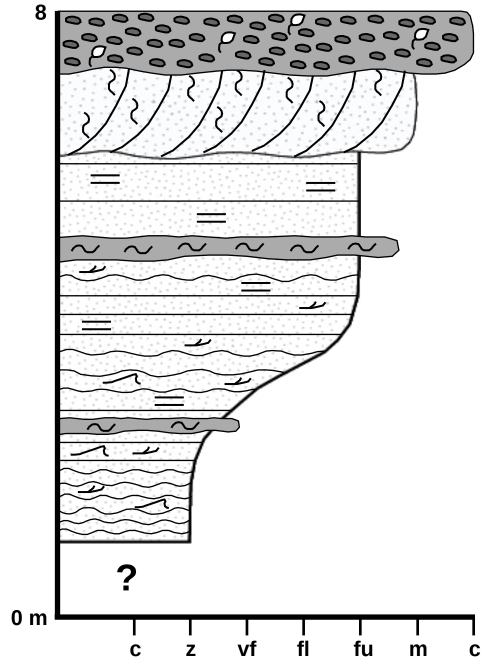

Figure 1.8: Idealized coarsening- and thickening-upward cycle from the Tuckfield Member. An average cycle is 8 m thick.

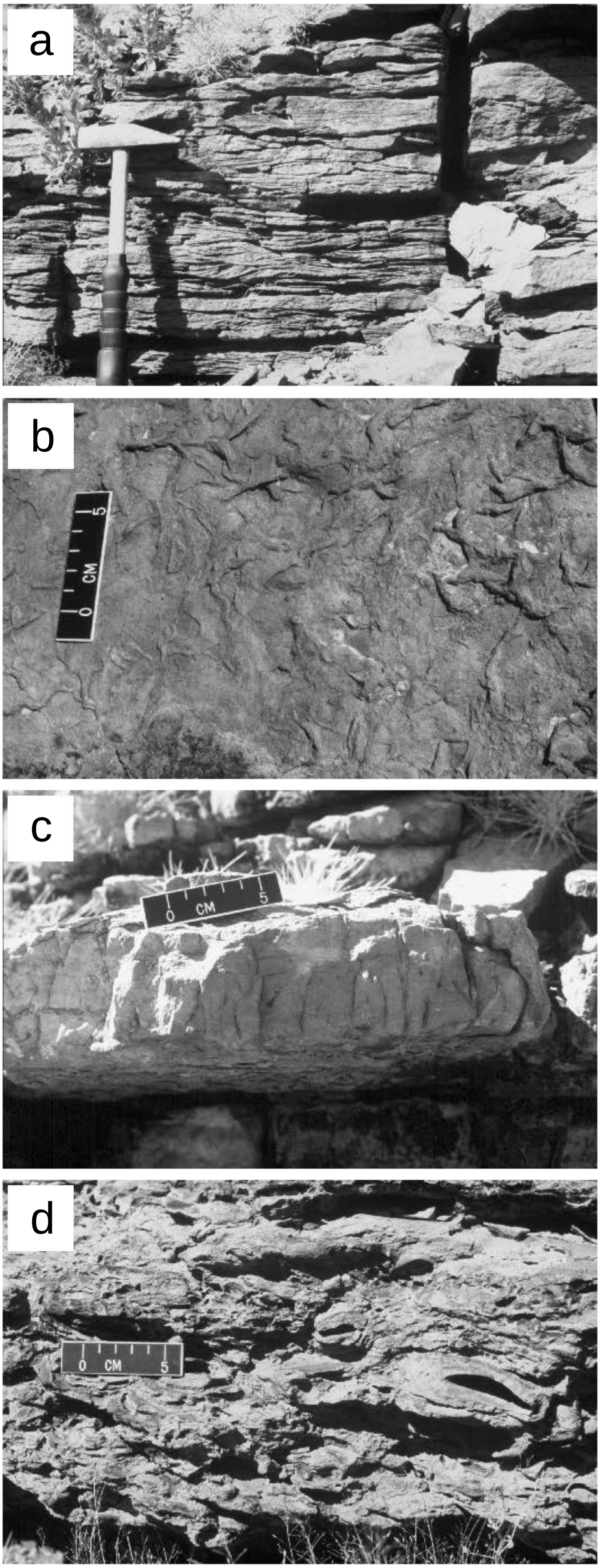

Figure 1.9: Typical facies of the Tuckfield Member. (a) Asymmetrical ripple cross-lamination found at the base of most cycles. (b) *Cruziana* ichnofacies typically preserved on bedding surfaces throughout the lower portion of cycles. (c) *Skolithos* ichnofacies typically preserved near the top of cycles. (d) Iron-rich, silty mud-pellet conglomerate that caps some cycles in the western part of the St George Ranges. Photographs from Location SG-8.

petrographic (grainsize, roundness, sorting, and porosity) and geochemical (XRF and quantitative XRD) information. The base of the cycle could not be analyzed because of poor outcrop exposure.

PETROGRAPHY

All samples studied in thin-section (Appendix 4) consist of predominantly subrounded to well-rounded quartz grains with detrital clay and minor amounts of mica. At the base of the sampled section, quartz grains tend to be more angular than near the top. As observed in outcrop, quartz sand coarsens upward from very fine to medium grained. The abundance of clay minerals decreases up the cycle (Figure 1.10).

Most beds are laminated at a millimeter-scale with graded to alternating layers of finer grained and coarser grained sediment. A preferred orientation of grains is often observed parallel to bedding. Sample porosities range between 20% and 42% (Appendix 5) and appear to be primary. Although no discernible trend is apparent in the studied cycle, these porosity values are consistent with values reported for the Poole Sandstone from elsewhere in the basin (Havord et al., 1997).

GEOCHEMISTRY

XRF data were collected from each sample to identify trends in bulk rock composition (Figure 1.11; Appendix 6). When plotted against the measured cycle, three oxides (SiO_2, Al_2O_3 and K_2O) display obvious and significant trends. The percentage of SiO_2 (quartz) generally increases up the cycle. The percentages of Al_2O_3 (clay and mica) and K_2O (mica) generally decrease up the cycle, closely mirroring the SiO_2 trend.

Quantitative XRD data were collected to identify the mineralogy of each sample (Figure 1.12; Appendix 6). As observed in thin section, a simple mineral composition occurs throughout the cycle. Each sample consists predominantly of quartz (80-92%) with lesser amounts of kaolinite (7-17%) and minor muscovite/illite (1-4%). Similar to the trend observed in the XRF data, the percentage of quartz increases up the cycle, whereas the percentage of kaolinite decreases up the cycle. No discernible trend is apparent in the muscovite/illite plot.

DEPOSITIONAL ENVIRONMENT

In the St George and Poole Ranges, the Tuckfield Member consists of a series of vertically stacked cycles. Each cycle contains lithologies and sedimentary structures

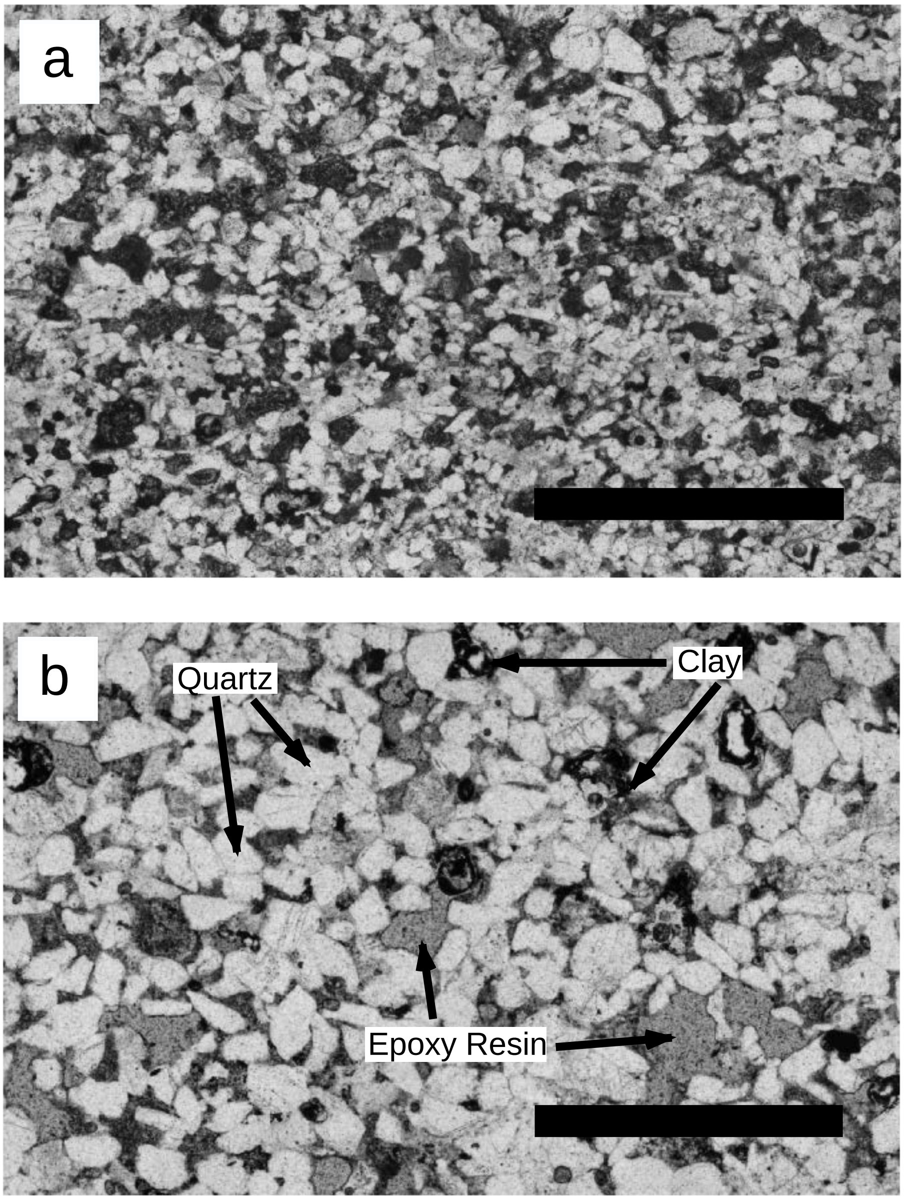

Figure 1.10: Photomicrographs taken under plane-polarized light from the (a) base and (b) top of one typical Tuckfield Member cycle. The cycle is from the upper portion (98-102 m) of a measured section located on the eastern edge of the St George Ranges (same cycle as depicted in Figures 1.11 and 1.12). The base of the measured section is located at 51K 0752252/UTM 7917068 (using the Australian Geodetic Datum 1966 coordinates). Note the rounded, monomineralic nature of the grains in both photomicrographs. In this cycle, quartz coarsens upward from very fine sand at (a) the base to medium sand at (b) the top. The scale in both photomicrographs equals 1 mm.

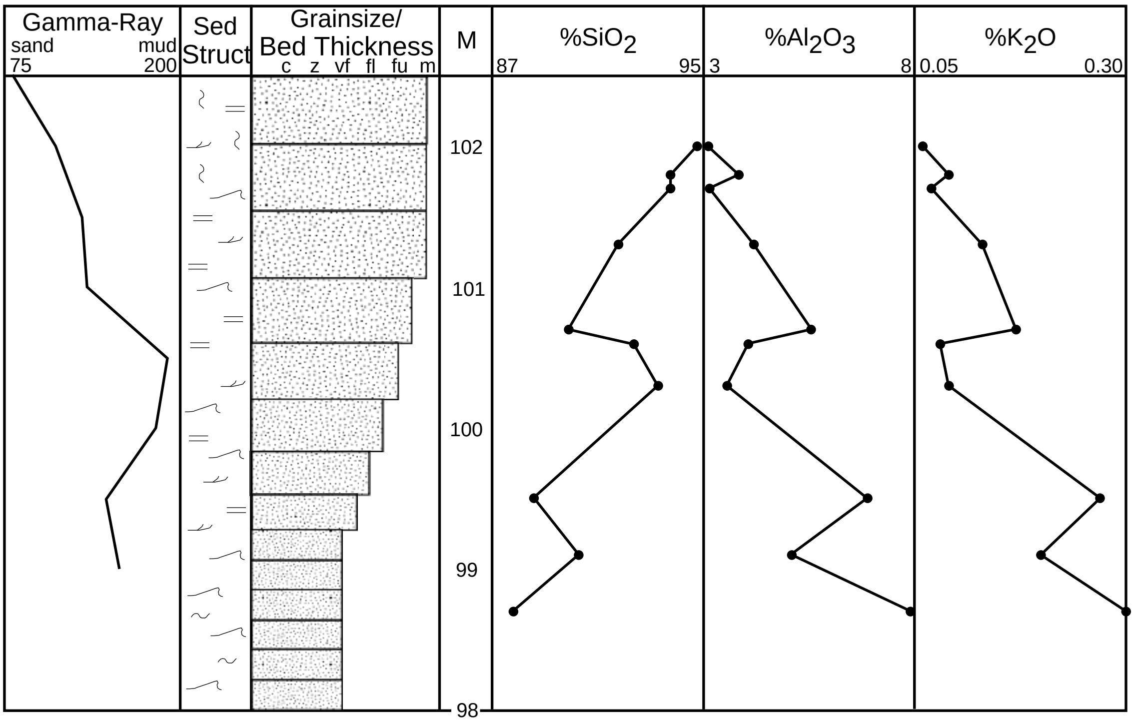

Figure 1.11: Lithology log with associated gamma-ray and XRF data for one typical Tuckfield Member cycle. The cycle is from the upper portion (98-102 m) of a measured section located on the eastern edge of the St George Ranges (same cycle as depicted in Figures 1.10 and 1.12). The base of the measured section is located at 51K 0752252/UTM 7917068 (using the Australian Geodetic Datum 1966 coordinates). Note that the lithology and gamma-ray logs record a coarsening-upward trend. This is also depicted in the XRF data, where the percentage of SiO_2 (quartz) increases up the cycle, and the percentages of Al_2O_3 (clay and mica) and K_2O (mica) decrease up the cycle.

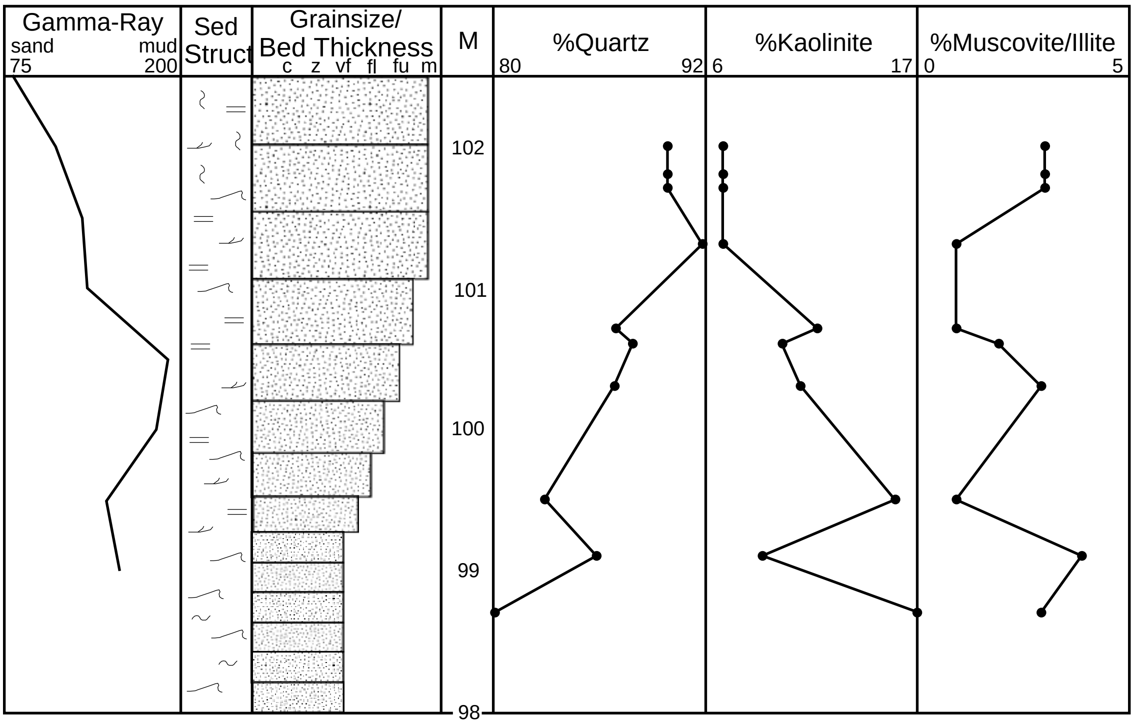

Figure 1.12: Lithology log with associated gamma-ray and quantitative XRD data for one typical Tuckfield Member cycle. The cycle is from the upper portion (98-102 m) of a measured section located on the eastern edge of the St George Ranges (same cycle as depicted in Figures 1.10 and 1.11). The base of the measured section is located at 51K 0752252/UTM 7917068 (using the Australian Geodetic Datum 1966 coordinates). Note that the lithology and gamma-ray logs record a coarsening-upward trend. This is also depicted in the quantitative XRD data, where the percentage of quartz increases up the cycle, and the percentage of kaolinite decreases up the cycle. No discernible trend in noted in the muscovite/illite plot.

that are indicative of a prograding sandy shorezone (as defined by Galloway and Hobday, 1996) (Figure 1.13). All data presented herein (field observations, gamma-ray logs, petrography, and geochemical analyses) are consistent with each cycle coarsening and shallowing upwards. Sedimentary structures near the base of most cycles (asymmetrical ripple cross-lamination, *Cruziana* ichnofacies) are indicative of deposition in a high-energy, lower to middle shoreface environment. Sedimentary structures near the top of most cycles (flat-lying beds, low-angle planar laminae, *Skolithos* ichnofacies) are indicative of deposition in a high-energy, upper shoreface to foreshore environment. Erosive beds throughout the Tuckfield Member may record storm events or mark the location of rip or tidal channels.

The mud-pellet conglomerates that cap many Tuckfield cycles were previously noted by Yeates et al. (1984). In the same paper, the authors suggest that similar iron-rich beds in the Liveringa Group (Lightjack Formation: Figure 1.3) may have precipitated where saltwater and freshwater mixed. I suggest that the Tuckfield conglomerates probably formed in a supratidal mud-flat environment. This would account for the presence of the finer grained sediment that is otherwise largely absent in the Tuckfield Member. By the Artinskian, the climate of northern Western Australia was starting to become progressively warmer and drier (Scotese et al., 1999). In such climates, supratidal deposits can be oxidized and deformed by desiccation. Therefore, supratidal environments in the Canning Basin would have been ideal for the formation of oxidized, iron-coated mud pellets. Subsequent drowning, associated with storm events or relative sea-level change, could have introduced the coarser grained sediment that now forms the matrix of the Tuckfield Member conglomerates.

SEQUENCE STRATIGRAPHIC FRAMEWORK

The discipline of sequence stratigraphy began in the mid-1970’s with the work of Peter Vail and his collegues at Exxon petroleum company (in Payton, 1977). Using seismic data, the Vail group recognized a series of unconformity-bounded sequences in the stratigraphic record. This work introduced the now popular concept of systems tracts and lead to the development of the sequence stratigraphic model.

Contemporaneously, the Vail group asserted that, through sequence analysis, an accurate chart of relative sea-level change could be constructed (Vail et al., 1977). Exxon’s global model recognized several orders of sea-level fluctuation, ranging from a few million years (3rd order cycles) to tens of millions of years (2nd order cycles) to

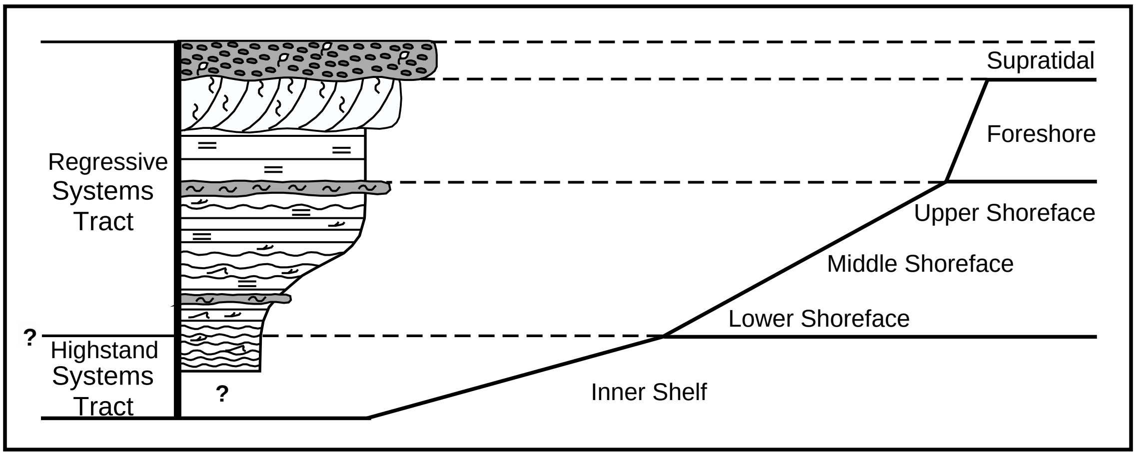

Figure 1.13: Depositional model for the idealized Tuckfield Member cycle (see Figure 1.8 for facies descriptions). The cycle consists of a relatively thin highstand systems tract that is gradationally overlain by thick regressive systems tract deposits. These sediments were deposited in an inner shelf to shorezone environment.

greater than one hundred million years (1st order cycles). Although higher frequency Milankovitch-scale cycles (20,000 to 100,000 years) were not included in Vail's original sea-level curve, they have been well documented elsewhere in the literature (e.g. Shackleton and Opdyke, 1976; Abbott and Carter, 1994; Tiedemann et al., 1994; Zachos et al., 1997).

In accordance with Vail's sea-level curve, the Exxon sequence stratigraphic model describes the idealized architecture of sediments deposited during a single sea-level cycle. These deposits are divided into three main, geometrically separate stratigraphic bodies, termed systems tracts (e.g. Vail et al., 1991). The *lowstand systems tract* consists of sediments deposited at and around a sea-level lowstand. The *transgressive systems tract* is deposited during the rising part of the sea-level cycle, whereas the *highstand systems tract* is deposited mainly during and shortly after a sea-level cycle peak.

In the original Exxon model, sedimentation does not occur on the shelf during the falling portion of the sea-level cycle since this is typically a time of erosion. However, subsequent studies (e.g. Hunt and Tucker, 1992; Posametier et al., 1992; Naish and kamp, 1997) have demonstrated that deposition may occur on the shelf if the correct balance of relative sea-level fall and rate of sediment supply is met. In such cases, the term *forced regressive systems tract* applies when sediments are bounded below by a regressive surface of erosion (Hunt and Tucker, 1992; Plint, 1988). The term *regressive systems tract* applies when regressive deposits shoal gradationally upwards from shelf into shoreface facies (Naish and Kamp, 1997).

Naish and Kamp (1997) first introduced and defined the regressive systems tract based upon Plio-Pleistocene cycles from the Rangitikei River Valley (Wanganui Basin, North Island, New Zealand). The deposits described by them consist of gradationally based, strongly progradational, shoreline sediments that accumulated during falling sea-level.

Similar in nature to the Rangitikei cyclothems, a typical Tuckfield Member cycle consists of gradationally based, strongly progradational, shoreline sediments that probably accumulated during falling sea-level. Therefore, the Tuckfield Member can be interpreted as almost entirely regressive systems tract deposits (Figure 1.13). The poorly exposed silty mudstone at the base of some cycles may represent inner shelf sediments that belong to the highstand systems tract. However, these finer-grained, poorly exposed deposits are typically thin and grade upward into the thicker shoreface and foreshore sediments that are herein ascribed to the regressive systems tract.

CONCLUSIONS

This is the first detailed investigation into the sedimentology and stratigraphy of the Early Permian Tuckfield Member of the Poole Sandstone. In the St George and Poole Ranges, at least 12 vertically stacked, coarsening- and thickening-upward Tuckfield Member cycles have been identified in outcrop. These cycles range in thickness from less than 5 m up to approximately 12 m. Each cycle contains lithologies and sedimentary structures that are indicative of a prograding sandy shorezone. Based on the data presented here, the Tuckfield Member is interpreted to consist predominantly of a vertically stacked series of regressive systems tract cycles.

Chapter 2

High-frequency sedimentary cycles from the onshore Canning Basin, Western Australia: an evaluation of the effects of mid-Permian orbital forcing

ABSTRACT

The Artinskian Tuckfield Member of the Poole Sandstone outcrops around the periphery of the St George and Poole Ranges of the Fitzroy Trough (onshore Canning Basin, Western Australia). In this area, the Tuckfield Member consists of a series of laterally extensive, coarsening- and thickening-upward cycles that were deposited predominantly in a shorezone environment. In outcrop, these cycles are typically 5 to 12 m thick. Gamma-ray and grainsize data, collected from 15 outcrops located throughout the study area, were analyzed to better define cyclicity. Spectral analysis identified several orders of meter- to decameter-scale cycles recorded in the Tuckfield Member. The average periodicities of the identified cycles occur in the ratio of ~36:10:4:2 m. This ratio correlates strongly with the known mid-Permian orbital periodicities of elongated eccentricity, eccentricity, obliquity, and precession (~410:100:40:20 thousand years). This favorable comparison indicates that Milankovitch-forcing and glacio-eustacy probably controlled the formation of depositional cyclicity in the Tuckfield Member. The 5 to 12 m cycle, predominant in outcrop, suggests that eccentricity and possibly obliquity were the main influences on global sea-level fluctuation during this time. If these interpretation are correct, Permo-Carboniferous glaciation persisted into at least the Artinskian stage of the Early Permian.

Key Words: Canning Basin, glacio-eustacy, Late Paleozoic glaciation, Milankovitch cyclicity, Permian, Poole Sandstone, Tuckfield Member

INTRODUCTION

Permo-Carboniferous sedimentary rocks record the longest known period of Phanerozoic glaciation. During this time continental ice-sheets flourished on Gondwana as it slowly drifted across the south pole (Crowell, 1975; Crowell, 1995). A direct record of this glaciation can be found on all present-day Gondwanan continents (Africa, Antarctica, Asia, Australia, and South America) as ice-affected landscapes and glacial deposits (e.g. Crowell, 1978; Hambrey and Harland, 1981; Visser, 1989; Gonzalez-Bonorino and Eyles, 1995). This record indicates that glaciation extended into the Sakmarian stage of the Early Permian. Although the Sakmarian probably marks the end of widespread Gondwanan glaciation (Scotese et al., 1999), there is debatable evidence that ice-sheets may have remained on parts of Gondwana up to at least the Triassic boundary (Veevers et al., 1994a; Veevers, 2000a). However, due to the ambiguous nature of this data, much uncertainty still exists concerning the exact timing of Permo-Carboniferous deglaciation.

Fortunately, the direct evidence that is restricted to ice-proximal environments (striated pavements, tillites, and outwash deposits) is not necessary to infer the presence of massive continental ice-sheets and polar ice-caps. Periodic to quasi-periodic oscillations in Earth's orbital parameters affect the distribution and amount of incident solar energy reaching Earth's surface (Hays et al., 1976; Berger, 1977). During ice-house periods, glaciers wax and wane in response to these orbital oscillations (e.g. De Boer and Smith, 1994; Naish et al., 1998; Zachos et al., 2001). This waxing and waning can directly affect global sea-level and influence sedimentation worldwide, resulting in the deposition of cyclic, vertically stacked, coarsening- or fining-upward marine sequences (Imbrie and Imbrie, 1979; Berger, 1988; Carter et al., 1999; Saul et al., 1999).

Since the work of Udden (1912), Permo-Carboniferous stratigraphic cyclicity has been recognized in marine sediments worldwide (e.g. Weller, 1931; Bush and Rollins, 1984; Veevers and Powell, 1987; Ross and Ross, 1988). This cyclicity has been convincingly linked to Milankovitch orbital modulations and glacio-eustacy (e.g. Wanless and Shephard, 1936; Heckel, 1977; Ross and Ross, 1985; Klein and Willard, 1989; Connolly and Stanton, 1992). Historically, investigations of Late Paleozoic cyclicity have focused on Carboniferous and earliest Permian strata (e.g. Ramsbottom, 1979; Algeo and Wilkinson, 1988; Goldhammer et al., 1994; Miller and Eriksson, 2000). Although these studies have been invaluable to our understanding of global sea-level fluctuation and climate change, they reveal little concerning the exact timing of Permian deglaciation. However, a few publications have suggested that mid- to Late Permian (post-Sakmarian) strata may also record Milankovitch-scale, glacio-eustatic cyclicity (Borer and Harris, 1991; Michaelsen and Henderson, 2000; Rampino et al., 2000). If these studies are correct, they support the idea that glaciers may have persisted on Gondwana (or elsewhere) up to at least the Triassic boundary (Rampino et al., 2000).

Australia is an ideal location in which to test for post-Sakmarian glacio-eustacy. Unlike other Gondwanan continents, Australia contains Permian successions that are predominantly marine and variably complete. Thick packages of Permian deposits outcrop and sub-crop in sedimentary basins throughout the continent. This chapter describes high-frequency, sedimentary cycles recorded within the Artinskian Tuckfield Member of the Poole Sandstone (onshore Canning Basin, Western Australia). These cycles are tested for a glacio-eustatic driving-mechanism by quantitatively comparing them to the known mid-Permian orbital parameters.

METHODS

This research is based upon field investigations of the Artinskian Tuckfield Member, where it is exposed around the periphery of the St George and Poole Ranges of the Fitzroy Trough (Figures 2.1 and 2.2; Appendix 1). Fifteen outcrop sections, ranging from 30 to 110 m thick, were evaluated for lithofacies, sedimentary structures, fossils, bed thickness variations, and vertical stacking patterns (Appendix 2).

Gamma-ray measurements were collected from each outcrop and plotted against the corresponding lithological log (Appendices 2 and 3). Measurements were collected at a 0.5 m vertical/stratigraphic spacing using a hand-held gamma-ray spectrometer. This instrument measures natural gamma-ray emissions that are related to the content of radiogenic isotopes of potassium, uranium, and thorium. These elements (particularly potassium) are common in clay minerals (Cant, 1992). Therefore, gamma-ray measurements should reflect the amount of clay present in terrigenous successions and may be used to detect quantitative changes in lithology.

To better constrain cyclicity in the Tuckfield Member, spectral analyses were run on gamma-ray and grainsize data from each measured section. Gamma-ray data were collected directly from outcrop (Appendix 3). Grainsize data were generated (at a 0.5 m spacing) from lithological logs using a simple coding procedure in which each grain-size division (silt, fine sand, etc.) is assigned a numeric value (Appendix 8). As a cross-check on the results, two different spectral programs were used to analyze each dataset (Appendices 9-11). "Timeseries," described in Weedon and Read (1995), uses the standard Blackman-Tukey method (Blackman and Tukey, 1958) to generate power spectra. "AnalySeries 1.1" (Paillard et al., 1996) uses a variety of different methods to generate power spectra. In this study, the Blackman-Tukey and Maximum Entropy (Haykin, 1983) methods are used. Results from the spectral analyses are compared with known mid-Permian orbital periodicities to determine the role (if any) of Milankovitch-forcing in the formation of depositional cyclicity.

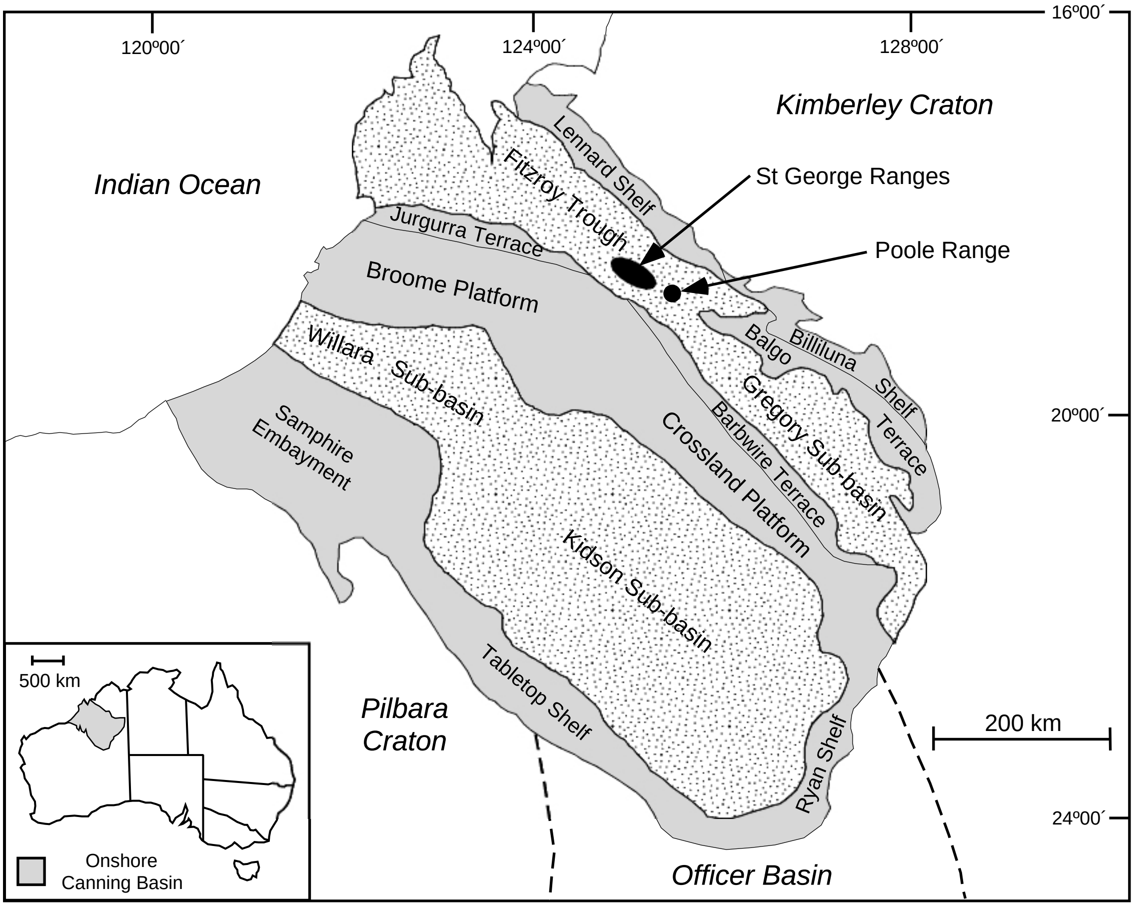

Figure 2.1: Simplified map of the onshore Canning Basin (adapted from Kennard et al., 1994; Apak and Carlsen, 1996) showing locations of the St George and Poole Ranges.

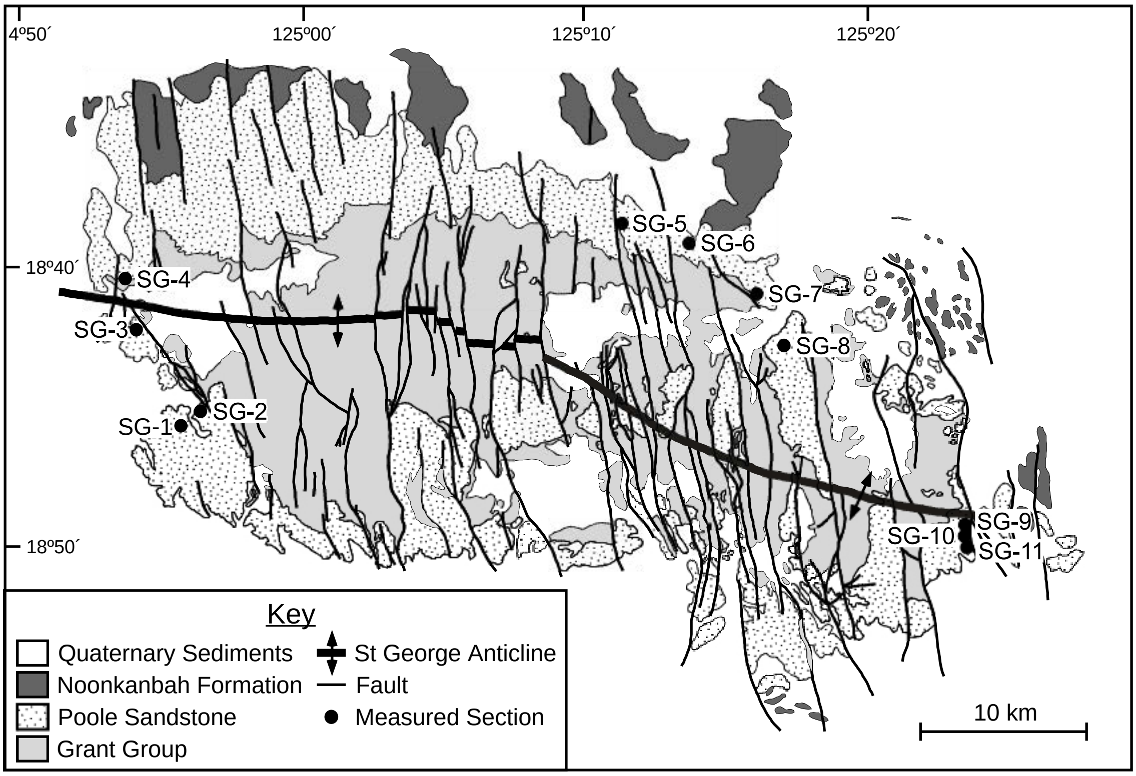

Figure 2.2a: Simplified geological map of the St George Ranges (adapted from Crowe and Towner, 1981) showing the location of the measured sections.

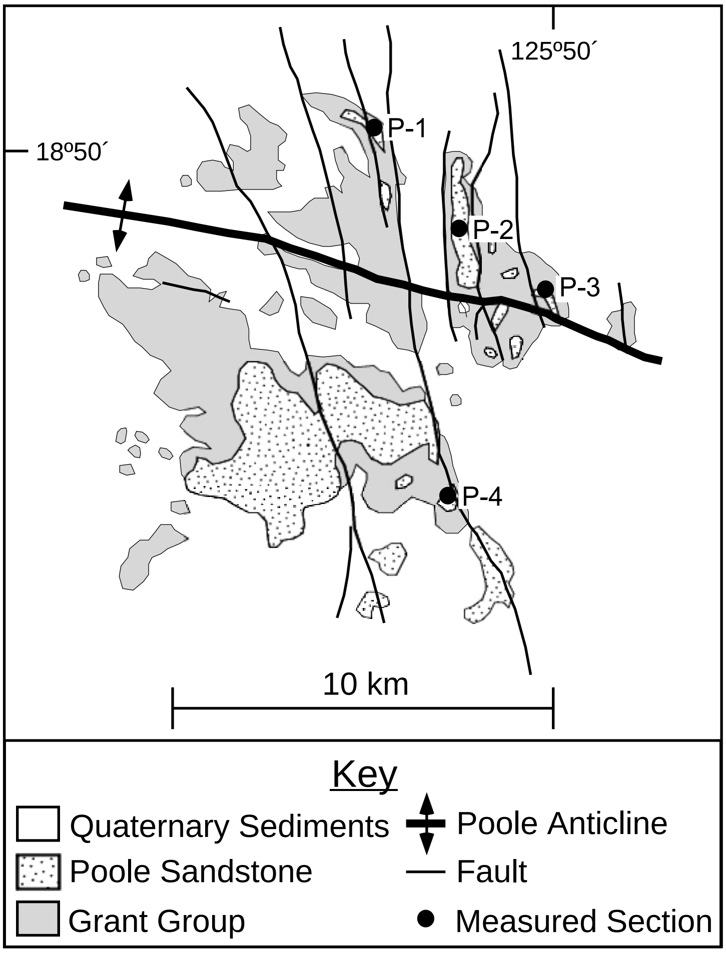

Figure 2.2b: Simplified geological map of the Poole Range (adapted from Crowe and Towner, 1981) showing the location of the measured sections.

GEOLOGIC SETTING

The onshore Canning Basin is the largest sedimentary basin in Western Australia. It lies between the Proterozoic Kimberley Craton to the northeast and the Archean Pilbara Craton to the southwest (Figure 2.1) (Purcell, 1984). Major northwest-trending faults, controlled by terrane boundaries in underlying basement rock, define the predominant structure of the basin (Hocking et al., 1994). Within the basin, two northwest-trending depositional troughs, flanked by narrow shelves and terraces, are separated by an uplifted mid-basin arch. The northern trough is divided by a basement high into the Fitzroy Trough to the northwest and the Gregory Sub-basin to the southeast. The southern trough is divided by a basement high into the Willara and Kidson Sub-basins (Kennard et al., 1994).

Since the Early Ordovician, the Canning Basin has experienced four phases of extension and transpression, each lasting approximately 70-80 million years. These tectonic phases resulted in the deposition of four tectono-stratigraphic megasequences: (i) Ordovician-Silurian; (ii) Devonian-Early Carboniferous; (iii) Late Carboniferous-Permian; and (iv) Jurassic-Cretaceous (Kennard et al., 1994). Subsidence associated with the Late Carboniferous-Permian megasequence was the most pronounced and resulted in the deposition of a thick Permo-Carboniferous succession throughout the basin. In the northern Fitzroy Trough, Late Carboniferous-Permian strata attain a thickness of more than 4 km (Eyles and Eyles, 2000).

The St George and Poole Ranges of the Fitzroy Trough

Although deposits of the Late Carboniferous-Permian megasequence are predominantly encountered in the sub-surface, a thick succession of Permian strata outcrops in the highly-faulted, anticlinal St George and Poole Ranges of the Fitzroy Trough (Figures 2.2 and 2.3). Strata from the St George and Poole Ranges record a variety of glacially-influenced, shallow-marine to non-marine depositional environments. These strata consist predominantly of siltstone and sandstone with only minor amounts of finer and coarser grained sediment.

At the base of this succession, the Sakmarian Carolyn Formation (upper Grant Group) is divided into the lower Wye Worry and upper Millajiddee Members (Crowe and Towner, 1976a). The Wye Worry Member consists predominantly of calcareous siltstone and sandy siltstone with locally abundant glacial dropstones (Crowe and Towner, 1981). General characteristics of the Wye Worry Member suggest that it was

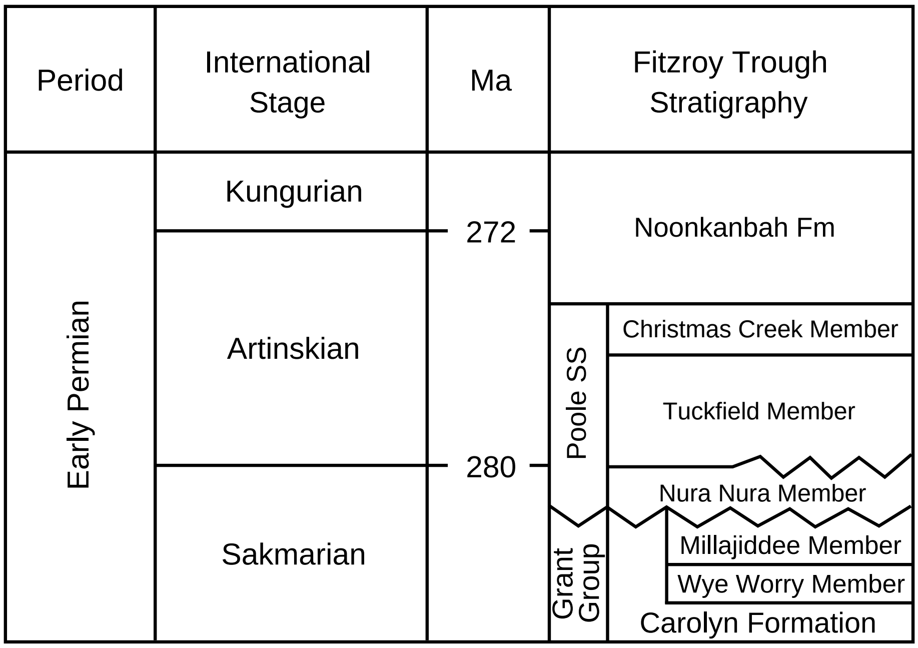

Figure 2.3: Stratigraphic column for the St George and Poole Ranges of the Fitzroy Trough, onshore Canning Basin (adapted from Kennard et al., 1994). Stage dates from Veevers, 2000b.

deposited in a fluvioglacial to shallow-marine deltaic setting (Apak, 1996). The Millajiddee Member consists predominantly of fine- to medium-grained sands (Crowe and Towner, 1981) that have been interpreted as fluvio-marine to deltaic, near-shore deposits (Apak, 1996). The Wye Worry and Millajiddee Members correspond approximately to the newly proposed Clianthus Formation (Apak, 1996) of Redfern and Millward (1994). However, the most recent geological maps of the St George and Poole Ranges (Crowe and Towner, 1981) pre-date Redfern and Millward's study. Because it is difficult to apply this new stratigraphic division (Redfern and Millward, 1994) directly to the field area, the previously defined stratigraphy of Crowe and Towner (1976a) is used here.

In the St George and Poole Ranges, the Sakmarian to Artinskian Poole Sandstone (defined by Guppy et al., 1952, 1958) unconformably overlies the Carolyn Formation. The Poole Sandstone consists of three distinct depositional units: the lowermost Nura Nura Member, the middle Tuckfield Member, and the uppermost Christmas Creek Member. The heterogenous Nura Nura Member consists of calcareous, thin-bedded sand and silt in the western part of the field area and poorly sorted, cross-bedded sandstone and conglomerate in the eastern part of the field area. It records deposition in a shallow-marine to fluvial environment (Crowe and Towner, 1976b). In the St George and Poole Ranges, the Christmas Creek Member consists almost entirely of cross-bedded, coarse-grained, fluvial sediments. The middle Tuckfield Member is the focus of this paper and is described in detail below.

Conformably overlying the Poole Sandstone, the poorly exposed Artinskian to Kungurian Noonkanbah Formation is the uppermost unit exposed in the St George and Poole Ranges (Yeates et al., 1984; Kennard et al., 1994). In this area, the Noonkanbah Formation is finer-grained than the underlying strata. It consists predominantly of shale and siltstone, with a rich fossil brachiopod assemblage. The Noonkanbah Formation is interpreted to record an episode of abrupt drowning and deposition in a marine environment (Yeates et al., 1984).

The Tuckfield Member of the Poole Sandstone

The middle Tuckfield Member of the Poole Sandstone outcrops around the periphery of the St George and Poole Ranges (Figure 2.2; Appendix 1). The sedimentology and stratigraphy of these deposits were described in detail by Adkins (2003; Chapter 1, this volume). So, only a brief description is given here.

In the St George and Poole Ranges, the Tuckfield Member consists of a series of vertically stacked, coarsening- and thickening-upward cycles (Appendix 2). In outcrop, these cycles are typically 7 to 12 m thick in the St George Ranges and 5 to 7 m thick in the Poole Range, with some thinner cycles (2 to 4 m) observed at most locations. A typical cycle consists upward of silty mudstone, siltstone, and sandstone. A supratidal, mud-pellet and plant-fragment conglomerate often caps cycles in the western part of the area (see Figures 2.4 and 2.5 for more detailed information). Primary sedimentary structures, trace fossils and the vertical succession of facies suggest that each cycle records an episode of shorezone progradation (Figure 2.4; Chapter 1, this volume). Although the Tuckfield Member was probably deposited in less than 20 m of water throughout the Fitzroy Trough (Brakel and Totterdell, 1993), relative cycle thicknesses and the occurrence of supratidal deposits in the St George Ranges suggest that the Poole Range records deposition in a slightly deeper, more shore-distal environment than the St George Ranges.

Tuckfield Member cycles are laterally continuous in the field area. Flat-lying benches usually correspond with cycle tops (Figure 2.6; Appendix 2). In Figures 2.5 and 2.7, heavy horizontal lines mark the tops of cycles. In Figure 2.7, eleven vertically stacked, coarsening- and thickening-upward cycles are traced in the Poole Range for a distance of over 10 km. Although Tuckfield Member cycles are also laterally continuous in the St George Ranges, it is difficult to correlate the measured sections from this area with absolute certainty. This difficulty can be attributed to the distance between measured outcrops (typically 5 to 10 km), the limited variation of sedimentary facies, and the highly faulted nature of the St George Ranges.

MILANKOVITCH THEORY AND THE ORBITAL PARAMETERS

Milankovitch theory is an astronomical theory of glaciation. It predicts that fluctuations in the seasonal and geographic distribution of incident solar energy drive climate change, the waxing and waning of glaciers, and therefore global sea-level (e.g. Imbrie and Imbrie, 1979). Three orbital perturbations affect this distribution of incident solar energy: eccentricity, obliquity, and precession (Figure 2.8). Eccentricity refers to the shape of Earth's orbit around the sun, which varies from elliptical to near circular. The period over which eccentricity varies from a maximum to a minimum and back is approximately 100,000 years. A superimposed regular variation of eccentricity also occurs at about 410,000 years. Obliquity refers to the angle of tilt in Earth's axis

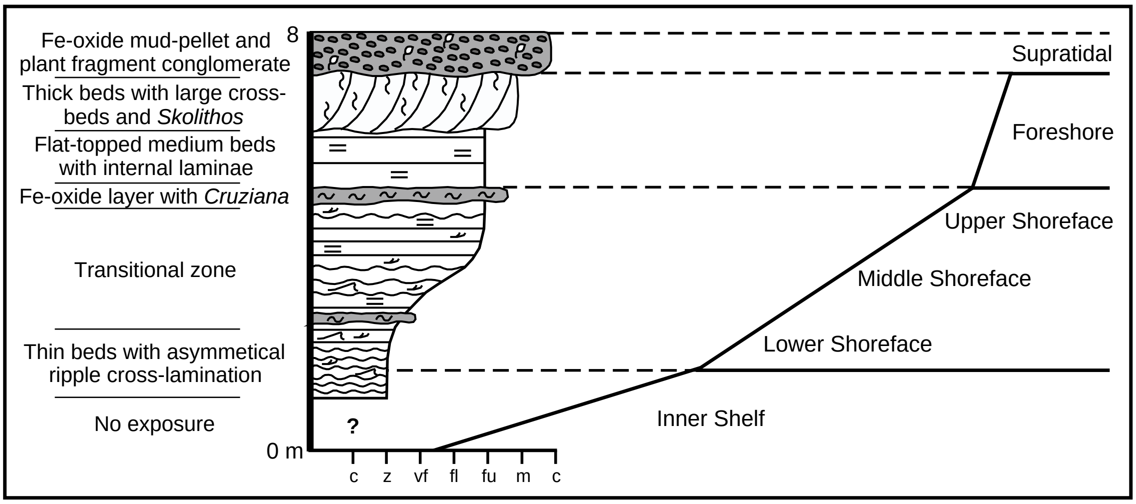

Figure 2.4: Idealized coarsening- and thickening-upward cycle from the Tuckfield Member (adapted from Adkins, 2003; Chapter 1, this volume). Each cycle, deposited in an inner shelf to shorezone environment, records an episode of coastal progradation. An average cycle is 8 m thick.

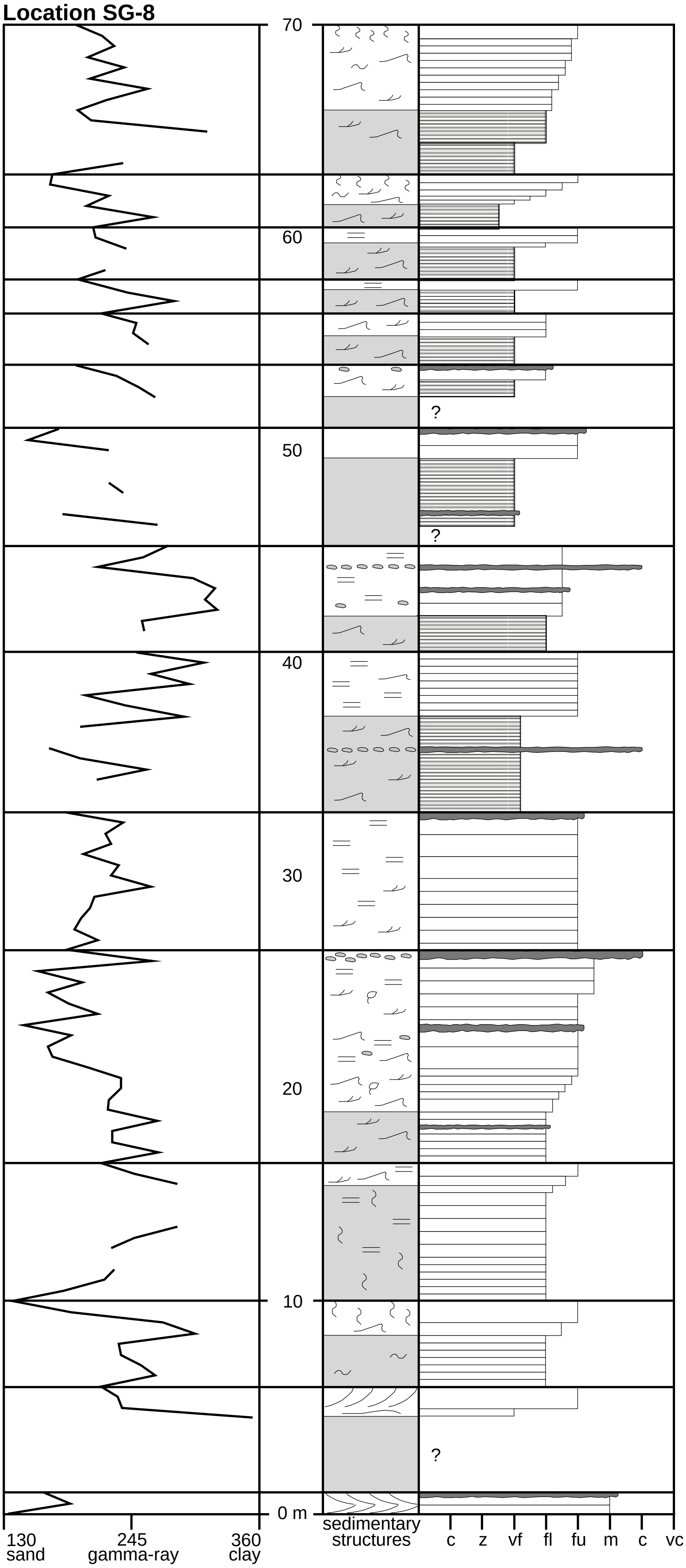

Figure 2.5a: Lithology log with associated gamma-ray data from the St George Ranges. The base of the measured section is located at 51K 0740868/UTM 7929491 (using the Australian Geodetic Datum 1966 coordinates). Heavy horizontal lines mark the tops of coarsening-and thickening-upward cycles. These lines generally correspond to the benches shown in Figure 2.6. Grainsize divisions from left to right on the x-axis of the lithology log are as follows: c (clay/mud); z (silt); vf (very fine sand); fl (lower half of fine sand); fu (upper half of fine sand); m (medium sand); c (coarse sand); vc (very coarse sand). Fine sand was divided into lower and upper halves to better depict variations in grainsize. See Figure 2.5b for key.

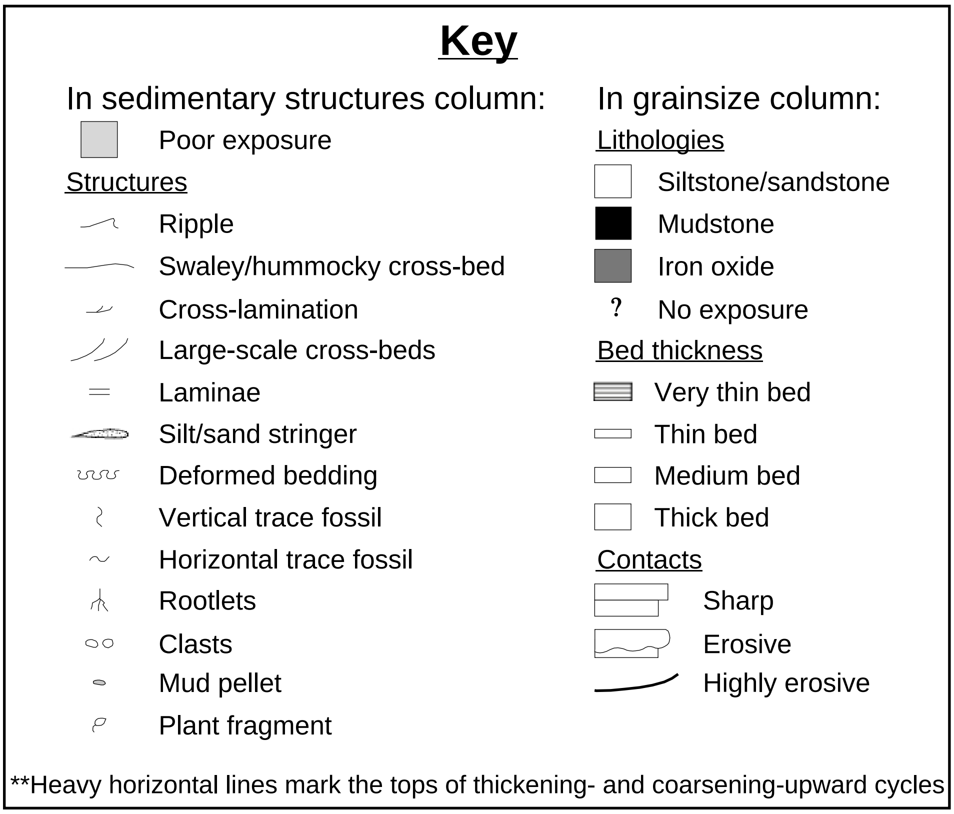

Figure 2.5b: Key for Figures 2.5a and 2.7.

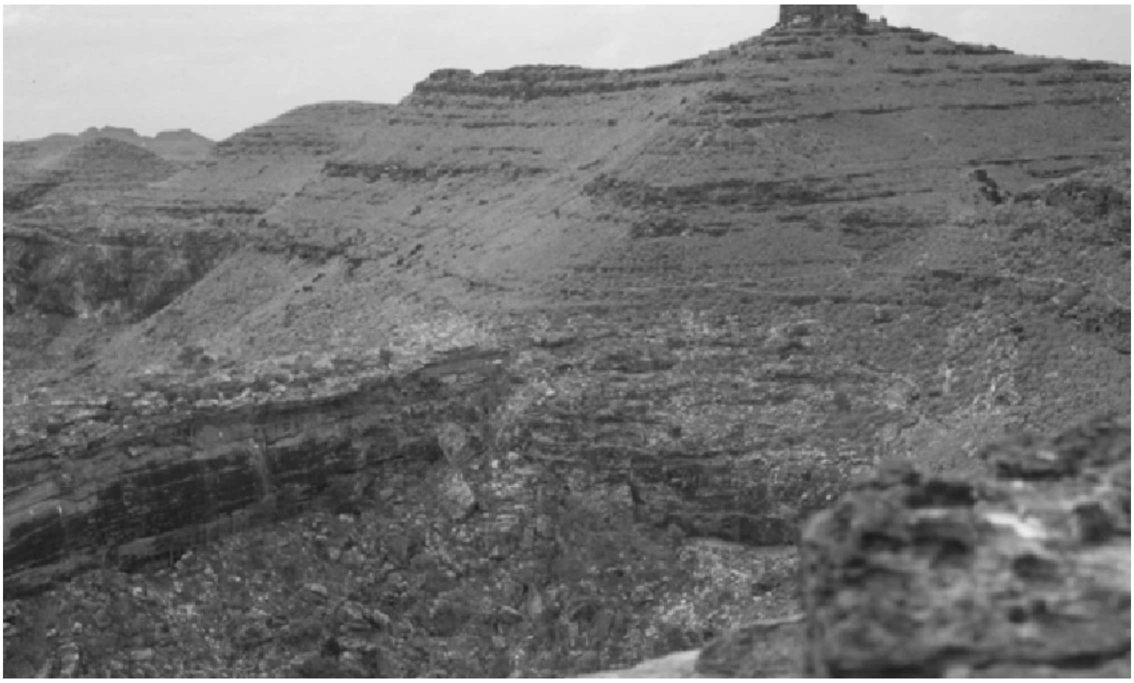

Figure 2.6: Outcrop of the Tuckfield Member, Poole Range. Note the laterally continuous, flat-lying benches that mark the tops of coarsening- and thickening-upward cycles. Photograph taken at 51K 0795184/UTM 7905636 (using the Australian Geodetic Datum 1966 coordinates), facing north. Photograph shows approximately 1 horizontal km of outcrop.

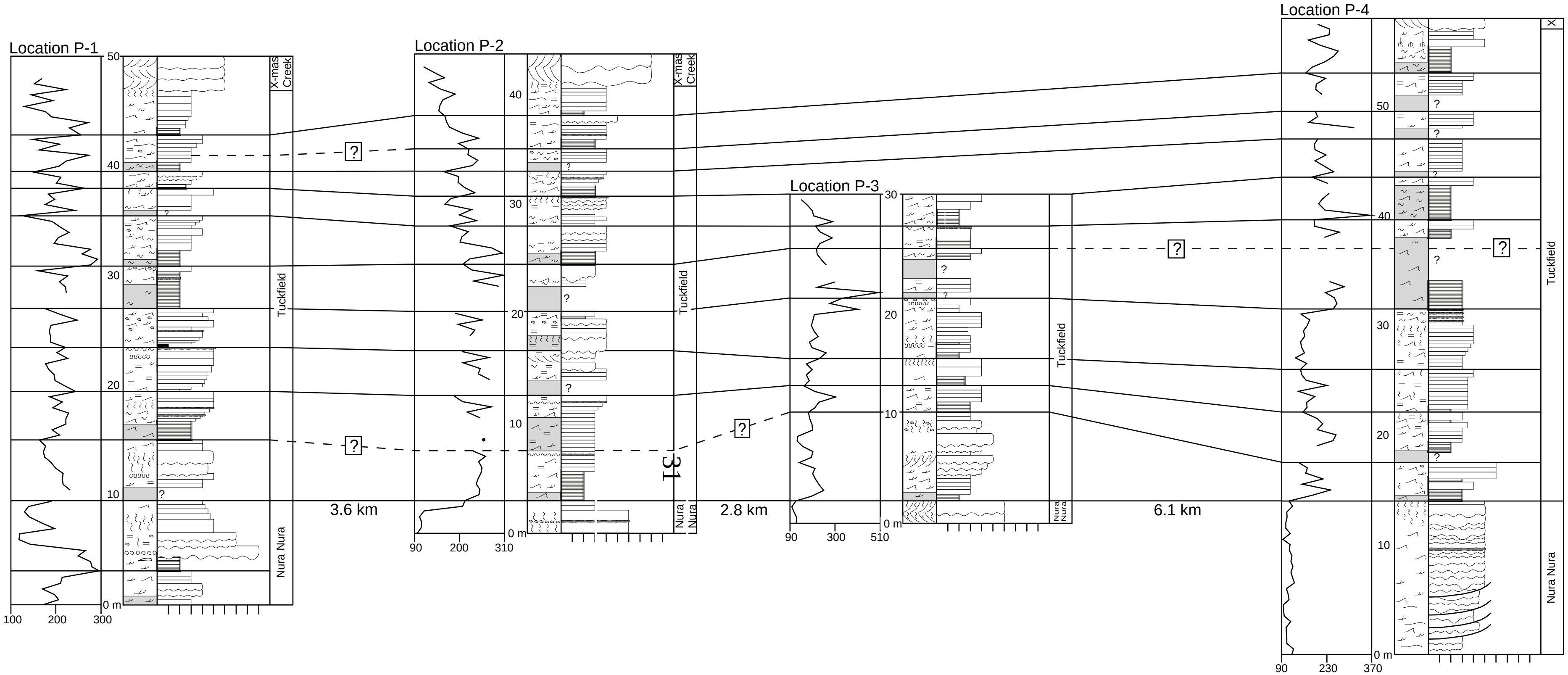

Figure 2.7: Cross-section through the Poole Range. Eleven coarsening- and thickening-upward Tuckfield Member cycles are traced for a distance of over 10 km. Heavy horizontal lines mark the tops of the coarsening- and thickening-upward cycles. These lines generally correspond with the benches shown in Figure 2.6. For each location, there is a lithology log with associated gamma-ray data. The base of Location P-1 is located at 51K 0793957/UTM 7914331 (using the Australian Geodetic Datum 1966 coordinates). The base of Location P-2 is located at 51K 0795598/UTM 7913141. The base of Location P-3 is located at 51K 0796826/UTM 7911692. The base of Location P-4 is located at 51K 0794992/UTM 7905489. Member names are given in the right-hand column of each measured section. Key as in Figure 2.5b.

Parameter	Schematic	Modern Period	Mid-Permian Period	Mid-Permian Ratio
Eccentricity	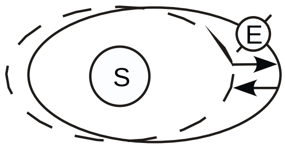	410,000 (elong) 100,000	410,000 (elong) 100,000	4.1:1 1
Obliquity	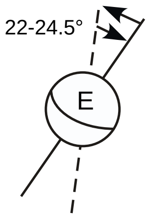	41,000	44,000 35,000	1:2.3 1:2.9
Precession	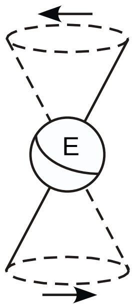	23,000 19,000	21,000 17,600	1:4.8 1:5.7

Figure 2.8: Schematic representation of the orbital parameters affecting Earth's climate (adapted from de Boer and Smith, 1994). The modern and retrodicted mid-Permian periodicities (from Berger and Loutre, 1994) are given for each parameter. Mid-Permian periodicities have been converted into ratios, relative to the 100,000 year cycle.

relative to the plane in which it rotates around the Sun. Obliquity varies between 22º and 24.5º and has a modern period of approximately 41,000 years. Precession refers to the wobble of Earth's axis of rotation that follows a roughly cone-shaped envelope. The modern precessional period is approximately 26,000 years with dual components of 23,000 and 19,000 years. For a more detailed review of the orbital parameters, see: Imbrie and Imbrie, 1979; Imbrie, 1985; Schwarzacher, 1993; or House, 1995.

The astronomical periods listed above are for the present. Berger and Loutre (1994) demonstrated that these values have changed throughout time. The astronomical periods for precession and obliquity have slowly lengthened during the past 2.5 billion years. This can be partially attributed to the combined lengthening of the Earth-Moon distance and the lengthening of the average day (Lambeck, 1980). Two hundred seventy (270) Ma (mid-Permian), obliquity had a periodicity with dual components of approximately 44,000 and 35,000 years. Precession had a periodicity with dual components of approximately 21,000 and 17,600 years (Figure 2.8). Eccentricity is not influenced by these variations. Therefore, the periods of eccentricity and elongated eccentricity (100,000 and 410,000 years) have remained relatively constant (Berger and Loutre, 1994).

SPECTRAL ANALYSIS

Spectral analysis is an objective, statistical method that can detect regular cyclicity in a dataset (Weedon, 1991). Although much speculation preceded their work, Hays et al. (1976) were the first to use spectral analysis to demonstrate that major climatic changes can be directly linked to variations in Earth's orbital parameters. This was achieved by identifying periodicities in oxygen isotope data (from planktonic foraminifera) that are consistent with the known periodicities of eccentricity, obliquity, and precession. Since that pivotal study, spectral analysis has been used to identify orbitally-induced, climatic variations recorded throughout the stratigraphic column (Reijmer et al., 1994; Weedon and Read, 1995; Weedon et al., 1999; Sierro et al., 2000).

In this study, gamma-ray data from each measured outcrop were analyzed using two spectral analysis programs (Appendices 9 and 10). Spectral plots generated from analysis of gamma-ray data from Location SG-8 are presented in Figure 2.9. In both plots (Figures 2.9a and 2.9b), spectral peaks represent cycles recorded in the rock record. The reciprocal of the frequency for each peak is equal to the average period of

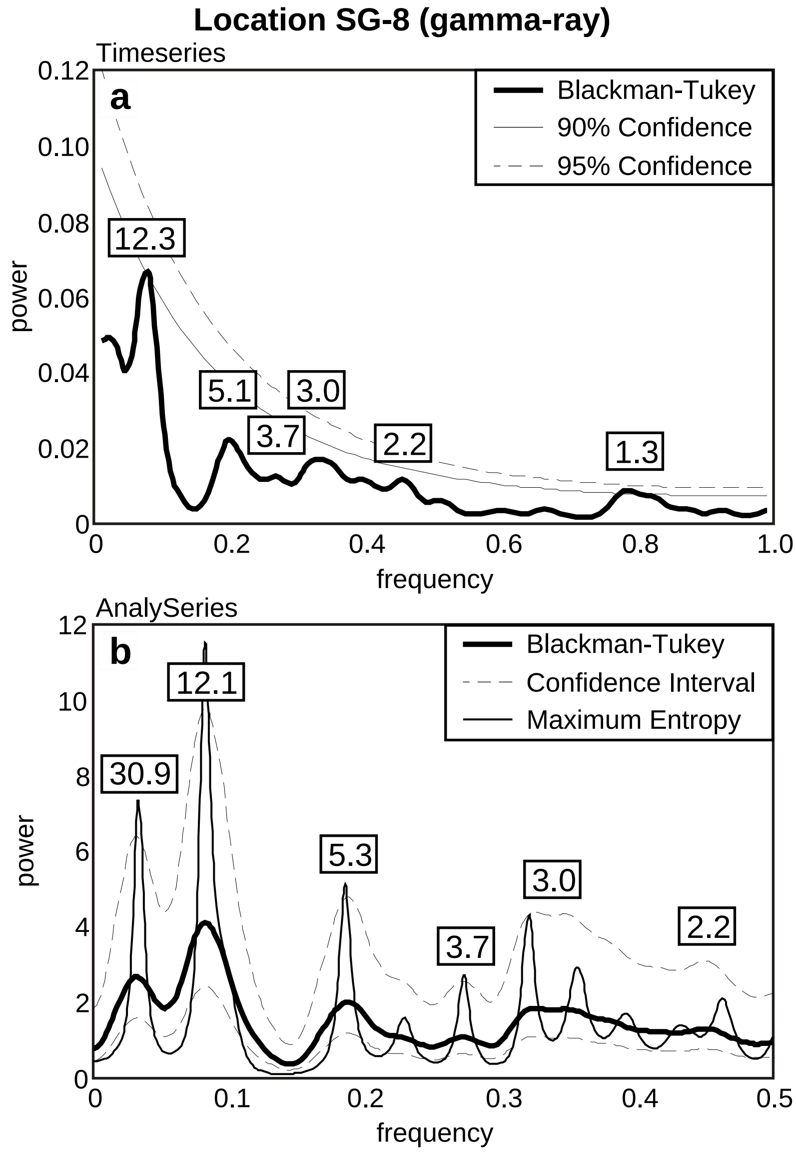

c

Cycle Thickness	Location SG-8 Ratios
30.9 meters	2.5:1
12.2 meters	1
5.2 meters	1:2.3
3.7 meters	1:3.3
3.0 meters	1:4.1
2.2 meters	1:5.5
1.3 meters	1:9.4

Figure 2.9: Spectral analyses of gamma-ray data from Location SG-8. Data were analyzed using two spectral programs as a cross-check on results. (a) displays spectrum (calculated using the Blackman-Tukey method) with 90% and 95% confidence lines. Results produced by “Timeseries” program. (b) displays two spectra (one with associated confidence interval, calculated using the Blackman-Tukey method; the second calculated using the maximum entropy method). Results produced by “AnalySeries 1.1" program. In (a) and (b), peaks in the spectra mark cycles. Average cycle periods are listed in rectangles above spectral peaks. (c) lists dominant cycles detected by the spectral analyses and their conversion into ratios relative to the 12.2 m cycle.

that cycle in meters (shown in rectangles above spectral peaks). Spectral peaks generated by the two programs were compared, averaged, and used to determine the periodicities of all significant cycles recorded at each location. For Location SG-8, cycles with periodicities of 30.9 m, 12.2 m, 5.2 m, 3.7 m, 3.0 m, 2.2 m and 1.3 m were detected (Figure 2.9c).

As a further check on the results, a similar process was performed on grainsize data from each measured outcrop (Appendices 9 and 11). Spectral plots generated from the analysis of grainsize data from Location SG-8 are presented in Figures 2.10a and 2.10b. Cycles with periodicities of 48.3 m, 13.9 m, 5.7 m, 4.6 m, 3.3 m, 2.4 m, 1.9 m and 1.6 m were detected (Figure 2.10c).

Table 2.1 summarizes the results of all spectral analyses performed in this study. The table is organized in a manner that will allow easy comparison of the detected periodicities from the 15 measured sections. This table is also organized to allow a comparison between the results presented here and the results presented in Tables 2.2-2.4, which will be discussed later in the text. Detected cycles can be grouped into six main categories/columns that are labeled A through F in Table 2.1. Additional cycles were detected in some datasets. They are listed in columns labeled 1 through 4.

In Table 2.1, periodicities detected from the analysis of gamma-ray data are listed in plain text. Periodicities detected from the analysis of grainsize data are listed in bold text. For most outcrops, periodicities from grainsize data compare favorably with periodicities from gamma-ray data. The largest discrepancies occur in Column A (e.g. Location SG-10), where cycles with the longest periods are listed. These discrepancies are probably related to the total length of the measured sections. Because spectral programs search for repetitive cycles, they cannot accurately detect periodicities greater than about half the total length of the dataset. Since the outcrops in this study range between 30 and 110 m thick, many of the periodicities listed in Column A are approaching the spectral programs' upper limit of detection. This may have resulted in some erroneous spectral peaks.

In addition to a favorable comparison between the gamma-ray and grainsize periods for each outcrop, the results from the 15 different locations also compare favorably with one another. In Column B (Table 2.1), most of the detected periodicities fall within a limited range. One notable observation is the difference in periodicities from the two areas. In the St George Ranges, the periodicities listed in Column B range between 7.4 m and 13.9 m with an average thickness of 10.9 m. In the Poole Range, the

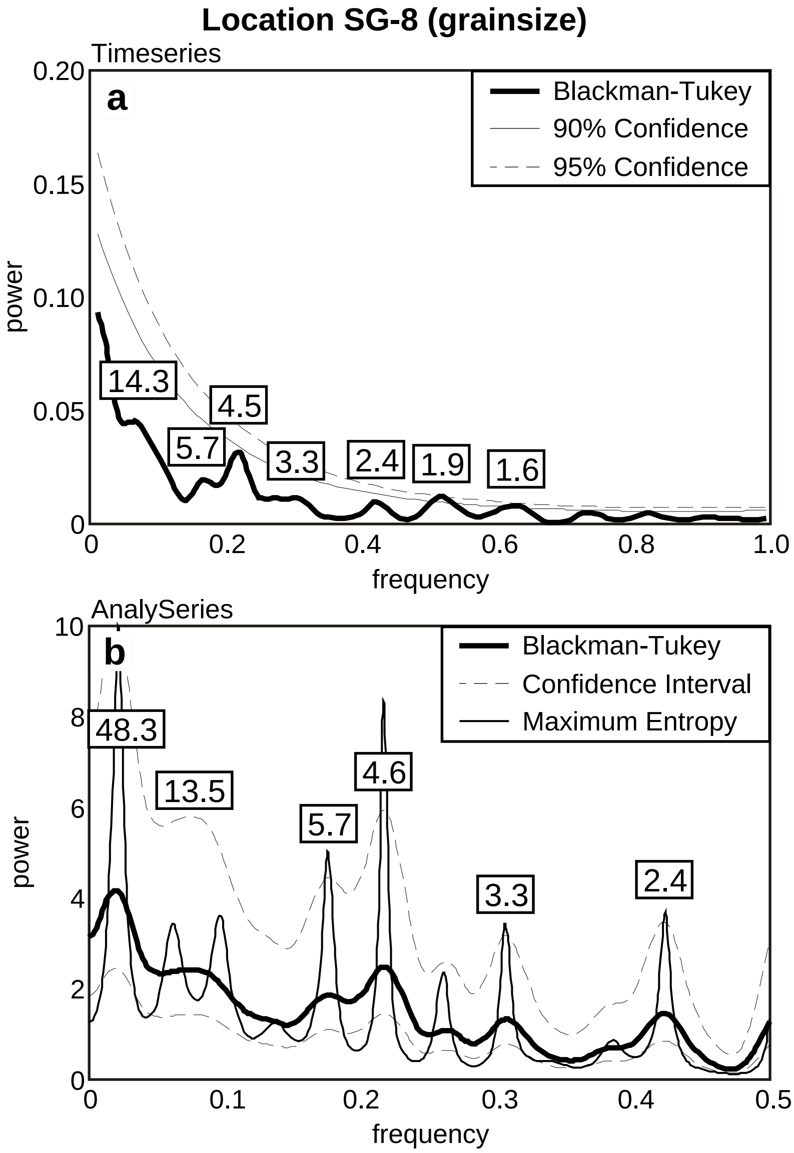

c

Cycle Thickness	Location SG-8 Ratios
48.3 meters	3.5:1
13.9 meters	1
5.7 meters	1:2.4
4.6 meters	1:3.0
3.3 meters	1:4.2
2.4 meters	1:5.8
1.9 meters	1:7.3
1.6 meters	1:8.7

Figure 2.10: Spectral analyses of grainsize data from Location SG-8. In (a) and (b), peaks in the spectra mark cycles. Average cycle periods are listed in rectangles above spectral peaks. (c) lists dominant cycles detected by spectral analyses and their conversion into ratios relative to the 13.9 m cycle. See Figure 2.9 for details concerning analyses.

Location	Periodicities (meters)									
	A	1	B	2	C	D	3	E	F	4
SG-1	39.7		10.8		6.7	3.8		2.5	1.7	1.5 1.3 1.1
	23.6		**?**		**4.9**	**3.3**		**2.3**	**1.6**	
SG-2	40.0		10.6	6.3	4.4	3.1	2.5	2.1	1.7	
	27.7		**11.6**	**6.6**	**4.4**	**3.9**	**3.1**	**2.3**	**2.1**	
SG-3	55.7		10.1	6.1						
	60.3	**17.8**	**10.1**	**6.0**	**4.7**	**3.5**	**3.0 2.4**	**2.1**	**1.7**	
SG-4	50.3		12.9		6.4	4.5			2.1	
	58.3		**11.4**		**5.2**	**3.1**				
SG-5	35.7		9.9		3.5	2.7		2.3	1.8	1.2
	21.2		**11.0**		**4.2**			**2.8**	**2.0**	
SG-6	45.1		13.5		6.6			3.5	2.1	
	27.0		**11.1**	**8.5**	**6.0**	**4.7**		**2.7**		
SG-7	49.7		11.2	5.8			3.1	2.1	1.5	
			8.7	**5.1**	**3.8**	**2.8**	**2.5**	**2.1**	**1.1**	
SG-8	30.9		12.2		5.2	3.7		3.0	2.2	1.3
	48.3		**13.9**		**5.7**	**4.6**		**3.3**	**2.4**	**1.9 1.6**
SG-9	39.1		9.0	5.0	3.9	2.7		2.3	2.1	
	29.7		**11.2**	**7.5**	**4.5**	**3.8**		**3.0**	**2.2**	
SG-10	33.5		10.0		5.3	4.0	2.7	2.3	1.8	
	53.5	**15.7**	**10.4**	**7.6 5.7**	**4.7**	**3.3**	**2.9**	**2.3**	**2.0**	
SG-11	34.4		11.6		4.4	3.4		2.6	2.3	
	44.0		**7.4**		**4.6**	**2.7**		**2.0**		
P-1			7.7		3.0	2.4		1.7	1.2	
			6.7		**3.5**	**2.0**		**1.4**	**1.2**	
P-2	23.4		6.1		3.8	2.9	2.0	1.3		
	12.1		**?**		**4.0**	**3.0**	**2.2**	**1.4**		
P-3	11.7		5.5		3.0	1.8		1.3		
			6.4		**3.4**	**2.4**			**1.1**	
P-4	25.9		6.9		4.1	2.4	2.0 1.7	1.3	1.2	
	20.9		**6.2**		**3.3**	**2.3**	**1.9 1.6**	**1.4**	**1.2**	
Average	36.2	16.8	9.8	6.4	4.4	3.2	2.4	2.2	1.8	1.4

Table 2.1: Summary of all detected cycles from the St George (SG) and Poole (P) Ranges. See Figure 2.2 for the location of the measured sections. Periodicities (in meters) detected from the analyses of gamma-ray data are shown in plain text. Periodicities detected from the analyses of grainsize data are shown in bold text. Columns are labeled A-F and 1-4 to facilitate comparison with Tables 2.2-2.4.

detected periodicities range between 5.5 m and 7.7 m with an average thickness of 6.5 m. Columns C through F show similar relationships with thinner cycles noted in the Poole Range than in the St George Ranges.

A COMPARISON OF CYCLICITY

To test for a glacio-eustatic driving mechanism, cycles detected in the Tuckfield Member (Table 2.1) were compared to the known mid-Permian orbital parameters (Figure 2.8). Since the periodicities of the Tuckfield cycles are spatial (given in meters) and the periodicities of the orbital parameters are temporal (given in years), a direct comparison could not be made. To effectively compare the two, all sets of periodicities had to be converted into sets of ratios.

Table 2.2 summarizes the conversion of the periodicities detected from the analysis of gamma-ray data into ratios. For this conversion, cycle periodicities in Column B (Table 2.1) were set to one (Table 2.2). Detected periodicities in each dataset were converted into ratios relative to the associated Column B periodicity (Table 2.1). For example, at Location SG-1 the cycle periodicity listed in column B is 10.8 m. The cycle periodicity listed in Column C is 6.7 m (Table 2.1). Since the number of 6.7 m cycles (Column C) in each 10.8 m cycle (Column B) equals 1.6 (10.8 ÷ 6.7 = 1.6), the Column C ratio in Table 2.2 for Location SG-1 is 1:1.6. At the base of Table 2.2, the average ratio for each column is given.

Table 2.3 summarizes the conversion of the periodicities detected from the analysis of grainsize data into ratios, using the above method. Again, the average ratios for each column is given at the base of the table.

The orbital parameters were converted into ratios by setting the 100,000 year cycle equal to one. For example, the number of 17,600 year cycles in each 100,000 year cycle is equal to 5.7 (100,000 ÷ 17,600 = 5.7). Therefore, the ratio used for the 17,600 year cycle is 1:5.7. The complete listing of Milankovitch ratios is given in Figure 2.8.

Table 2.4 lists the average gamma-ray ratios, the average grainsize ratios, and the ratios for the mid-Permian orbital parameters. These three sets of results compare favorably with one another. There is also a favorable comparison between the gamma-ray ratios and the grainsize ratios for the "extra," non-Milankovitch-band periodicities (Table 2.4).

Location	Computed Gamma-Ray Ratios									
	A	1	B	2	C	D	3	E	F	4
SG-1	3.7:1		1		1:1.6	1:2.8		1:4.3	1:6.4	1:7.2 1:8.3 1:9.8
SG-2	3.8:1		1	1:1.7	1:2.4	1:3.4	1:4.2	1:5.0	1:6.2	
SG-3	5.5:1		1	1:1.7						
SG-4	3.9:1		1		1:2.0	1:2.9			1:6.1	
SG-5	3.6:1		1		1:2.8	1:3.7		1:4.3	1:5.5	1:8.3
SG-6	3.3:1		1		1:2.0			1:3.9	1:6.4	
SG-7	4.4:1		1	1:1.9			1:3.6	1:5.3	1:7.5	
SG-8	2.5:1		1		1:2.3	1:3.3		1:4.1	1:5.5	1:9.4
SG-9	4.3:1		1	1:1.8	1:2.3	1:3.3		1:3.9	1:4.3	
SG-10	3.4:1		1		1:1.9	1:2.5	1:3.7	1:4.3	1:5.6	
SG-11	3.0:1		1		1:2.6	1:3.4		1:4.5	1:5.0	
P-1			1		1:2.6	1:3.2		1:4.5	1:6.4	
P-2	3.8:1		1		1:1.6	1:2.1	1:3.1	1:4.7		
P-3	2.1:1		1		1:1.8	1:3.1		1:4.2		
P-4	3.8:1		1		1:1.7	1:2.9	1:3.5 1:4.1	1:5.3	1:5.8	
Average	3.7:1		1	1:1.8	1:2.1	1:3.1	1:3.7	1:4.5	1:5.9	1:8.6

Table 2.2: Computed ratios of cycle periodicities detected from the analysis of gamma-ray data (plain text in Table 2.1). Columns are labeled A-F and 1-4 to facilitate comparison with Tables 2.1, 2.3, and 2.4. For the conversion of periodicities into ratios, periodicities in Column B were assumed to equal one. All other periodicities detected in each dataset (e.g. Location SG-1) were converted into ratios relative to the Column B value. The average ratio of each column is listed at the bottom of the table.

Location	Computed Grainsize Ratios									
	A	1	B	2	C	D	3	E	F	4
SG-1	?		1		?	?		?	?	
SG-2	2.4:1		1	1:1.8	1:2.6	1:3.0	1:3.7	1:5.0	1:5.5	
SG-3	6.0:1	1.8:1	1	1:1.7	1:2.1	1:2.9	1:3.4 1:4.2	1:4.8	1:5.9	
SG-4	5.1:1		1		1:2.2	1:3.7				
SG-5	1.9:1		1		1:2.6			1:3.9	1:5.5	
SG-6	2.4:1		1	1:1.3	1:1.9	1:2.4		1:4.1		
SG-7			1	1:1.7	1:2.3	1:3.1	1:3.5	1:4.1	1:7.9	
SG-8	3.5:1		1		1:2.4	1:3.0		1:4.2	1:5.8	1:7.3 1:8.7
SG-9	2.7:1		1	1:1.5	1:2.5	1:2.9		1:3.7	1:5.1	
SG-10	5.1:1	1.5:1	1	1:1.4 1:1.8	1:2.2	1:3.2	1:3.6	1:4.5	1:5.2	
SG-11	5.9:1		1		1:1.6	1:2.7		1:3.7		
P-1			1		1:1.9	1:3.4		1:4.8	1:5.6	
P-2	?		1		?	?	?	?		
P-3			1		1:1.9	1:2.7			1:5.8	
P-4	3.4:1		1		1:1.9	1:2.7	1:3.3 1:3.9	1:4.4	1:5.2	
Average	3.8:1	1.7:1	1	1:1.6	1:2.2	1:3.0	1:3.7	1:4.3	1:5.8	1:8.0

Table 2.3: Computed ratios of cycle periodicities detected from the analysis of grainsize data (bold text in Table 2.1). Columns are labeled A-F and 1-4 to facilitate comparison with Tables 2.1, 2.2, and 2.4. For the conversion of periodicities into ratios, periodicities in Column B were assumed to equal one. All other periodicities detected in each dataset (e.g. Location SG-1) were converted into ratios relative to the Column B value. The average ratio of each column is listed at the bottom of the table.

	Column	A	1	B	2	C	D	3	E	F	4
Tuckfield	Gamma-Ray Ratio	3.7:1		1	1:1.8	1:2.1	1:3.1	1:3.7	1:4.5	1:5.9	1:8.6
Tuckfield	Grainsize Ratio	3.8:1	1.7:1	1	1:1.6	1:2.2	1:3.0	1:3.7	1:4.3	1:5.8	1:8.0
Milankovitch	Ratio	4.1:1		1		1:2.3	1:2.9		1:4.8	1:5.7	
Milankovitch	Period (yrs)	410,000		100,000		44,000	35,000		21,000	17,600	
Milankovitch	Parameter	Eccentricity				Obliquity			Precession		

Table 2.4: Comparison of cyclicity detected from the analyses of gamma-ray and grainsize data. In Row 1, columns are labeled A-F and 1-4 to facilitate comparison with Tables 2.1-2.3. Row 2 lists the average ratios detected from the analyses of gamma-ray data. Row 3 lists the average ratios detected from the analyses of grainsize data. Below the heavy, horizontal line, information concerning mid-Permian orbital cyclicity (ratios, periodicities, and parameters) is presented. Note the favorable comparison of the three sets of ratios.

DISCUSSION

The favorable comparison between the Tuckfield Member cycles and the mid-Permian orbital parameters indicates that orbital cyclicity was probably the driving force in the formation of the Tuckfield Member cycles. However, this positive correlation does not necessarily mean that the Tuckfield Member cycles are glacio-eustatic in origin. For example, Fielding and Webb (1996) used spectral analysis to identify Milankovitch-scale cyclicity in Late Permian alluvial deposits from the Bainmedart Coal Measures in Antarctica. They attributed the observed cyclicity to changing sediment supply that was controlled by orbitally-forced climate change, not glacio-eustatic sea-level fluctuations.

Although the Bainmedart Coal Measures record Milankovitch-scale cyclicity and are similar in age to the Tuckfield Member, these deposits cannot be used as a direct analog. The depositional environment of the two areas are too dissimilar for a worthwhile comparison. To gain a better understanding of the Tuckfield Member cycles, it is best to compare them with other mid- to Late Permian shallow-marine, cyclic deposits (Table 2.5). The number of publications documenting such deposits are extremely limited. Three notable exceptions are considered here (Table 2.5).

In Australia, the Artinskian to Ufimian Pebbley Beach Formation of the southern Sydney Basin consists of a series of coarsening-upward, shallow-marine, siliciclastic cycles (Chapter 5, this volume). Spectral analysis of gamma-ray data from the Pebbley Beach Formation reveals several orders of cyclicity, with periodicities of 8.5 m, 4.9 m, 3.2 m, 1.8 m and 1.3 m (Table 2.5). These Pebbley Beach cycles have been attributed to changes in eccentricity (8.5 m cycle), obliquity (4.9 and 3.2 m cycles), and precession (1.8 and 1.3 m cycles).

The Upper Guadalupian (latest Permian) Yates Formation of the Permian Basin (USA) consists of a series of outer- to inner-shelf, alternating carbonate/siliciclastic cycles. Borer and Harris (1991) utilized Fischer plots and spectral analysis to constrain cyclicity within this unit. They identified large-scale (30 m) cycles that contained 4 smaller-scale cycles of varying thickness. The 30 m cycles were interpreted to be 400,000 year eccentricity cycles, whereas the smaller-scale cycles were interpreted to be 100,000 year eccentricity cycles (Table 2.5).

At the Permo-Triassic boundary, the Gartnerkofel section from the Carnic Alps in Austria consists of dolomitized limestone and interbedded thin marls and shales of shallow-marine origin (Rampino et al., 2000). Spectral analysis of gamma-ray data

	Elongated Eccentricity	Eccentricity	Obliquity	Precession
Tuckfield Member (This study)	36.2 m	9.8 m	3.2-4.4 m	1.8-2.2 m
Pebbley Beach Fm (Chapter 5, this volume)		8.5 m	3.2-4.9 m	1.3-1.8 m
Yates Formation (Borer and Harris, 1991)	30.0 m			
Gartnerkofel Section (Rampino et al., 2000)	36.0 m	9.5-13.0 m	4.4-5.4 m	2.0-2.3 m

Table 2.5: Comparison of some mid- to Late Permian (post-Sakmarian) shallow-marine cyclic successions. Note the similarity in detected periodicities.

from the Gartnerkofel section revealed several orders of cyclicity with periodicities of 36.0 m, 9.5-13.0 m, 4.4-5.4 m and 2.0-2.3 m. These cycles have been attributed to changes in elongated eccentricity (36.0 m), eccentricity (9.3-13.0 m), obliquity (4.4-5.4 m), and precession (2.0-2.3 m) (Table 2.5) (Rampino et al., 2000).

These three deposits are ideal analogs for the Tuckfield Member cycles. All four examples consist of cyclic, shallow-marine deposits with a significant siliciclastic component. Cycle thicknesses and bundling patterns are similar in the four areas. The Tuckfield Member, Yates Formation, and Gartnerkofel section each record cyclicity with a periodicity of 30 to 36 m (Table 2.5). The three studies independently attributed this scale of cyclicity to changes in Earth's elongated eccentricity. The Tuckfield Member, Pebbley Beach Formation, and Gartnerkofel section each record cycles with periodicities of approximately 10 m, 4 m and 2 m (Table 2.5). The three studies independently attributed these cycles to changes in Earth's eccentricity (10 m cycle), obliquity (4 m cycle), and precession (2 m cycle). The similarities in depositional environment and noted cyclicity from these distant areas support the theory that glacio-eustatic sea-level fluctuations probably controlled the formation of depositional cyclicity in each area.

Dominant Cyclicity

In the St George Ranges, cycles apparent in outcrop are typically 7 to 12 m thick (Figure 2.5; Appendix 2). In the Poole Range, cycles apparent in outcrop are typically 5 to 7 m thick (Figure 2.7; Appendix 2). These values correspond to periodicities that have been attributed to fluctuations in Earth's eccentricity (Tables 2.1 and 2.4, Column B). In addition to these dominant cycles, thinner cycles (2-4 m thick) also outcrop in the study area. These thinner cycles may be incomplete 100,000 year cycles. However, it is also possible that these thinner cycles record a higher-frequency 40,000 year periodicity superimposed upon the dominant 100,000 year periodicity.

Non-Milankovitch Cyclicity

Additional cycles, not corresponding to the orbital parameters, were detected at some locations (Columns 1-4 in Tables 2.1-2.4). These additional cycles are relatively few and not unexpected when the sensitive nature of spectral analysis is considered. The positive correlation between the gamma-ray and grainsize ratios for these "extra" non-Milankovitch-band cycles indicates that they probably represent real events and are not simply erroneous peaks in the spectral plots. These "extra" cycles may record localized tectonic activity or short- to long-term changes in sediment supply.

The Stratigraphic Effects of Deglaciation

Eyles and Eyles have published several recent papers on the Permo-Carboniferous system of Australia (e.g. Eyles et al., 1997; Eyles et al., 1998; Eyles et al., 2001; Eyles and Eyles, 2000). Much of their work has focused on the development of large-scale, 30+ million-year, diamictite/shale/sandstone sequences that occur throughout Western Australia (e.g. Eyles et al., 2002; Eyles et al., 2003). Within these sequences, the lowermost diamictite succession is typically composed of rapidly deposited, glacially influenced, marine strata. The middle succession typically consists of fossiliferous cool water shales. The upper sandstone succession typically comprises shallow marine, wave- and storm-influenced sandstone (Eyles et al., 2002; Eyles et al., 2003).

These studies suggest that tectonism, not glacio-eustacy, is responsible for the formation of the observed sequences. In their model, the lower diamictite part of the sequence records basin infilling of coarse debris produced by faulting and glaciation of the adjacent craton. The middle shale part of the sequence marks a phase of sediment under-filling, characterized by tectonic subsidence, an increase in relative sea-level, and a reduction in sediment supply. The upper sandstone part of the sequence records a late stage in the tectonic cycle when subsidence rates have decreased and sediment supply overcomes accommodation space (Eyles et al., 2002; Eyles et al., 2003).

In the Canning Basin, the upper sandstone unit of Eyles and Eyles' tripartite sequence consists of the Clianthus Formation (i.e. Wye Worry and Millajiddee Members), the Poole Sandstone, and the Noonkanbah Formation (Eyles et al., 2002). As discussed earlier, these are the rocks that outcrop in the St George and Poole Ranges. These strata appear to provide a direct record of Permian deglaciation superimposed upon the larger, tectonic sequence described by Eyles et al. (2002).

During the earliest Permian, continental ice covered much of Australia. Palynological analysis indicates that the glacial climax was reached in the northern regions of Western Australia (Pilbara Craton) during the Sakmarian (Crowell and Frakes, 1971). In the Canning Basin, glacially-influenced deposits of the Wye Worry Member (Carolyn Formation) record the presence of these nearby icesheets.

By the latest Sakmarian, continental glaciers had started to retreat from the area (Redfern and Millward, 1994) as Australia slowly drifted northward into a more temperate climatic zone (Scotese et al., 1999). A lack of glacial sediments of this age in the Canning Basin provides evidence of this retreat. The non-cyclic, shallow-marine to fluvial deposits of the Millajiddee (Carolyn Formation) and Nura Nura (Poole Sandstone) Members record a gradual reduction in water depths that coincided with short pulses of regional tectonism (Kennard et al., 1994; Eyles and Eyles, 2000).

By the Artinskian, the Canning Basin had reached a phase of tectonic equilibrium (Kennard et al., 1994). Therefore, the waxing and waning of glaciers, which remained on Antarctica (Eyles et al., 1997, 1998) and possibly parts of southern Australia (Crowell, 1975) and the north pole (Scotese et al., 1999), were able to drive local sea-level fluctuation within the Canning Basin. These fluctuations caused the deposition of high-frequency, shallow-marine sedimentary cycles such as those of the Tuckfield Member.

In the St George and Poole Ranges, the fluvial Christmas Creek Member marks the final episode of shorezone progradation associated with the high-frequency sea-level change recorded by the Tuckfield Member. This progradation was followed by abrupt drowning and deposition of the marine Noonkanbah Formation. This abrupt transgression may record one of the last major episodes of ice-sheet decay during the Permian.

CONCLUSIONS

A thick succession of Permian strata outcrops in the St George and Poole Ranges of the Fitzroy Trough (onshore Canning Basin). This succession records the effects of gradual Gondwanan deglaciation during the mid-Permian.

Outcrop exposures around the periphery of the St George and Poole Ranges have allowed for detailed measurements of the Artinskian Tuckfield Member (Poole Sandstone). In the Poole Range, eleven vertically stacked, laterally extensive, coarsening- and thickening upward cycles were identified in outcrop. In the St George Ranges, at least 14 such cycles can be identified in outcrop. Spectral analysis of gamma-ray and grainsize data were used to better constrain this cyclicity. Ratios between identified Tuckfield Member cycles correlate strongly with the predicted mid-Permian orbital parameters of eccentricity, obliquity, and precession. Although all three orbital perturbations are recorded in the Tuckfield Member, eccentricity and possibly obliquity were the main influences on depositional cyclicity during this time.

Additionally, Tuckfield Member cycles compare favorably with mid- to Late Permian shallow-marine cyclic deposits identified in Australia, Europe, and North America. This favorable comparison, combined with their strong correlation to Milankovitch periodicities, suggests that the Tuckfield Member cycles are glacio-eustatic in origin. Therefore, Permo-Carboniferous glaciation must have extended into at least the Artinskian stage of the Early Permian.

Chapter 3

Milankovitch-band cyclicity preserved in non-marine Permian sediments from the onshore Canning Basin, Western Australia

ABSTRACT

The Early Permian Tuckfield Member of the Poole Sandstone is exposed along the southeastern margin of the Grant Range (Fitzroy Trough, onshore Canning Basin). In this area, the Tuckfield Member outcrops as a less than 50 m thick package of laterally discontinuous, highly ferruginous, thinning-upward cycles. At the outcrop scale, cycles range in thickness from 2 to 8 m. A typical cycle consists of a fining-upward succession of sandstone and siltstone. Sandstone clasts, individual mud pellets, and locally continuous mud-pellet and plant-fragment conglomerate occur throughout the studied interval. Sedimentary structures and the vertical stacking of facies suggest that the Tuckfield Member predominantly records braided channel deposition on a sand-rich coastal plain in the Grant Range area.

To constrain the origin of the depositional cyclicity that is apparent in outcrop, spectral analyses were performed on gamma-ray data from two locations. Several orders of meter- to decameter-scale cycles were identified. Statistical analysis shows that the ratios between these cycles correlate strongly with the known mid-Permian orbital periodicities of eccentricity, obliquity, and precession. This comparison suggests that Milankovitch-forcing of climate was responsible for the formation of the non-marine depositional cyclicity recorded in the Tuckfield Member.

Key Words: Canning Basin, Milankovitch cyclicity, Permian, Poole Sandstone, Tuckfield Member

INTRODUCTION

Depositional cyclicity has long been recognized in both marine and non-marine sedimentary succession (e.g. Uden, 1912; Barrell, 1913). The formation of such cycles has been attributed to many factors, including tectonism (e.g. Tankard, 1986), changing sediment supply (e.g. Smith and Ashley, 1985), and relative sea-level fluctuation (e.g. Ross and Ross, 1995). During the twentieth century, many studies demonstrated that Milankovitch-forcing of climate can influence global sea-level (e.g. Veevers and Powell, 1987; Boardman and Heckel, 1989). Likewise, other studies showed that orbitally driven climatic variations are able to affect local sedimentation (e.g. Talbot, 1985; Spaulding, 1991). Therefore, it is not surprising that depositional cyclicity can often be linked to Earth's orbital parameters (e.g. Heckel, 1986; Read, 1995; Carter and Naish, 1998).

Historically, research projects investigating orbitally influenced depositional cyclicity have concentrated on marine, mainly pelagic strata. However, in the past 20 years, a limited number of studies have reported Milankovitch-scale cyclicity in non-marine successions, ranging from lacustrine to fluvial to desert environments (e.g. Astin, 1990; Olsen, 1990; Clemmensen et al., 1994; Fielding and Webb, 1996). Nevertheless, examples of orbitally influenced depositional cyclicity in strictly non-marine environments are relatively rare.

This paper outlines the cyclic development of a non-marine sandy coastal plain in the Phanerozoic onshore Canning Basin (Figure 3.1). The Early Permian Tuckfield Member (Poole Sandstone) (Figure 3.2) was measured at two locations along the southeastern margin of the Grant Range (Fitzroy Trough) (Figure 3.3; Appendix 1). These outcrops were evaluated on a bed-by-bed basis for lithology, fossils, sedimentary structures, bed thickness variations, and vertical stacking patterns (Appendix 2). Gamma-ray emissions were measured at a 0.5 m vertical spacing (Appendix 3). Sedimentary logs from the two measured locations concentrate on the documentation of repetitive cyclicity. Based upon these observations, an idealized cycle model has been developed for the Tuckfield Member in this area.

To better define the observed cyclicity, spectral analyses were performed on gamma-ray data from each location (Appendix 10). As a cross-check on the results, two spectral analysis programs ("Timeseries" and "AnalySeries 1.1") were used to analyze each dataset (Appendix 9). "Timeseries," described in Weedon and Read (1995), uses the standard Blackman-Tukey method (Blackman and Tukey, 1958) to generate power spectra. "AnalySeries 1.1" (Paillard et al., 1996) uses the Blackman-Tukey and Maximum Entropy (Haykin, 1983) methods to generate power spectra. The results from the spectral analyses are here compared with the known Mid-Permian orbital periodicities to determine the role that Milankovitch-forcing played in the formation of the depositional cyclicity.

GEOLOGIC SETTING

Three hundred million years ago at the Permo-Carboniferous boundary, Australia was part of the super-continent Pangea (Figure 3.4). Widespread glaciation extended from the south pole up to approximately 45° south latitude and covered portions of present-day Africa, Antarctica, Asia, Australia, and South America (Crowell, 1978). During this time, the onshore segment of the intracratonic Canning

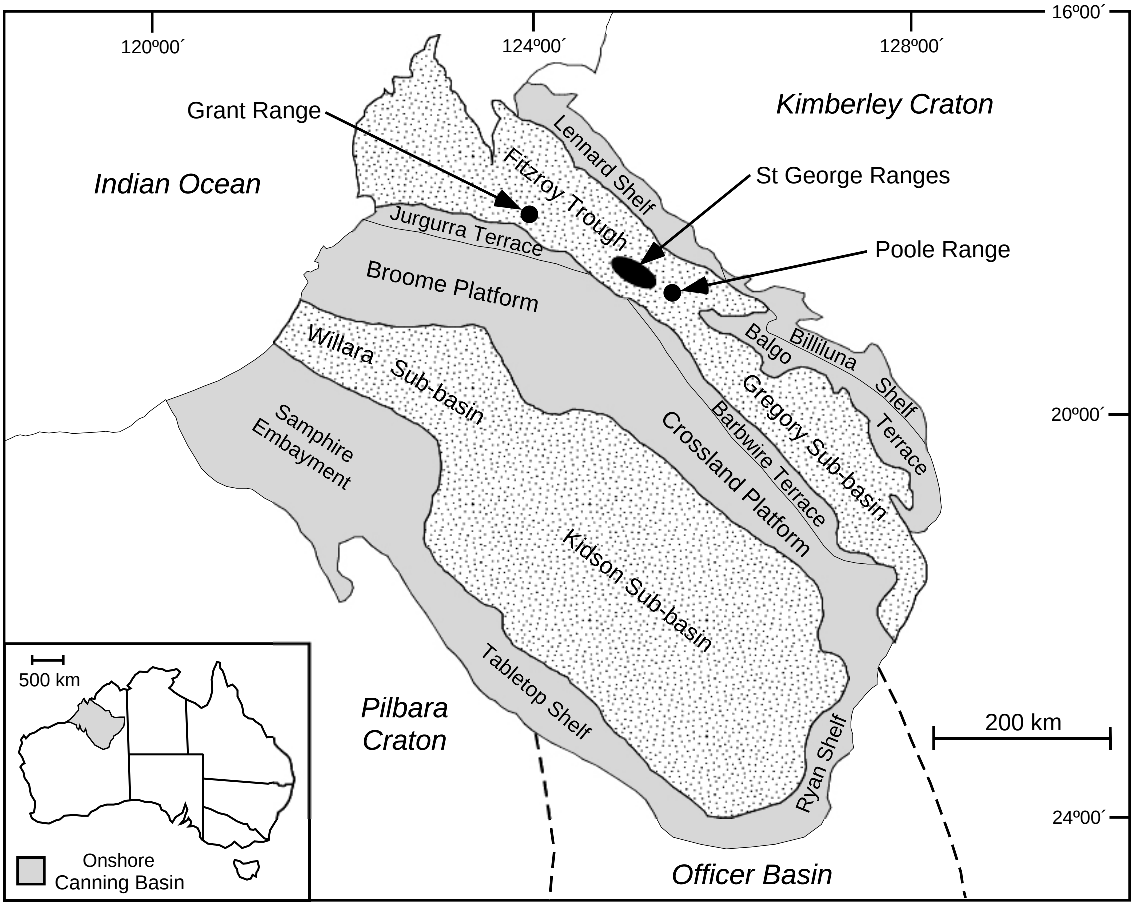

Figure 3.1: Simplified map of the onshore Canning Basin (adapted from Kennard et al., 1994; Apak and Carlsen, 1996) showing locations of the Grant, St George, and Poole Ranges. The basin's modern coordinates are given.

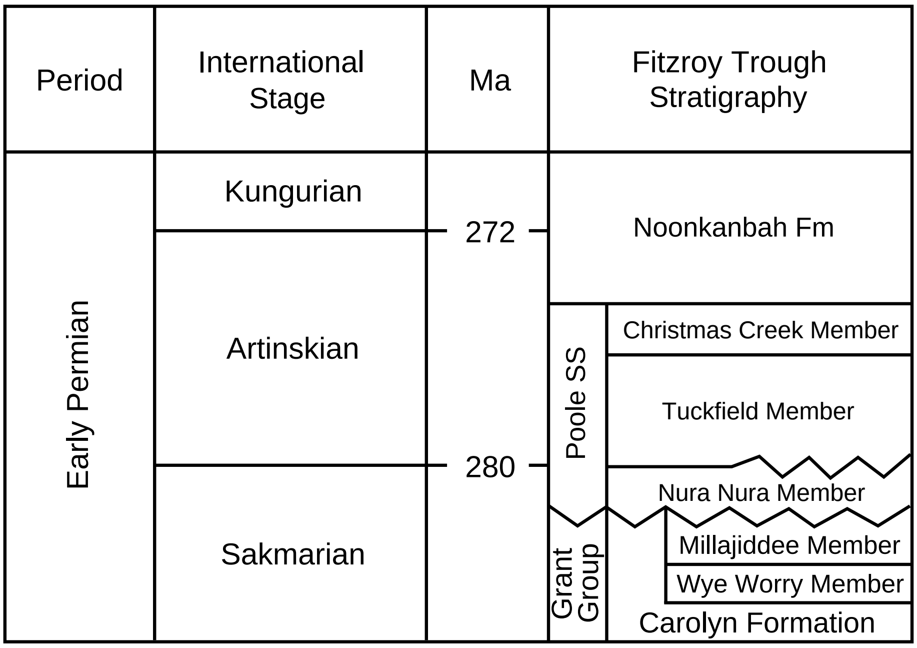

Figure 3.2: Early Permian stratigraphic column for the Fitzroy Trough, onshore Canning Basin (adapted from Kennard et al., 1994). In the Grant Range, the Christmas Creek Member of the Poole Sandstone is not present. The Noonkanbah Formation disconformably to conformably overlies the Tuckfield Member. Stage dates from Veevers, 2000b.

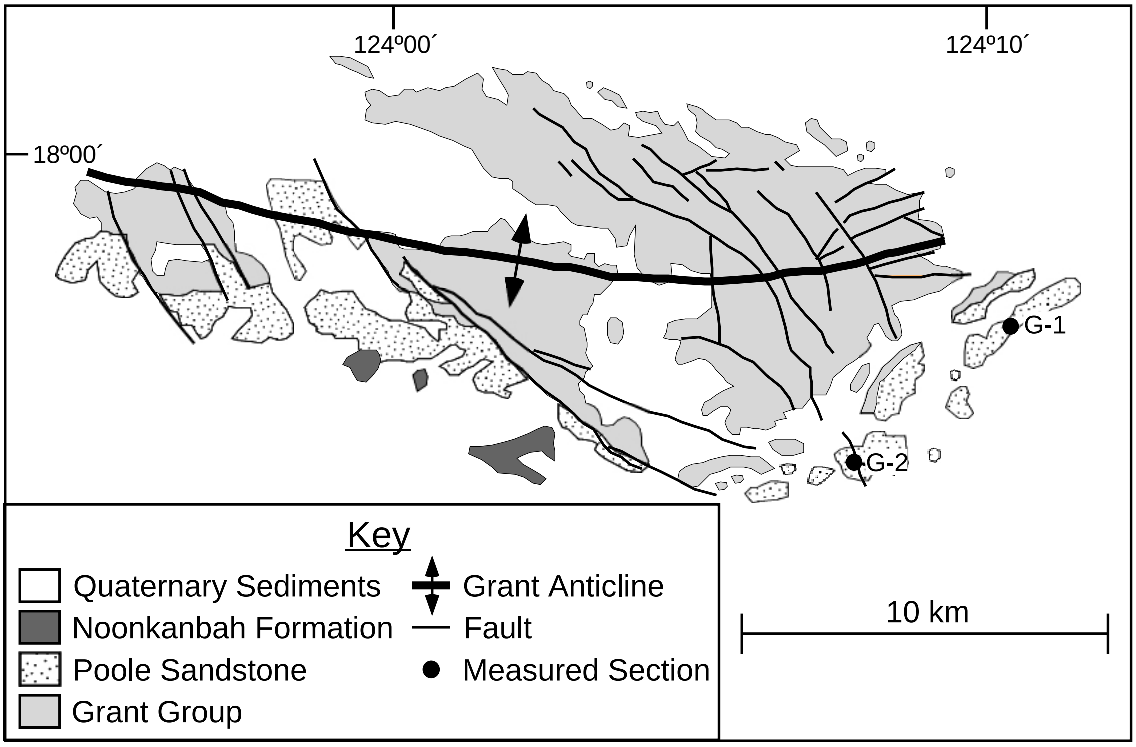

Figure 3.3: Simplified geological map of the Grant Range (adapted from Crowe and Towner, 1981) showing the location of the measured sections.

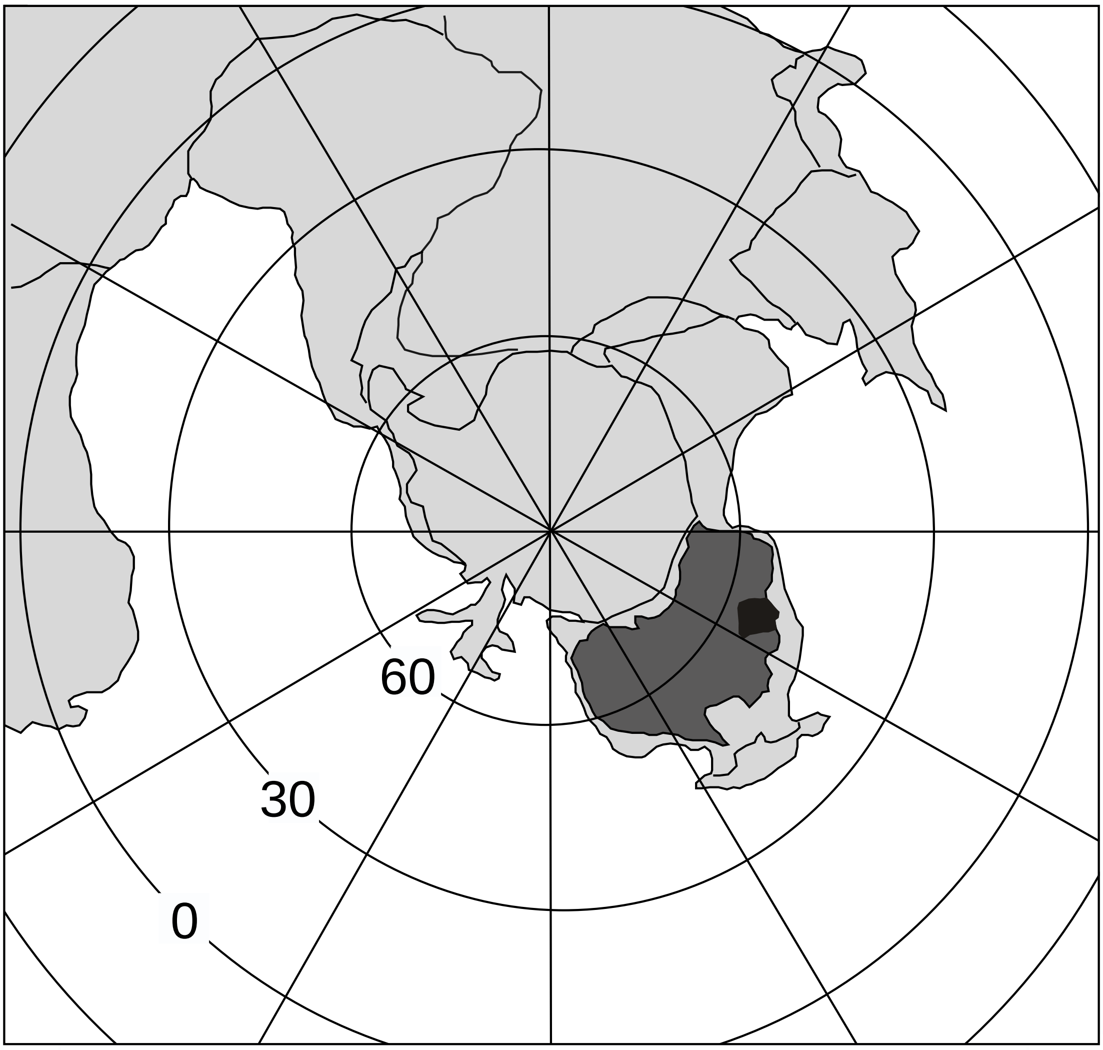

Figure 3.4: Early Permian (Sakmarian) paleo-geographic reconstruction (adapted from Smith et al., 1981; Veevers, 2000c). Australia is shown in dark gray. During this time, glaciation extended from the south pole (center of diagram) up to approximately 45º south latitude. The Canning Basin (shown in black) was located at approximately 50º south latitude. Evidence from the Canning Basin suggests that glacial conditions persisted into the early Sakmarian in northern Western Australia.

Basin (northern Western Australia) lay at approximately 50º south latitude (Figure 3.4) (Veevers, 2000c). Adjacent to the southern edge of the basin, the uplifted Pre-Cambrian Pilbara Craton was a focal point of glaciation. Ice, carrying coarse-grained clastic material, flowed northward from the craton into the basin's four major fault-bounded depocenters (Figure 3.1) (O'Brien et al., 1998). Today, abundant glacial dropstones (Wye Worry Member, Carolyn Formation, Grant Group: Figure 3.2) in the Fitzroy Trough (Crowe and Towner, 1981) and on the adjacent Lennard Shelf (O'Brien et al., 1998) indicate that glacial conditions extended into the northwestern section of the Canning Basin as late as the early Sakmarian.

By the latest Sakmarian, ice had withdrawn from northern Western Australia (Redfern and Millward, 1994). This glacial retreat corresponded with the beginning of widespread deglaciation across Gondwana (southern Pangea). In the Canning Basin, the deposition of the Poole Sandstone (a transgressive, shallow-marine sand sheet) coincided with the termination of local glaciation (Kennard et al., 1994).

Throughout the Canning Basin, the Poole Sandstone (defined by Guppy et al., 1952; 1958) consists of a laterally extensive package of shallow-marine to non-marine sediments. In the Fitzroy Trough, the Poole Sandstone is divided into three distinct depositional units: the lower Nura Nura Member, the middle Tuckfield Member, and the upper Christmas Creek Member (Figure 3.2). Recent studies have focused on depositional cyclicity that is preserved in shallow-marine sediments of the Artinskian Tuckfield Member (Chapters 1 and 2, this volume). These studies were conducted in the St George and Poole Ranges of the Fitzroy Trough (Figure 3.1) where the Tuckfield Member outcrops as a vertically stacked series of laterally continuous cycles (Figure 3.5a). In these ranges, a typical cycle is approximately 5 to 12 m thick and consists of a coarsening- and thickening-upward package of progradational shorezone sediments. Identified cycles are interpreted to record glacio-eustatic sea-level fluctuations. Although major ice sheets withdrew from northern Western Australia during the earliest Sakmarian, these cycles provide indirect evidence that glaciation persisted on Gondwana (or elsewhere) into at least the Artinskian stage of the Early Permian (Chapters 1 and 2, this volume).

THE TUCKFIELD MEMBER IN THE GRANT RANGE

This study focuses on exposures of the Tuckfield Member along the southeastern margin of the Grant Range (Figure 3.3). The Grant Range is a relatively

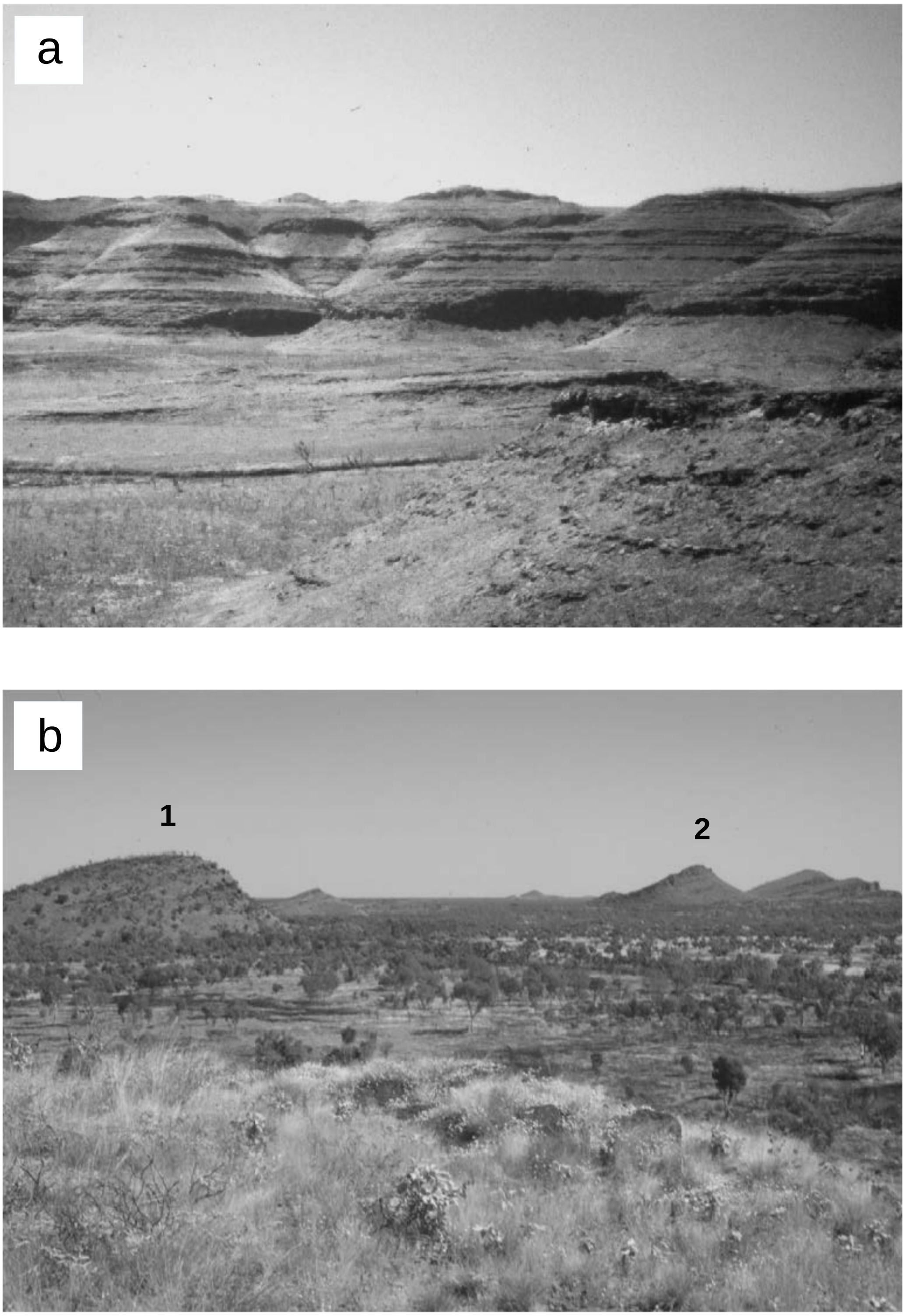

Figure 3.5: Typical outcrops of the Tuckfield Member (Poole Sandstone) in (a) the St George and Poole Ranges and (b) the Grant Range. Note that the laterally continuous cycles that are characteristic of the St George and Poole Ranges are not so readily apparent in the Grant Range. Field of view in photograph (a) is approximately 1 km wide. Photograph taken on eastern edge of St George Ranges: 51K 0752494/UTM 7917909 (using the Australian Geodetic Datum 1966 coordinates), facing-west. Pho tograph (b) taken at 51K 0619547/UTM 8000617 (using the Australian Geodetic Datum 1966 coordinates), facing northeast. The distance between Hill 1 and Hill 2 is approximately 3 km.

small (approximately 300 km^2) anticlinal feature that is located approximately 100 km northwest of the St George Ranges (Figure 3.1). In the Grant Range, the Tuckfield Member outcrops as a series of small (typically less than 50 m high), disconnected hills (Figure 3.5b). Upon first inspection, these deposits appear cyclic and are reminiscent of the shallow-marine sedimentary cycles observed in the St George and Poole Ranges (Chapters 1 and 2, this volume). Deposits from all three ranges outcrop as alternating, cyclic bands of more resistant and less resistant (often unexposed) rock.

However, closer study reveals that Tuckfield Member deposits in the two areas (Grant Range and St George/Poole Ranges) are inherently different. Although locally continuous, Grant Range cycles have a limited lateral extent (usually less than 100 m) and typically cannot be traced from outcrop (hill) to outcrop (hill). In the Grant Range, the Tuckfield Member (i) is more ferruginous; (ii) is not fossiliferous (no marine trace or body fossils observed); and (iii) contains more sandstone clasts and individual mud pellets than in the St George and Poole Ranges.

Two outcrop sections from the Grant Range were measured in detail (Appendices 2 and 3). The sedimentary log and associated gamma-ray data from Location G-1 are presented in Figure 3.6. In this representative log, the cyclic alternation between areas of exposure and non-exposure is evident. Due to superficial similarities, it would be easy to assume that these cyclic deposits conform to the coarsening- and thickening-upward cycle model developed for the shallow-marine sediments of the St George and Poole Ranges (Figure 3.7a). However, a fining- and thinning-upward cycle model is not only a reasonable alternative but also typically a more appropriate one (Figure 3.7b). In Figure 3.6a, heavy horizontal lines mark the boundaries between successive fining- and thinning-upward cycles. At the outcrop scale, a typical cycle ranges between 2 and 8 m thick.

Cycle Model

In the Grant Range, most Tuckfield Member cycles follow a similar progression of sediment facies. Because these deposits outcrop as a vertically stacked series of cycles, a generalized cycle model can be used to describe the basic sedimentology of the Tuckfield Member in this area (Figure 3.7b).

At its base, a typical cycle consists of medium- to thick-bedded, fine- to medium-grained sandstone. These sands usually contain large-scale, trough to planar cross-beds and have erosive bases. Internal laminae (parallel to bedding) and

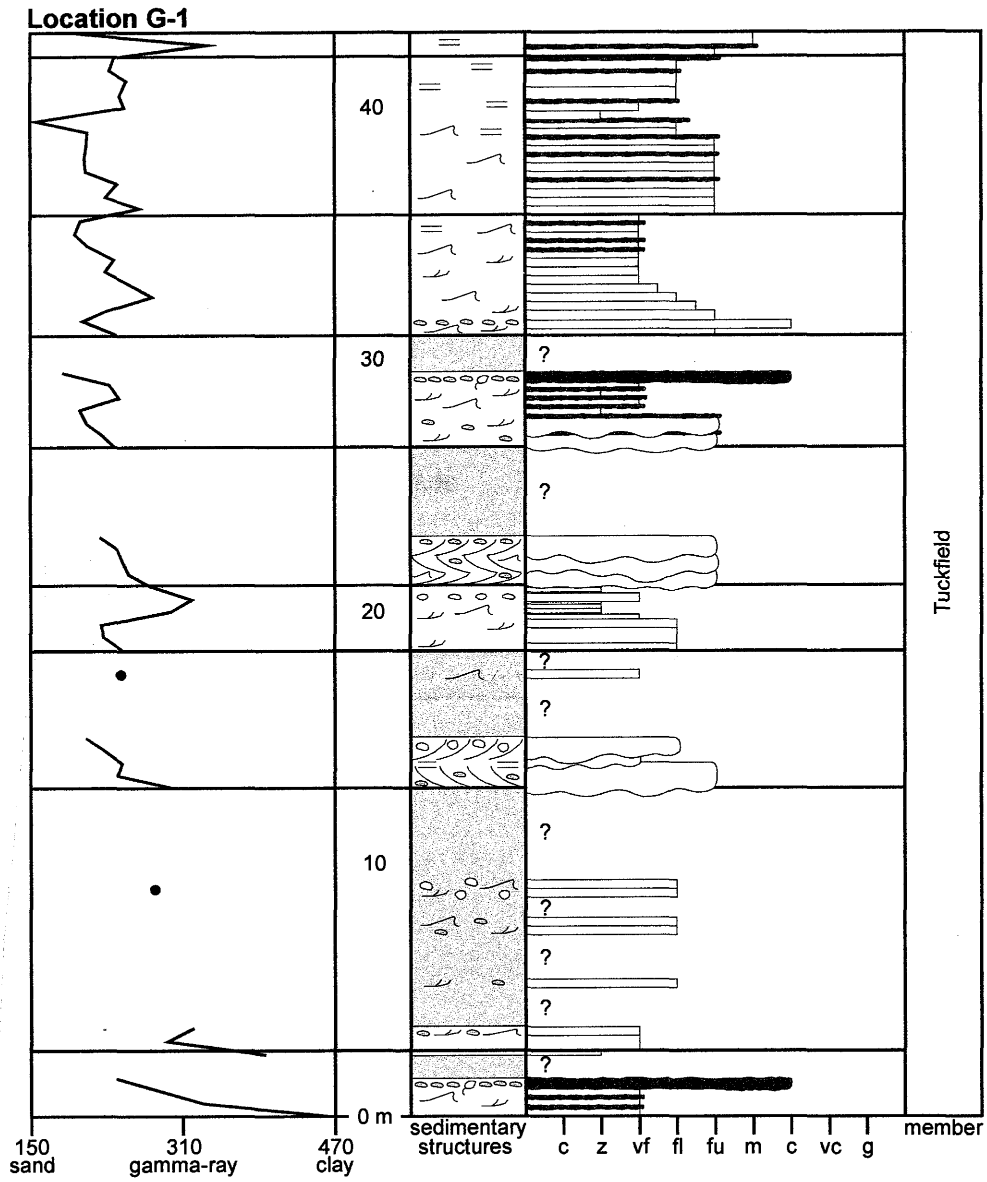

Figure 3.6a: Lithology log with associated gamma-ray data from the Grant Range. The base of the measured section is located at 51K 0624696/UTM 8004945 (using the Australian Geodetic Datum 1966 coordinates). Heavy horizontal lines mark the tops of fining- and thinning-upward cycles. Grainsize increments from left to right on x-axis are as follows: c (clay/mud); z (silt); vf (very fine sand); fl (lower half of fine sand); fu (upper half of fine sand); m (medium sand); c (coarse sand); vc (very coarse sand). Fine sand was divided into lower and upper halves to better depict variations in grainsize. Member names are given in the right-hand column. See Figure 3.6b for key.

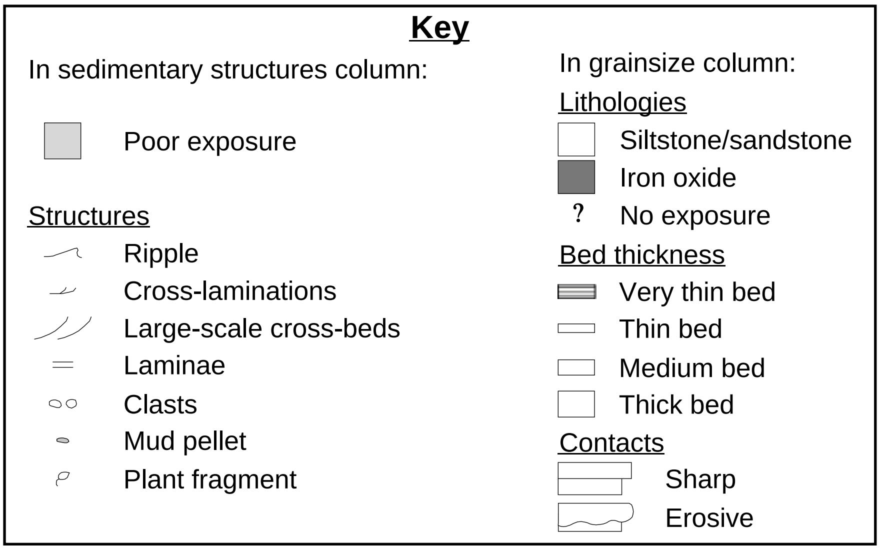

Figure 3.6b: Key for Figure 3.6a.

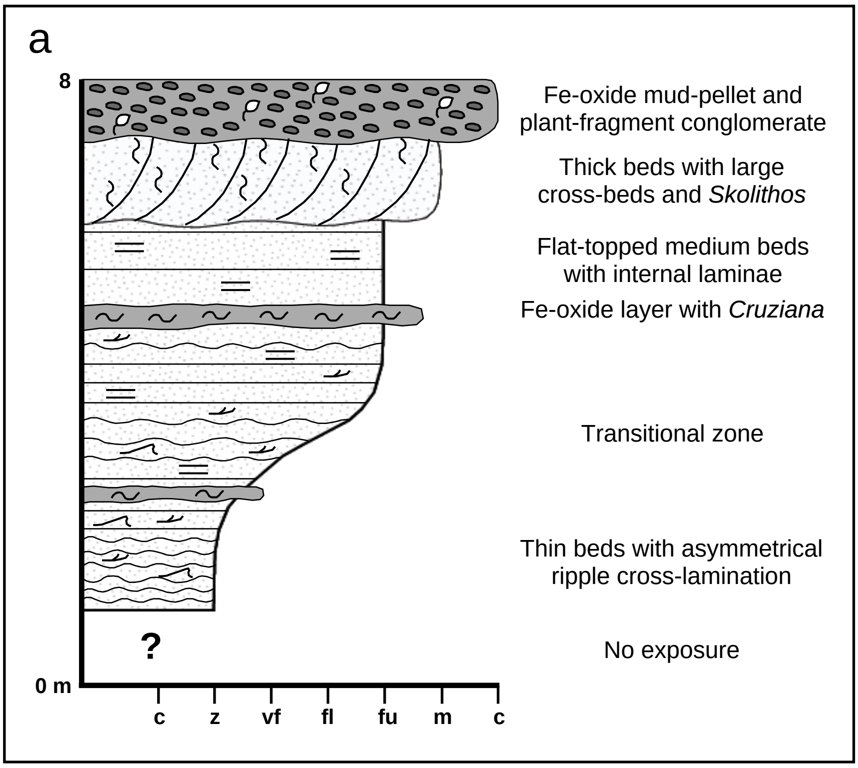

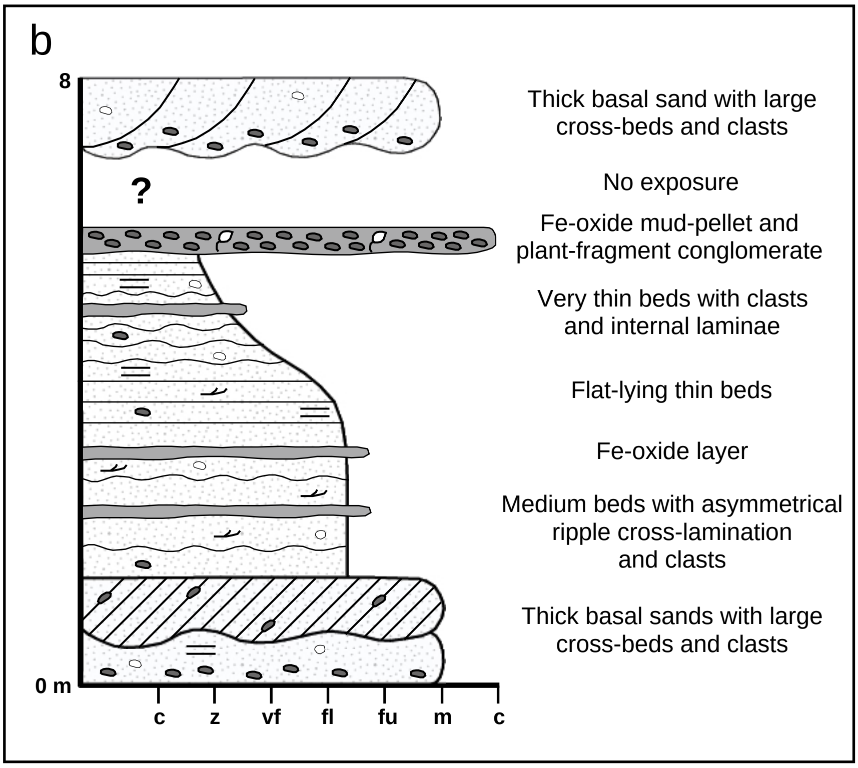

Figure 3.7: Idealized cycle models for the Tuckfield Member. (a) depicts the coarsening- and thickening-upward cycle that is typical of the St George and Poole Ranges (Adkins, 2003; Chapter 1, this volume). (b) depicts the fining- and thinning-upward cycle that is typical of the Grant Range. Note the lack of trace fossils and abundance of individual sandstone and mud clasts in model (b).

symmetrical ripple marks are occasionally preserved. Surficial ferruginization is common. Rounded sandstone clasts (typically up to 2 cm in diameter) (Figure 3.8a) and elongated mud pellets (typically up to 5 cm long) occur in abundance throughout these basal sands. The mud pellets typically have silty mud centers and thick (up to 1 cm) iron-oxide outer shells. These elongated clasts are usually oriented parallel to either bedding or cross bedding.

The basal sands are generally overlain by thin- to medium-bedded, fine-grained sandstone. These finer-grained sands progressively grade upward into very thin-bedded sandstone and siltstone. In this fining- and thinning-upward package, beds tends to be locally continuous with non-erosive to slightly erosive bases. Rippled cross-laminated beds are gradually replaced by beds with flat-lying internal laminae. Symmetrical ripple marks occur throughout the cycle but are more prevalent near the base, whereas flat-topped beds are more prevalent near the top of the cycle. Thin layers of concentrated iron oxide and surficial ferruginization are common. Elongated mud pellets and rounded sandstone clasts also occur throughout this portion of the cycle. Often, a densely packed mud-pellet and plant-fragment conglomerate with an iron-rich sandy matrix will occur mid-cycle (Figure 3.8b). These conglomerates typically range in thickness from a few centimeters up to approximately 0.5 m. Cycles are usually capped by a poorly exposed, scree-covered, gentle slope.

Depositional Environment

All noted observations (e.g. fining-upward sequences, laterally discontinuous cycles, sedimentary structures, absence of marine fossils) suggest that the Tuckfield Member records non-marine, braided channel deposition on a sand-rich coastal plain in the Grant Range. Highly erosive, laterally discontinuous, cross-bedded sands with abundant clasts occur at the base of most cycles. These beds probably mark the location of small scour channels. The coarse-grained basal sands typically grade upward into thin-bedded, finer-grained sands and silts that are characteristic of upper channel-fill deposits. The poorly exposed, fine-grained sediments that cap many cycles may record overbank deposition.

The most diagnostic facies that occurs in the Tuckfield Member is the iron-rich, mud-pellet and plant-fragment conglomerate. In the St George Ranges, these rocks typically cap prograding, shallow-marine, sedimentary cycles (Figure 3.7a) (Adkins, 2003; Chapter 1, this volume). Based upon their stratigraphic position and unique

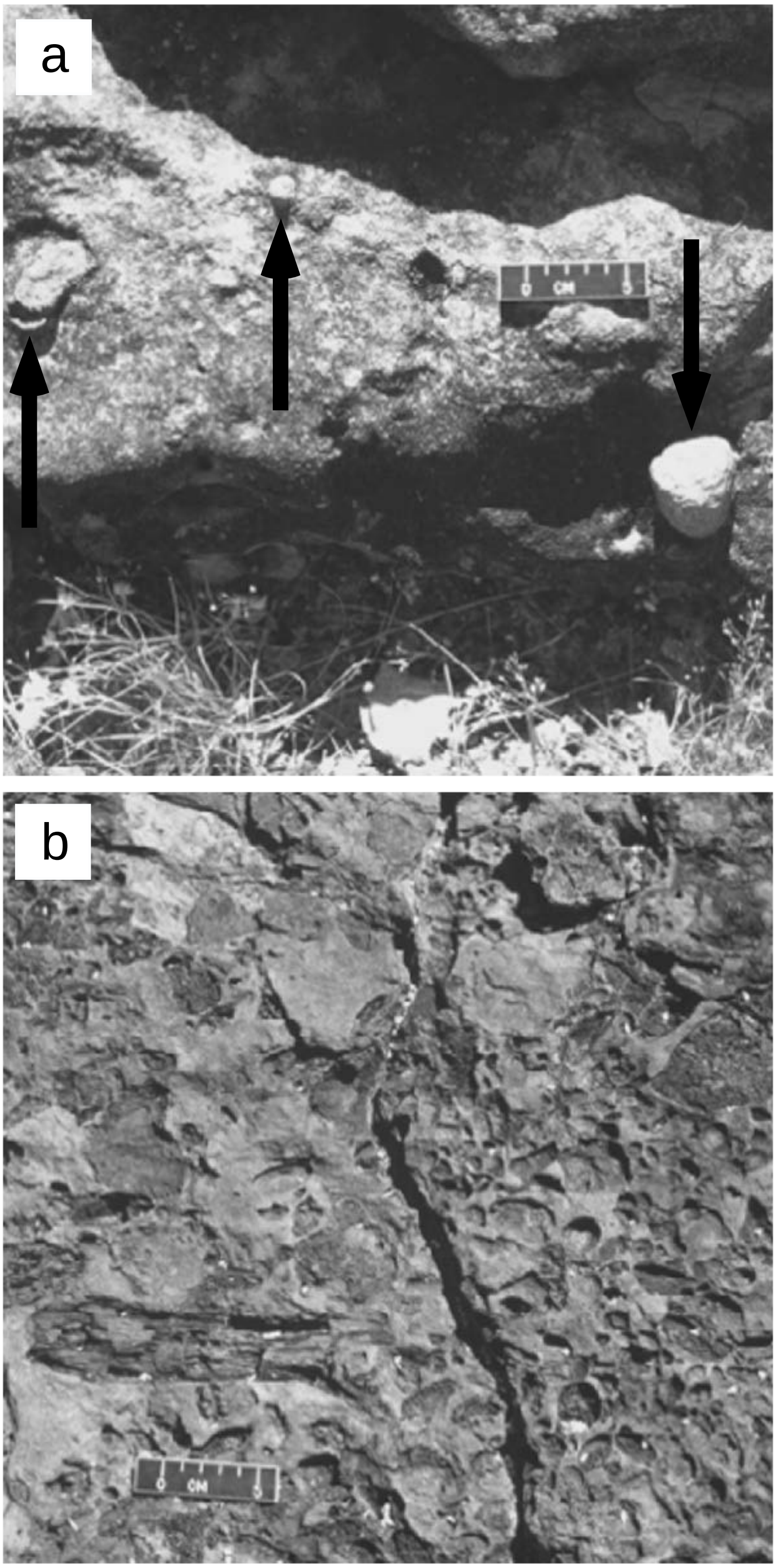

Figure 3.8: In the Grant Range, sandstone clasts and mud pellets occur throughout the Tuckfield Member. (a) Photograph of basal sands with rounded sandstone clasts (marked by arrows). (b) Bedding plane view of a typical mud-pellet and plant-fragment conglomerate. In this photograph, the impressions of ripped-up, iron-coated mud pellets (abundant circular features) and plant-fragments (elongated feature above scale) are clearly visible. Many mud pellets and plant fragments still remain in the sandy matrix and can be seen in cross-section. Similar to the sandstone clasts shown in (a), individual mud pellets also occur throughout the entire Tuckfield succession. Photographs from Location G-2. Scale in both photographs is 5 cm.

sedimentary features (fine-grained sediment, abundant plant fragments, iron-rich nature), Adkins (2003; Chapter 1, this volume) interpreted these conglomerates to be supratidal/overbank mudflat deposits. If this interpretation is correct, the abundance of mud pellets (both individual and in conglomerates) in the Grant Range succession again indicates that the entire sequence was probably deposited in a non-marine, coastal plain environment.

Today, Tuckfield Member deposits in the Grant Range are dominated by relatively coarse-grained sediment (very fine to medium-grained sand). However, the number of silty mud pellets that occur throughout this succession suggest that finer-grained silts and muds must have been deposited in a nearby area, probably in an overbank setting. In the St George and Poole Ranges, the shallow-marine sediments of the Tuckfield Member outcrop as laterally continuous beds. The lateral continuity of these deposits is generally only interrupted by widespread areal faulting (Figure 3.5a). In contrast, the non-marine sediments of the Grant Range outcrop as isolated hills that are separated by distances of 1 to 3 km (Figures 3.3 and 3.5b). The occurrence of these outcrops appears to be unrelated to faulting (Figure 3.3). Therefore, it is possible that some of the areas of apparent non-deposition (between outcrops/hills) in the Grant Range actually mark the locations of previous overbank mudflats. Post-uplift erosion may have removed these less resistant deposits, leaving sediments that were predominantly associated with and trapped between the more resistant channel sands.

SPECTRAL ANALYSIS

To better define the depositional cyclicity recorded in the Grant Range, spectral analyses were performed on the gamma-ray dataset from each location (Appendix 10).[**] The results from these analyses are presented in Figures 3.9 (Location G-1) and 3.10 (Location G-2). In both figures, the upper plots (Figures 3.9a and 3.10a) were generated by the "Timeseries" program and the lower plots (Figures 3.9b and 3.10b) were generated by the "AnalySeries 1.1" program. Spectral peaks in all four diagrams (Figures 3.9a, 3.9b, 3.10a and 3.10b) represent cycles recorded in the rock record. The reciprocal of the frequency for each peak is equal to the average period of that cycle in

[**] Spectral analyses were also performed on grainsize data from Locations G-1 and G-2 (Appendices 8 and 11). Although these analyses do support the conclusions of Chapter 3, the spectral plots are generally not as well-developed as the plots generated from the analyses of gamma-ray data. Therefore, they are not discussed in this chapter. However, they are available for consideration in Appendix 11.

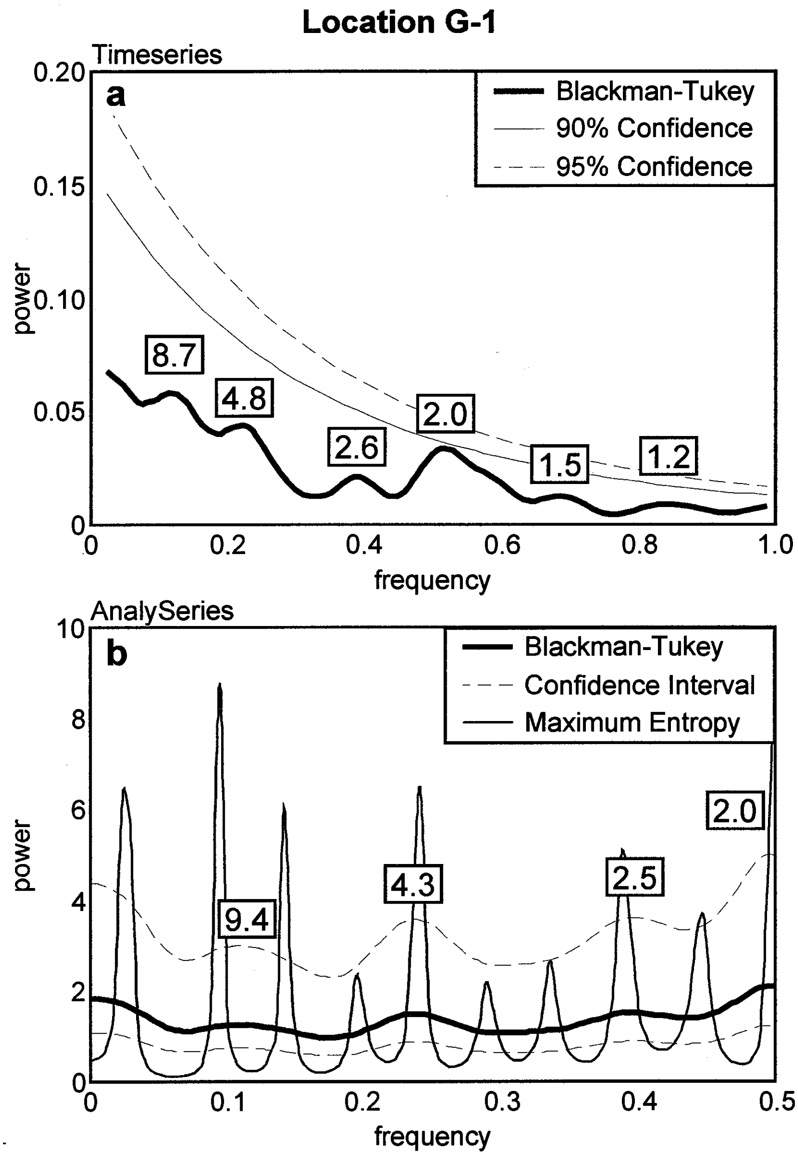

c

Cycle Thickness	Location G-1 Ratios
9.1 meters	1
4.6 meters	1:2.0
2.6 meters	1:3.5
2.0 meters	1:4.6
1.5 meters	1:6.1
1.2 meters	1:7.6

Figure 3.9: Spectral analyses of gamma-ray data from Location G-1. Data were analyzed using two spectral programs as a cross-check on results. (a) displays spectrum (calculated using the Blackman-Tukey method) with 90% and 95% confidence lines. Results produced by "Timeseries" program. (b) displays two spectra (one with associated confidence interval, calculated using the Blackman-Tukey method; the second calculated using the maximum entropy method). Results produced by "AnalySeries 1.1" program. In (a) and (b), peaks in the spectra mark cycles. Average cycle periods are listed in rectangles above spectral peaks. (c) lists dominant cycles detected by the spectral analyses and their conversion into ratios relative to the 9.1 m cycle.

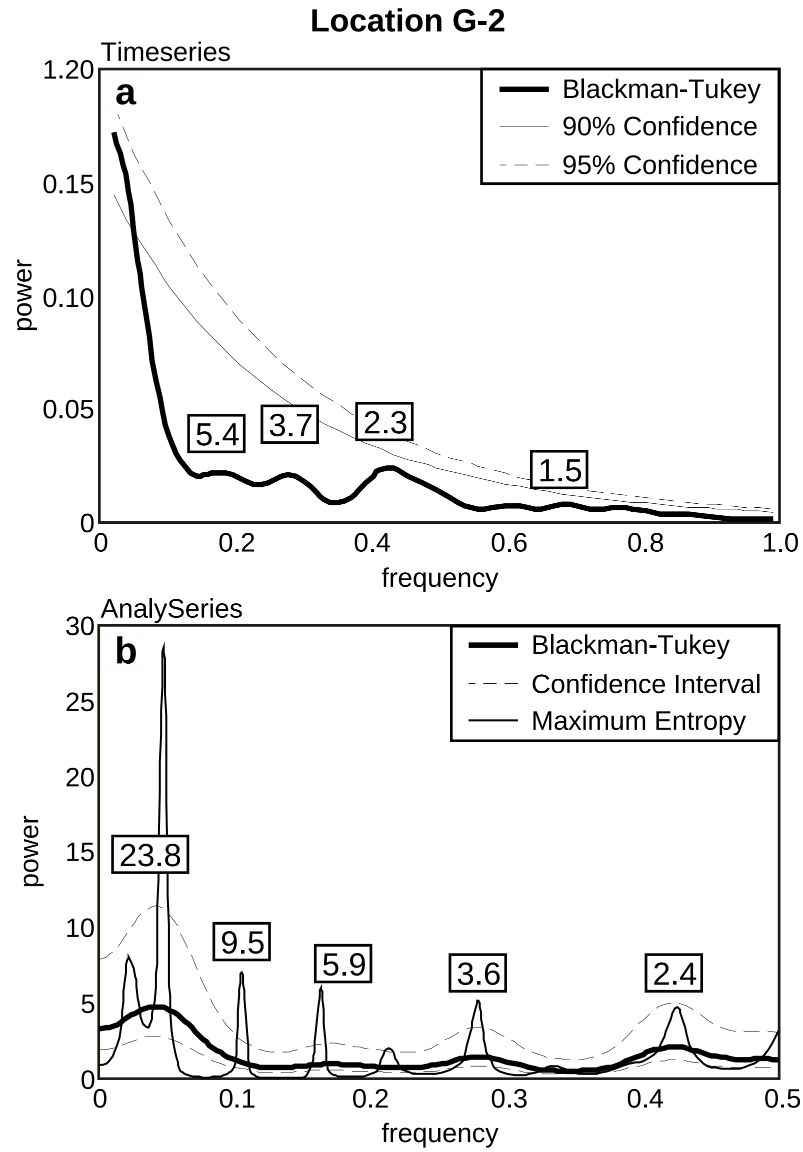

c

Cycle Thickness	Location G-2 Ratios
23.8 meters	2.5:1
9.5 meters	1
5.7 meters	1:1.7
3.7 meters	1:2.6
2.4 meters	1:4.0
1.5 meters	1:6.3

Figure 3.10: Spectral analyses of gamma-ray data from Location G-2. Data were analyzed using two spectral programs as a cross-check on results. (a) displays spectrum (calculated using the Blackman-Tukey method) with 90% and 95% confidence lines. Results produced by “Timeseries” program. (b) displays two spectra (one with associated confidence interval, calculated using the Blackman-Tukey method; the second calculated using the maximum entropy method). Results produced by “AnalySeries 1.1" program. In (a) and (b), peaks in the spectra mark cycles. Average cycle periods are listed in rectangles above spectral peaks. (c) lists dominant cycles detected by the spectral analyses and their conversion into ratios relative to the 9.5 m cycle.

meters (shown in rectangles above spectral peaks). For each location, the spectral peaks generated by the two programs were compared, averaged, and used to determine the periodicities of all significant cycles recorded at that location (Figures 3.9c and 3.10c). According to these analyses, cycles with average periodicities of 9.1 m, 4.6 m, 2.6 m, 2.0 m, 1.5 m and 1.2 m were detected at Location G-1 (Figure 3.9c). Cycles with average periodicities of 23.8 m, 9.5 m, 5.7 m, 3.7 m, 2.4 m and 1.5 m were detected at Location G-2 (Figure 3.10c).

MILANKOVITCH CYCLICITY

Rhythmic changes in Earth's orbital path can influence the formation of depositional cyclicity. Although orbitally influenced cycles are typically associated with marine strata, recent studies have demonstrated that Milankovitch-scale cyclicity can also be recorded in non-marine successions (Olsen, 1986; Olsen, 1994; Olsen and Kent, 1999). Many of these studies have attributed the formation of non-marine cycles to orbitally-controlled (i) changes in precipitation (Olsen, 1994); (ii) large-scale climatic variations (e.g. arid versus humid) (Clemmensen et al., 1994); and/or (iii) seasonal fluctuations in sediment supply (Fielding and Webb, 1996). Additionally, it has long been postulated that sea-level fluctuations (including glacio-eustatic) can alter baselevel and thereby influence cyclothem development in fluvial and other non-marine environments (e.g. Allen, 1964). For these reasons, it is prudent to consider Milankovitch-forcing as a potential driving mechanism in the formation of any highly cyclic non-marine succession.

To test for orbital cyclicity in the Tuckfield Member (Grant Range), the identified cycles (Figures 3. 9 and 3.10) are here compared with the known astronomic rhythms. The orbital parameters are well established for the present-day with periodicities of approximately 410,000 years (elongated eccentricity), 100,000 years (eccentricity), 41,000 years (obliquity), and 19,000 to 23,000 years (precession) (Berger, 1988; DeBoer and Smith, 1994). However, due to long-term alterations in the Earth-Moon-Sun rotational system, the values for obliquity and precession have slowly changed throughout geologic time. During the mid-Permian, obliquity is retrodicted to have had a periodicity with dual components of 44,000 and 35,000 years. Precession is retrodicted to have had a periodicity with dual components of 21,000 and 17,600 years. The periodicities for eccentricity (100,000 years) and elongated eccentricity (410,000 years) have remained relatively constant (Berger and Loutre, 1994).

To effectively compare the identified Tuckfield Member cycles (Figures 3.9 and 3.10) with the mid-Permian orbital periodicities, each set of numbers (e.g. all cycles identified at Location G-1) must first be converted into a set of ratios. For Location G-1, this conversion is shown in Figure 3.9c. For example, if the 9.1 m cycle is set at one, the number of 4.6 m cycles in each 9.1 m cycle is 2.0 (9.1 ÷ 4.6 = 2.0). For Location G-2, a similar conversion is shown in Figure 3.10c. The mid-Permian orbital periodicities were converted into ratios by setting the 100,000 year cycle equal to one. For example, the number of 44,000 year cycles in each 100,000 year cycle is equal to 2.3 (100,000 ÷ 44,000 = 2.3). The complete listing of the mid-Permian Milankovitch ratios is given in the second line of Table 3.1.

In addition to listing the mid-Permian orbital periodicities and their associated ratios, Table 3.1 also lists the ratios from Locations G-1 and G-2 (originally given in Figures 3.9c and 3.10c) and the average cycle periodicities detected in deposits from the St George and Poole Ranges (from the analyses of gamma-ray data: Chapter 2, this volume). Clearly, the non-marine cycles identified in the Grant Range (Locations G-1 and G-2) compare favorably with the orbital periodicities and with the shallow-marine cycles detected in the other areas. Extra, non-Milankovitch-band cycles (in unmarked columns) detected in the St George and Poole Ranges have been interpreted to be the result of tectonic events or short-term changes in sediment supply (Chapter 2, this volume). The extra cycle detected at Location G-1 (1:7.6) may also record tectonism or short-term changes in sediment supply. However, it is equally possible that this cycle is merely a spurious peak in the spectral plot.

It should also be noted that the shallow-marine, Milankovitch-band cyclicity recorded in the St George and Poole Ranges appears to conform more closely to the expected Milankovitch periodicities than do the non-marine cycles recorded in the Grant Range. Although this may be a true representation, it is probable that this is simply a result of sampling. The values listed for the St George and Poole Ranges (Table 3.1) are averaged from 15 measured sections. The values listed under Locations G-1 and G-2 (Table 3.1) each represent one measured section. Obviously, the more samples that are averaged together, the more accurate the results will be.

DEPOSITIONAL MODEL FOR THE FITZROY TROUGH

During the Artinskian when the Tuckfield Member was deposited, the Fitzroy Trough was comprised of a complex system of shallow-marine to non-marine

Periodicities	Eccentricity 410,000	100,000		Obliquity 44,000	35,000		Precession 21,000	17,600	
Expected Milankovitch Ratios	4.1:1	1		1:2.3	1:2.9		1:4.8	1:5.7	
Location G-1 Ratios		1		1:2.0	1:3.5		1:4.6	1:6.1	1:7.6
Location G-2 Ratios	2.5:1	1		1:1.7	1:2.6		1:4.0	1:6.3	
Average St George & Poole Ratios	3.7:1	1	1:1.8	1:2.1	1:3.1	1:3.7	1:4.5	1:5.9	1:8.6

Table 3.1: Results of spectral analyses. Line 1 lists Milankovitch orbital parameters with their associated periodicities. Line 2 lists Milankovitch parameters in ratios relative to the 100,000 year cycle. Line 3 lists the ratios computed for the Location G-1 periodicities (taken from Figure 3.9c). Line 4 lists the ratios computed for the Location G-2 periodicities (taken from Figure 3.10c). For comparison, average ratios from the St George and Poole Ranges (detected from the analyses of 14 gamma-ray datasets: Chapter 2, this volume) are shown in Line 5. Note the favorable comparison between the Milankovitch ratios and the Tuckfield Member ratios (from both shallow-marine sediments [St George and Poole Ranges] and non-marine sediments [Locations G1 & G-2: Grant Range]). Extra, non-Milankovitch-band cycles (in unmarked columns) detected in the St George and Poole Ranges have been interpreted to record tectonic events or short-term changes in sediment supply (Chapter 2, this volume). The extra cycle detected at Location G-1 (1:7.6) may also record tectonism or short-term changes in sediment supply. However, it is equally possible that this cycle is merely a spurious peak in the spectral plot.

depositional environments (Figure 3.11). In the St George and Poole Ranges, the Artinskian Tuckfield Member outcrops as a series of shallow-marine cycles. Recent studies (Chapters 1 and 2, this volume) have directly linked these cycles to Earth's orbital parameters and attributed the formation of depositional cyclicity to glacio-eustatic sea-level fluctuation. In the nearby Grant Range, the Tuckfield Member outcrops as a series of non-marine cycles. This study demonstrates a favorable comparison between these non-marine cycles and the known mid-Permian orbital periodicities. This favorable comparison indicates that Milankovitch-forcing of climate influenced the formation of non-marine cyclicity in the Grant Range.

As previously mentioned, Earth's orbital perturbations can affect global sea-level. Additionally, orbital cyclicity can influence precipitation, large-scale climatic variations, and seasonal fluctuations in sediment supply. Therefore, it could be difficult to determine the exact mechanism of formation for many non-marine cyclic successions. However, the strong correlation between the identified non-marine and shallow-marine Tuckfield Member cycles (Table 3.1) suggests that the same mechanism probably controlled the formation of depositional cyclicity in both environments. Adkins (Chapter 2, this volume) proposed that global sea-level fluctuation, related to the waxing and waning of Gondwanan glaciers, drove the deposition of shallow-marine cyclicity in the St George and Poole Ranges. This same sea-level fluctuation may have affected local base-level in the Fitzroy Trough, thereby forcing the rhythmic migration of non-marine, coastal plain environments. As these glacially-driven changes in base-level forced the Grant Range coastal plain to migrate, local channel-shifting may have resulted in the deposition of the vertically stacked, fining- and thinning-upward cycles observed in outcrop.

CONCLUSIONS

In the Grant Range, at least eight vertically stacked, fining- and thinning-upward Tuckfield Member cycles have been identified. Each cycle contains lithologies and sedimentary structures that are indicative of non-marine, braided channel deposition on a sand-rich coastal plain. Spectral analysis of gamma-ray data was used to constrain the depositional cyclicity that is observed in outcrop. Identified cycles correlate strongly with the known mid-Permian orbital periodicities of eccentricity, obliquity, and precession. This favorable comparison indicates that Milankovitch-forcing of climate is responsible for the formation of these cycles. Additionally, the calculated ratios for the

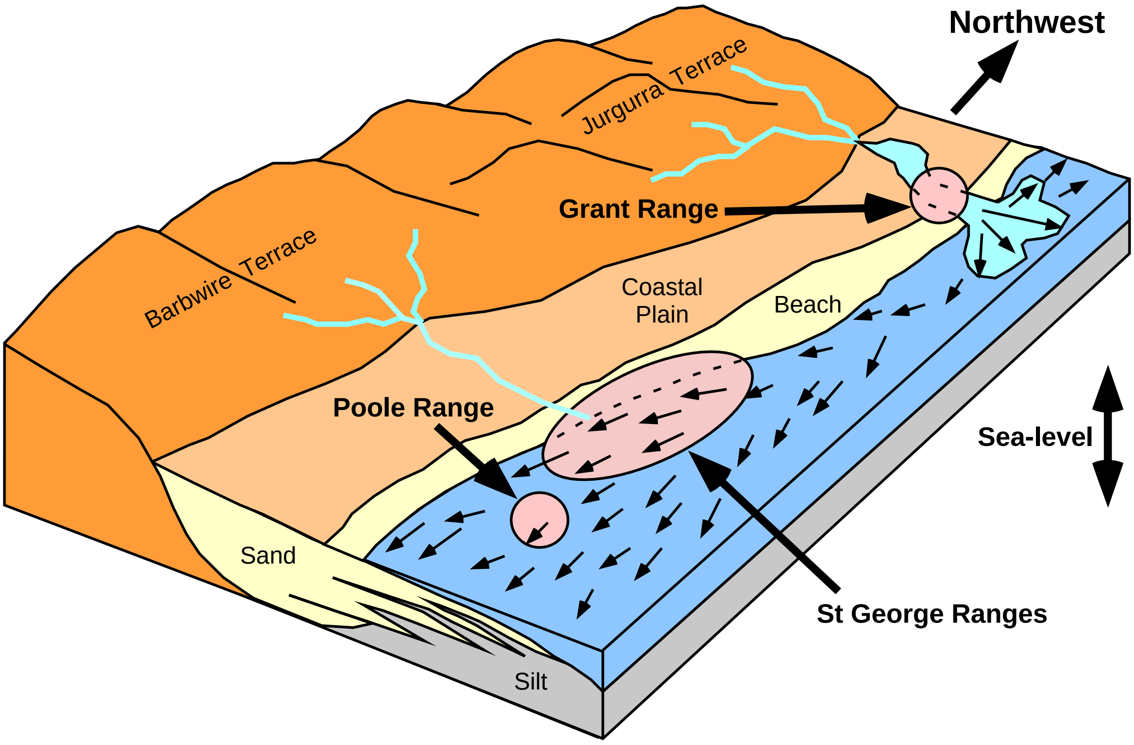

Figure 3.11: Simplified depositional model for the Fitzroy Trough during the mid-Permian. In the St George and Poole Ranges, glacio-eustatic sea-level fluctuation resulted in the deposition of coarsening- and thickening-upward shallow-marine cycles. These same sea-level fluctuations caused cyclic migration of the coastal plain that resulted in the deposition of fining- and thinning-upward, non-marine cycles within the Grant Range.

non-marine cyclicity that was identified in the Grant Range is similar to the correlative calculated ratios for the shallow-marine cyclicity that was identified in the St George and Poole Ranges (eccentricity, obliquity, and precession). This suggests that glacio-eustatic sea-level fluctuations probably controlled both the formation of shallow-marine and non-marine (coastal plain) cyclicity in the mid-Permian Fitzroy Trough. These findings act as a reminder that Milankovitch-forcing of climate should never be dismissed as a potential driving-mechanism in the formation of non-marine depositional cyclicity.

Chapter 4

The stratigraphic evolution and petroleum potential of the Early Permian Poole Sandstone, onshore Canning Basin, Western Australia

ABSTRACT

The Early Permian Poole Sandstone occurs throughout the northwestern region of the onshore Canning Basin, Western Australia. Although the Poole Sandstone has long been identified as a potential petroleum reservoir, its sub-surface stratigraphic evolution has not been studied in any detail. This investigation focuses on the sedimentology and stratigraphy of the unit as it occurs in the northern Fitzroy Trough/Lennard Shelf region. In this area, the Poole Sandstone can be traced throughout the sub-surface as a continuous package of predominantly shallow-marine sediments. The two distinct depositional units that together comprise the Poole Sandstone are easily recognized on sub-surface gamma-ray logs. The lower Nura Nura Member unconformably overlies the Early Permian Grant Group and probably consists of a heterogeneous package of predominantly clastic sediments. Its unconformable nature, combined with the lateral variability of the Nura Nura deposits, makes the lower bounding surface of the Poole Sandstone difficult to identify in well logs with certainty. In contrast, the bounding surface between the Nura Nura Member and the overlying Tuckfield Member is easily recognized, as is the bounding surface between the Tuckfield Member and the overlying Noonkanbah Formation

Because the Tuckfield Member is well constrained within the study area, it is possible to perform detailed stratigraphic analyses of this unit. In the northern Fitzroy Trough/Lennard Shelf region, the Tuckfield Member ranges from 39 to 68 m thick and consists of a coarsening-upward package of predominantly shallow-marine clastic sediments. This large-scale coarsening-upward cycle is comprised of four distinct, smaller-scale coarsening-upward cycles of approximately equal thickness. The Tuckfield Member and each of its four internal cycles can be traced laterally throughout the field area for a distance of over 200 km. Parallel to the paleo-coastline, these cycles maintain a near constant thickness. Oblique to the paleo-coastline, these cycles both thicken and deepen basinward.

To gain a better understanding of the observed cyclicity, spectral analyses were performed on gamma-ray data from the Terrace 1 log. These analyses indicate that the Poole Sandstone probably records a variety of sea-level fluctuations of both orbital and tectonic origin.

Key Words: Canning Basin, cyclicity, Fitzroy Trough, Permian, Poole Sandstone, Tuckfield Member

INTRODUCTION

The onshore segment of the Phanerozoic Canning Basin has potential for significant hydrocarbon production (e.g. Kennard et al., 1994). Lying mainly within the Great Sandy and Gibson Deserts of Western Australia, the onshore Canning Basin covers an area larger than Texas (430,000 km^2) and has a basin fill of up to 18 km (Yeates et al., 1984). The sediments that fill the basin were predominantly deposited from the Early Ordovician to the Early Cretaceous in a shallow-marine environment. These sediments contain thick reservoir-quality sandstone and carbonate units (Kennard et al., 1994).

To date, hydrocarbon exploration within the Canning Basin has met with limited success. However, several small petroleum fields, identified in the basin's northern regions (Middleton, 1992; Griffin et al., 1993), suggest that larger hydrocarbon accumulations may also exist. With fewer than 300 exploration wells scattered throughout the area (Apak and Carlsen, 1996), parts of the onshore Canning Basin are relatively untested and the potential for commercial petroleum discovery remains high.

Exploration within the basin has historically focused on its northwestern region. Since the 1920s, more than 250 petroleum wells have been drilled throughout the Canning Basin area. Of these, approximately 45% are located in the Fitzroy Trough (15%) and on the adjacent Lennard Shelf (30%) (Apak and Carlsen, 1996) (Figure 4.1). In this region, commercial hydrocarbon accumulations have been identified in terrigenous Permo-Carboniferous strata (e.g. the Early Permian Grant Group) and carbonate reservoirs from the Devonian reef complex (Griffin et al., 1993; Apak and Carlsen, 1996). Additionally, a few historically non-productive Permo-Carboniferous units have been identified as potential petroleum reservoirs (Towner, 1981; Jackson et al., 1994).

The Early Permian Poole Sandstone (defined by Guppy et al., 1952, 1958) is one such unit. It has largely been marked as a potential petroleum reservoir based upon favorable porosity/permeability values and recorded hydrocarbon shows (e.g. Havord et al., 1997). Although it may be economically important, little is known about the sub-surface stratigraphic evolution of this unit. To date, few detailed sedimentological and/or stratigraphic analyses have been performed on the Poole Sandstone. The studies that do exist concentrate predominantly on high-frequency cyclicity that is recorded in relatively limited outcrop exposures (Grant, St George, and Poole Ranges: Figure 4.1) of the middle Tuckfield Member (Adkins, 2003; Chapters 1-3, this volume). To

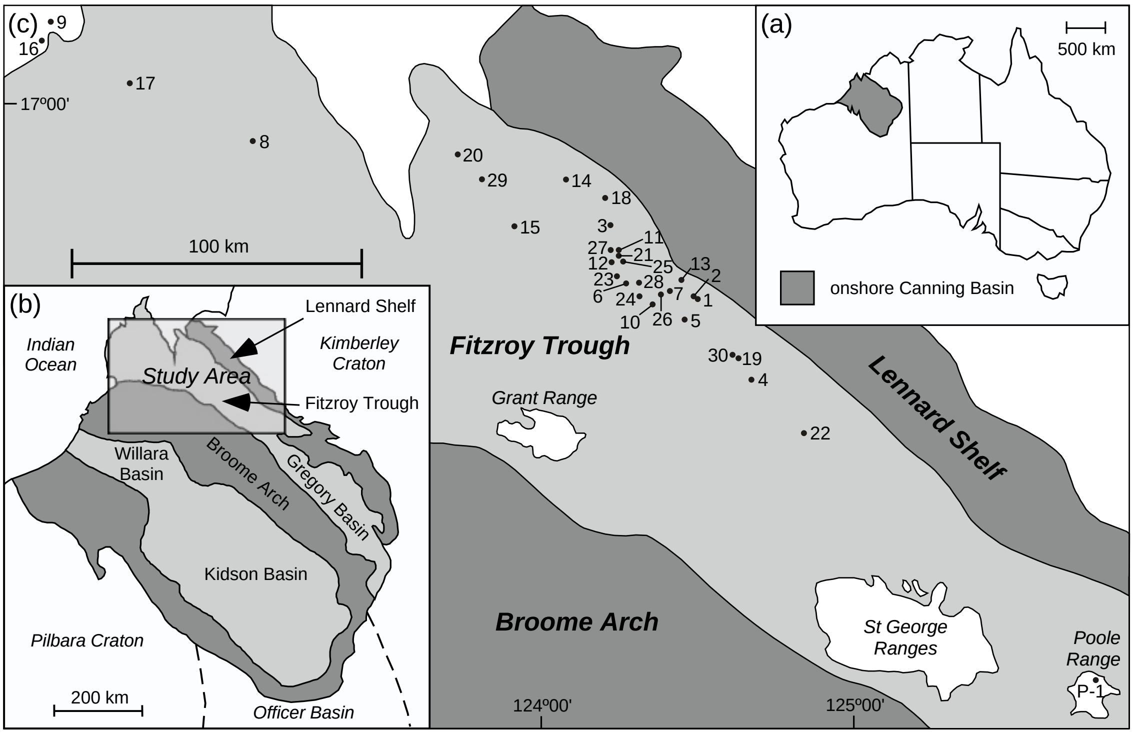

Figure 4.1: Simplified map of Australia (a) showing location of the onshore Canning Basin (b). The northern Fitzroy Trough/Lennard Shelf study area (c) is labeled on map (b). Map (c) shows the location of the 30 sub-surface wells (labeled 1-30) and the location of the Grant, St George, and Poole Ranges. See Table 4.1 for further information on the wells. Maps (b) and (c) are adapted from Kennard et al., 1994.

effectively evaluate the hydrocarbon potential of the Poole Sandstone, it is necessary to first understand its sub-surface stratigraphic evolution. This chapter provides a detailed analysis of the sub-surface Poole Sandstone (concentrating on the middle Tuckfield Member) as it occurs in the northwestern region of the onshore Canning Basin (Figure 4.1).

DATABASE AND METHODS

This research focuses on sub-surface data from the northern Fitzroy Trough and the adjacent Lennard Shelf. Gamma-ray logs, obtained from hydrocarbon exploration wells, were collected from an area that covers approximately 15,000 km^2 and includes more than 70 petroleum wells (Figure 4.1). The Early Permian Nura Nura and Tuckfield Members of the Poole Sandstone were identified on each of the 70+ logs. Of these logs, 30 were chosen for inclusion in this study (Figure 4.1 and Table 4.1). The chosen logs are of high quality, record complete preservation of the Poole Sandstone (e.g. no section is faulted out), and provide non-repetitive lateral coverage of the study area. For example, all of the Sundown wells (1-5) occur within approximately 1 km^2. Therefore, their logs are near replicas of each other. To avoid the use of repetitive data, only one of these wells (Sundown 2) is included in this investigation.

Based upon the 30 chosen gamma-ray logs, cross-sections and an isopach map of the Tuckfield Member were constructed. These diagrams are used to establish the depositional environment and lateral variability of the unit. Additionally, sub-surface data from this area is compared with outcrop observations taken from the nearby Poole Range (Figure 4.1). The similarity between the two datasets allows sub-surface stratigraphic and sedimentological interpretations to be made with confidence.

In the study area, several orders of cyclicity, recognized in the Tuckfield Member, can be traced laterally for more than 200 km. To define the observed cyclicity better, spectral analyses were performed on gamma-ray measurements taken at a one-meter vertical spacing (from a depth of 775 m in the Noonkanbah Formation to a depth of 950 m in the Grant Group) on the Terrace 1 log (Appendix 12). To verify the results, this dataset was analyzed using two different spectral analysis programs (Appendix 9). The “Timeseries” program (described by Weedon and Read, 1995) uses the standard Blackman-Tukey method (Blackman and Tukey, 1958) to generate power spectra, whereas the “AnalySeries 1.1” program (Paillard et al., 1996) uses both the Blackman-Tukey and Maximum Entropy (Haykin, 1983) methods to generate power spectra. The

Location & Well Name	Latitude	Longitude	Tuckfield Top (m)	Nura Nura Top (m)	Tuckfield Thickness (m)
1) Blina 5	17º 37' 34"	124º 30' 10"	588	637	49
2) Blina 8	17º 37' 11"	124º 29' 29"	608	657	49
3) Canegrass 1	17º 23' 30"	124º 13' 32"	555	598	43
4) Crimson Lake 1	17º 53' 05"	124º 40' 33"	712	776	64
5) Hakea 1	17º 41' 37"	124º 27' 50"	550	603	53
6) Hangover 1	17º 34' 40"	124º 16' 34"	769	824	55
7) Janpam 1	17º 36' 08"	124º 24' 52"	784	835	51
8) Jum Jum 1	17º 07' 21"	123º 04' 57"	1545	1596	51
9) Kambara 1	16º 44' 35"	122º 26' 16"	805	844	39
10) Katy 1	17º 38' 40"	124º 21' 29"	704	759	55
11) Loyd 2	17º 28' 11"	124º 15' 06"	818	867	49
12) Loris 1	17º 30' 24"	124º 13' 44"	917	970	53
13) Mariana 1	17º 33' 57"	124º 27' 10"	632	677	45
14) May River 1	17º 14' 50"	124º 05' 01"	439	480	41
15) Millard 1	17º 23' 39"	123º 55' 05"	1177	1234	57
16) Minjin 1	16º 48' 08"	122º 24' 45"	770	819	49
17) Moogana 1	16º 56' 17"	122º 41' 27"	1118	1159	41
18) Orange Poole 1	17º 18' 15"	124º 12' 34"	319	358	39
19) Philydrum 1	17º 48' 60"	124º 37' 56"	582	643	61
20) Point Torment 1	17º 09' 58"	123º 44' 15"	894	939	45
21) Runthrough 1	17º 29' 23"	124º 14' 56"	982	1031	49
22) Scarpia 1	18º 03' 13"	124º 50' 36"	484	552	68
23) Sundown 2	17º 33' 19"	124º 14' 42"	784	838	54
24) Sunup 1	17º 37' 12"	124º 18' 58"	756	812	56
25) Terrace 1	17º 30' 23"	124º 15' 50"	825	877	52
26) Thompsons 1	17º 36' 41"	124º 23' 10"	814	865	51
27) Wattle 1	17º 28' 14"	124º 13' 35"	902	951	49
28) West Blackstone 1	17º 34' 32"	124º 18' 57"	766	817	51
29) West Kora 1	17º 14' 48"	123º 49' 00"	978	1022	44
30) West Philydrum 1	17º 48' 20"	124º 36' 52"	574	638	64

Table 4.1: Detailed information about the 30 wells used in this study.

detected cycles are herein compared with cyclicity identified in shallow-marine Tuckfield Member deposits from the Poole Range (Figure 1.4) (Chapter 2, this volume). This comparison plays a critical role in determining the significance of the cyclicity observed in the study area.

Due to poor imaging associated with shallow sub-surface depths and the relatively thin nature of the Poole Sandstone, seismic data was not used in this study.

GEOLOGIC SETTING

The Fitzroy Trough is a northwest-trending graben bounded by the Beagle Bay and Pinnacle Fault Systems to the northeast and by the Fenton Fault System to the southwest (Towner, 1981). Development of both the Fitzroy Trough and the larger Canning Basin began during the Ordovician when thrust-related shearing in basement rock to the north (Shaw et al., 1992a) resulted in extension and rapid subsidence of the Canning Basin area. The Fitzroy Trough contains over 15 km of Paleozoic and minor Mesozoic sediments that can be divided into four distinct tectono-stratigraphic megasequences: (i) Ordovician-Silurian; (ii) Devonian-Early Carboniferous; (iii) Late Carboniferous-Permian; and (iv) Jurassic-Cretaceous. Each of these megasequences corresponds to a transgressive-regressive package that records an episode of crustal stretching and subsidence followed by an extended period of tectonic quiescence (Kennard et al., 1994).

To the northeast, the Beagle Bay and Pinnacle Fault Systems separate the northern Fitzroy Trough from the adjacent Lennard Shelf. A thin succession (generally less than 2 km thick) of Paleozoic basin strata overlies shallow basement rock in the Lennard Shelf area. These strata typically thicken (Towner, 1981) and deepen (from diagrams in: Towner, 1981; Gibson, 1983; Purcell and Poll, 1984) basinward. They consist of mainly Devonian reef and reef-associated deposits with lesser accumulations of Ordovician and Carboniferous-Triassic rocks (Towner, 1981). The major faults that separate the Fitzroy Trough from the Lennard Shelf are predominantly near-vertical normal faults that offset sediments in the area by as much as several kilometers (Yeates et al., 1984). Offset associated with these faults is greatest at depth and lessens higher in the section (e.g. Towner, 1981; Gibson, 1983). The Early Permian Poole Sandstone is one of the oldest stratigraphic units that is relatively continuous across the northern Fitzroy Trough/Lennard Shelf area.

Within the Canning Basin, the Poole Sandstone consists of a laterally extensive package of shallow-marine and non-marine sediments. Three distinct depositional units comprise the Poole Sandstone: the lower Nura Nura Member, the middle Tuckfield Member, and the upper Christmas Creek Member (Crowe and Towner, 1976a). Although the middle Tuckfield Member occurs throughout the Canning Basin, the lower Nura Nura Member is restricted to the northwestern region of the basin (Crowe and Towner, 1977) and the upper Christmas Creek Member has only been identified in outcrop exposures of the St George and Poole Ranges (Crowe and Towner, 1976a).

OUTCROP CHARACTERISTICS

The best exposures of the Poole Sandstone are found in the Grant, St George, and Poole Ranges of the Fitzroy Trough (Figure 4.1). Detailed stratigraphic analyses of the unit (concentrating on the middle Tuckfield Member) were recently conducted in all three areas (Adkins, 2003; Chapters 1-3, this volume). In these ranges, the Sakmarian to Artinskian Nura Nura Member unconformably overlies fluvio-marine to deltaic, near-shore deposits of the upper Grant Group (Figure 4.2) (Apak, 1996). In these ranges, the Nura Nura Member is less than 30 m thick (Crowe and Towner, 1981) and consists of a heterogeneous mix of clastic sediments. These sediments record deposition in a variety of shallow-marine to non-marine environments (Crowe and Towner, 1976b).

In the Grant, St George, and Poole Ranges, the Artinskian Tuckfield Member conformably to unconformably overlies the Nura Nura Member (Figure 4.2) (Crowe and Towner, 1981). The unit ranges in thickness from less than 50 m in the Grant and Poole Ranges to greater than 100 m in parts of the St George Ranges. In outcrop, this unit records a variety of depositional environments that range from non-marine coastal plain settings (Grant Range) to shallow-marine shoreface settings (Poole Range) (Adkins, 2003; Chapters 1-3, this volume).

In the Poole Range area, the Tuckfield Member outcrops as an approximately 40 m thick package of vertically stacked, coarsening- and thickening-upward cycles (Figure 4.3). Well-defined natural benches usually correspond with cycle tops and can be traced laterally throughout the range (Figures 4.3 and 4.4). Individual cycles are typically 5 to 7 m thick, but some thinner cycles (2 to 4 m) also occur within the Tuckfield Member succession (Figure 4.3) (Chapter 2, this volume). Each cycle systematically coarsens upward from silty mudstone to siltstone to sandstone. Primary

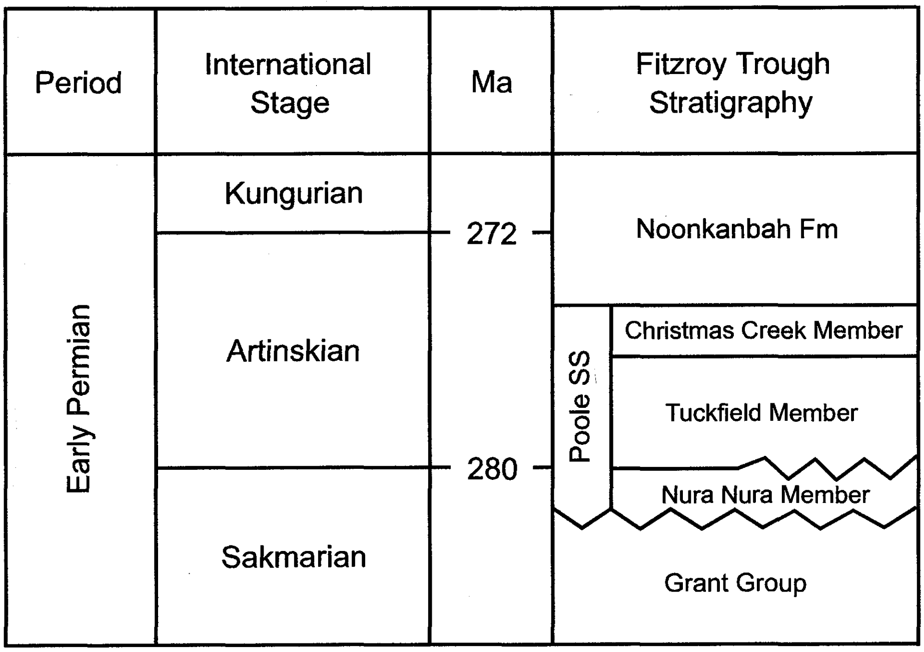

Figure 4.2: Early Permian stratigraphic column for the Fitzroy Trough/Lennard Shelf area (adapted from Kennard et al., 1994). In this area, the Christmas Creek Member is confined to the St George and Poole Ranges. Outside these ranges, the Noonkanbah Formation conformably overlies the Tuckfield Member. Stage dates from Veevers, 2000b.

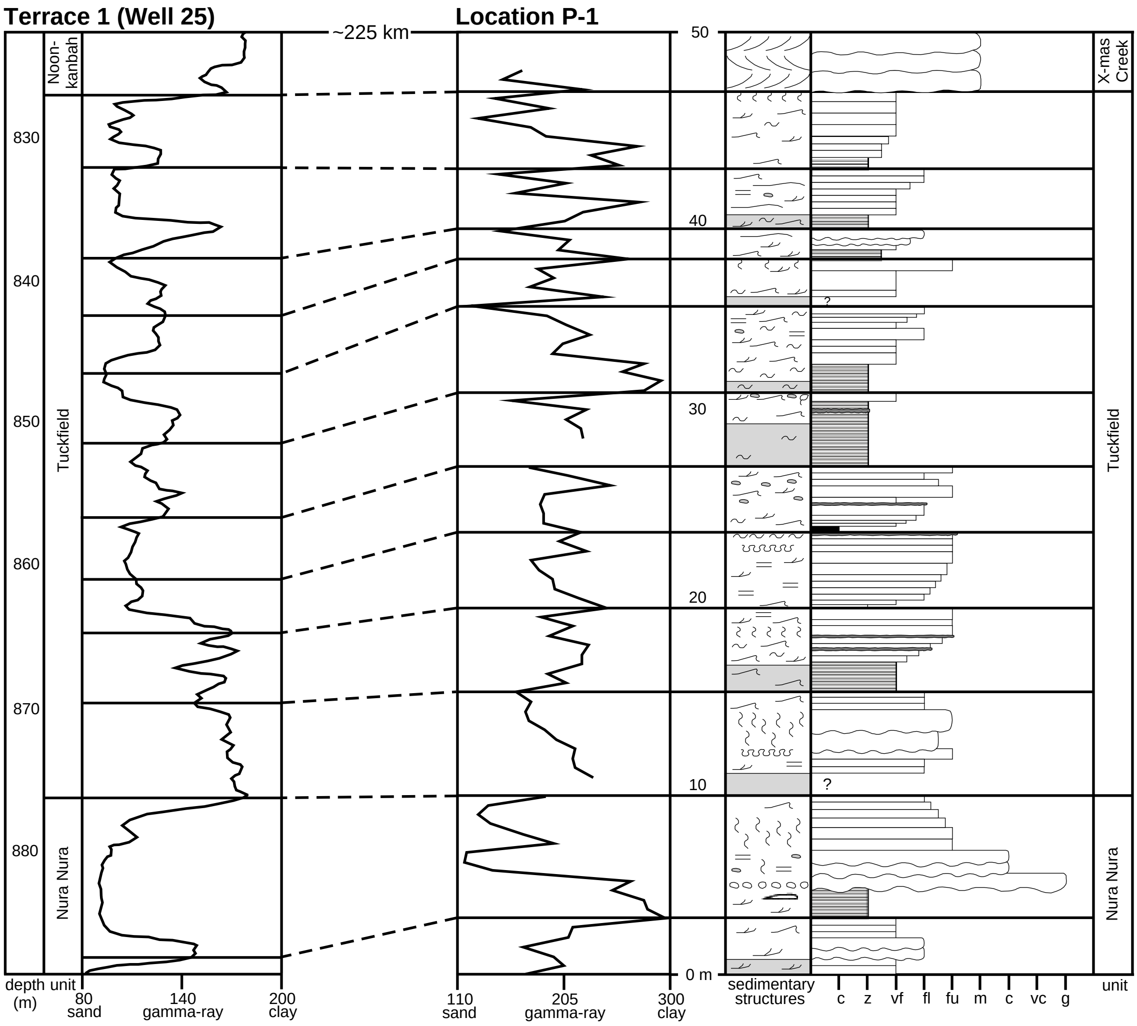

Figure 4.3a: Sub-surface gamma-ray log from Terrace 1 (Well 25 on Figure 4.1 & Table 4.1) and lithology log with associated gamma-ray data from the Poole Range (Location P-1 on Figure 4.1). The base of the Poole Range section is located at 51K 0793957/UTM 7914331 (using the Australian Geodetic Datum 1966 coordinates). Horizontal lines mark the tops of coarsening- and thickening-upward cycles, as depicted on the lithology log (Location P-1). These lines generally correspond to the benches shown in Figure 4.4. Although a distance of more than 200 km separates Terrace 1 and Location P-1, there is a distinct positive correlation between the 2 gamma-ray logs. Grainsize increments from left to right on the x-axis of the lithology log are as follows: c (clay/mud); z (silt); vf (very fine sand); fl (lower half of fine sand); fu (upper half of fine sand); m (medium sand); c (coarse sand); vc (very coarse sand). Fine sand was divided into lower and upper halves to better depict variations in grainsize. Member and formation names are given in the columns labeled "unit." See Figure 4.3b for key.

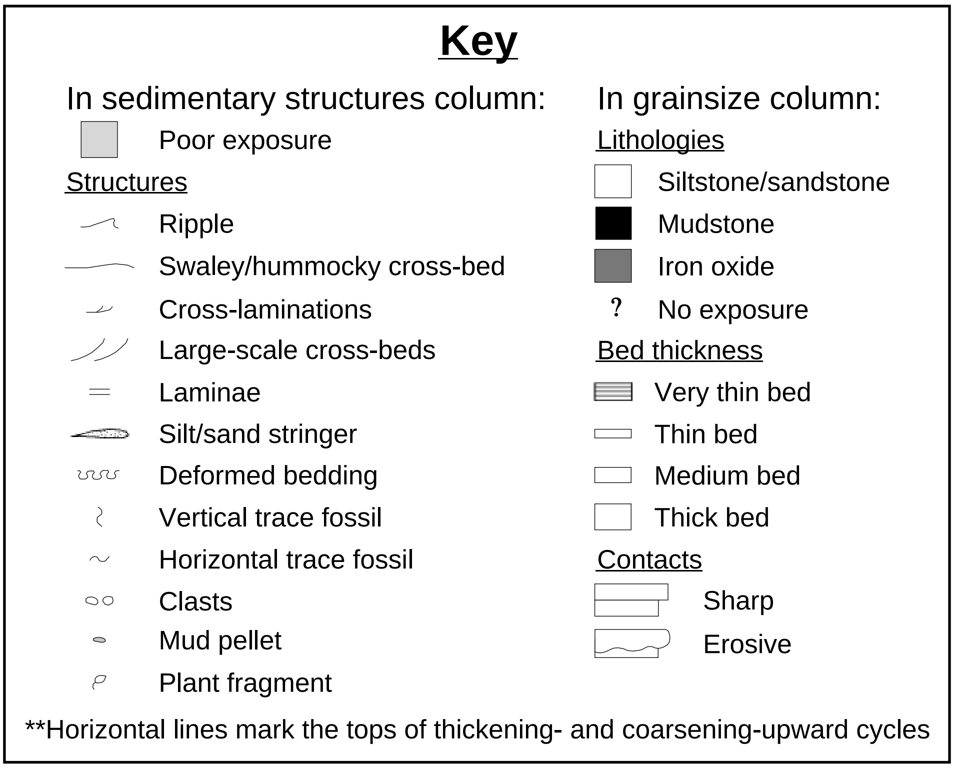

Figure 4.3b: Key for Figure 4.3a (Location P-1).

Figure 4.4: Outcrop of the Tuckfield Member, Poole Range. Note the laterally continuous, flat-lying benches that mark the tops of coarsening- and thickening-upward cycles. Photograph taken at 51K 0795184/UTM 7905636 (using the Australian Geodetic Datum 1966 coordinates), facing north. Photograph shows approximately 1 horizontal km of outcrop.

sedimentary structures, trace fossils and the vertical succession of facies suggest that each cycle records an episode of shorezone progradation (Adkins, 2003, Chapter 1, this volume).

In the Grant Range, the Tuckfield Member outcrops as a less than 50 m thick package of laterally-discontinuous, thinning-upward cycles. At the outcrop scale, cycles range in thickness from 2 to 8 m and consists of a fining-upward succession of sandstone and siltstone. Sandstone clasts, individual mud pellets, and locally continuous mud-pellet and plant-fragment conglomerates occur throughout the stratigraphic interval. Primary sedimentary structures and the vertical succession of facies suggest that the Tuckfield Member was predominantly deposited on a sand-rich coastal plain in the Grant Range area (Chapter 3, this volume).

Poorly sorted, coarse-grained, fluvial sediments of the Artinskian Christmas Creek Member conformably overlie the Tuckfield Member (Figure 4.2) in the St George and Poole Ranges. This unit is relatively thin (less than 10 m thick) and restricted to the St George/Poole Ranges area (Crowe and Towner, 1976a). Outside this area, poorly exposed, fine-grained, fossiliferous, marine sediments of the Noonkanbah Formation conformably overlie the Tuckfield Member (Guppy et al., 1952, 1958).

SUB-SURFACE CHARACTERISTICS

There are no outcrop exposures of the Poole Sandstone in the northern Fitzroy Trough/Lennard Shelf area (Towner, 1981; Gibson, 1983; Griffin et al., 1993). However, the unit can be traced throughout the region via sub-surface seismic (e.g. Purcell and Poll, 1984; O'Brien et al., 1998) and well-log data (e.g. Havord et al., 1997; O'Brien et al., 1998). Although little can be learned about the internal structure of the Poole Sandstone from local seismic lines, gamma-ray logs from the area provide a wealth of information concerning the sedimentology and stratigraphy of the unit.

Although stratigraphic successions are customarily described in ascending order, the reverse approach is used here. This is because the upper bounding surface of the Poole Sandstone is typically more pronounced and easier to identify on gamma-ray logs than the lower bounding surface of the unit.

In the study area, the contact between the Tuckfield Member and the overlying Noonkanbah Formation is easily identified on sub-surface gamma-ray logs (Figures 4.5 and 4.6). In the Fitzroy Trough/Lennard Shelf area, the Noonkanbah Formation is greater than 200 m thick and consists of predominantly fine-grained marine sediment

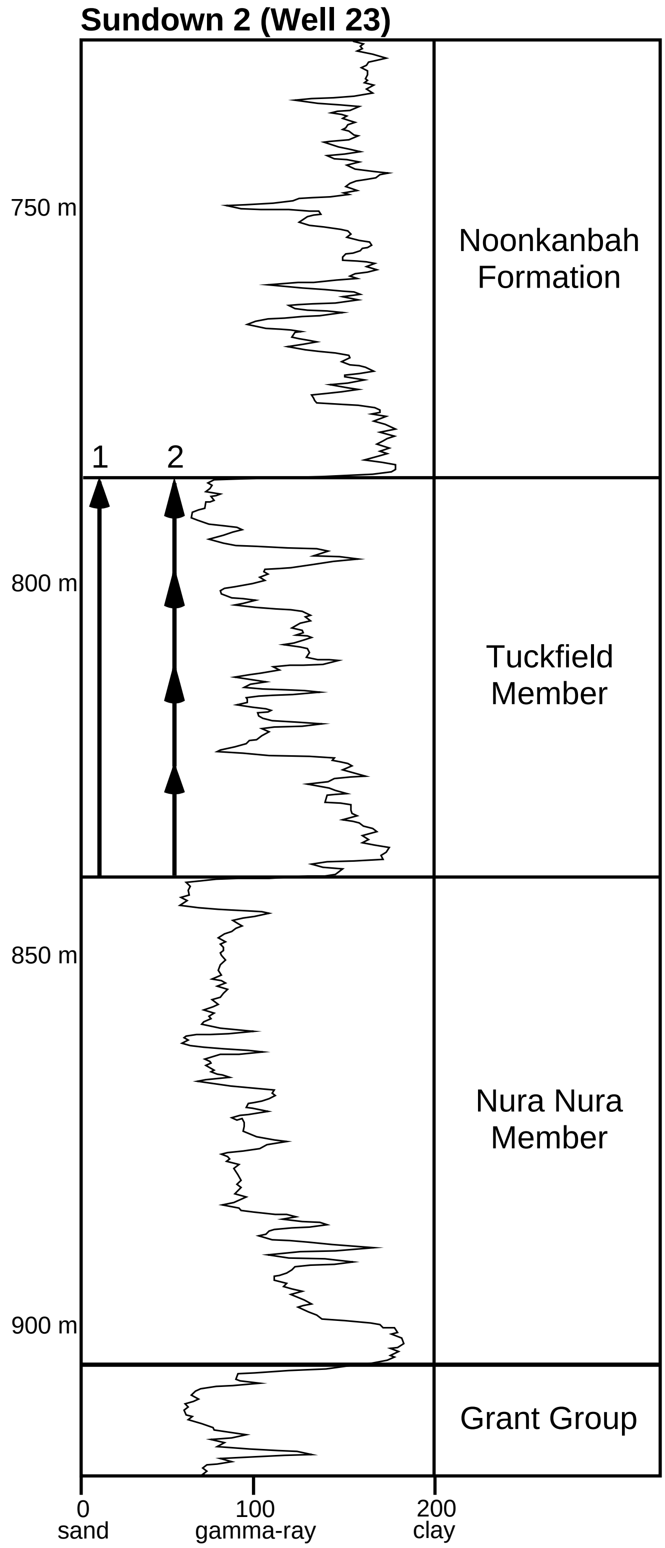

Figure 4.5: Gamma-ray log from the Sundown 2 well focusing on the Early Permian Poole Sandstone. In the study area, the upper and lower boundaries of the Tuckfield Member are typically marked by a sudden upward increase in gamma-ray values. Although the contact between the Nura Nura Member and the underlying Grant Group is easily identified on this log, it is not so apparent at other locations throughout the region (see Figure 4.6). Note that the Tuckfield Member consists of one major coarsening-upward sequence (arrows marked by 1) that is comprised of 4 smaller-scale, coarsening-upward sequences (arrows marked by 2).

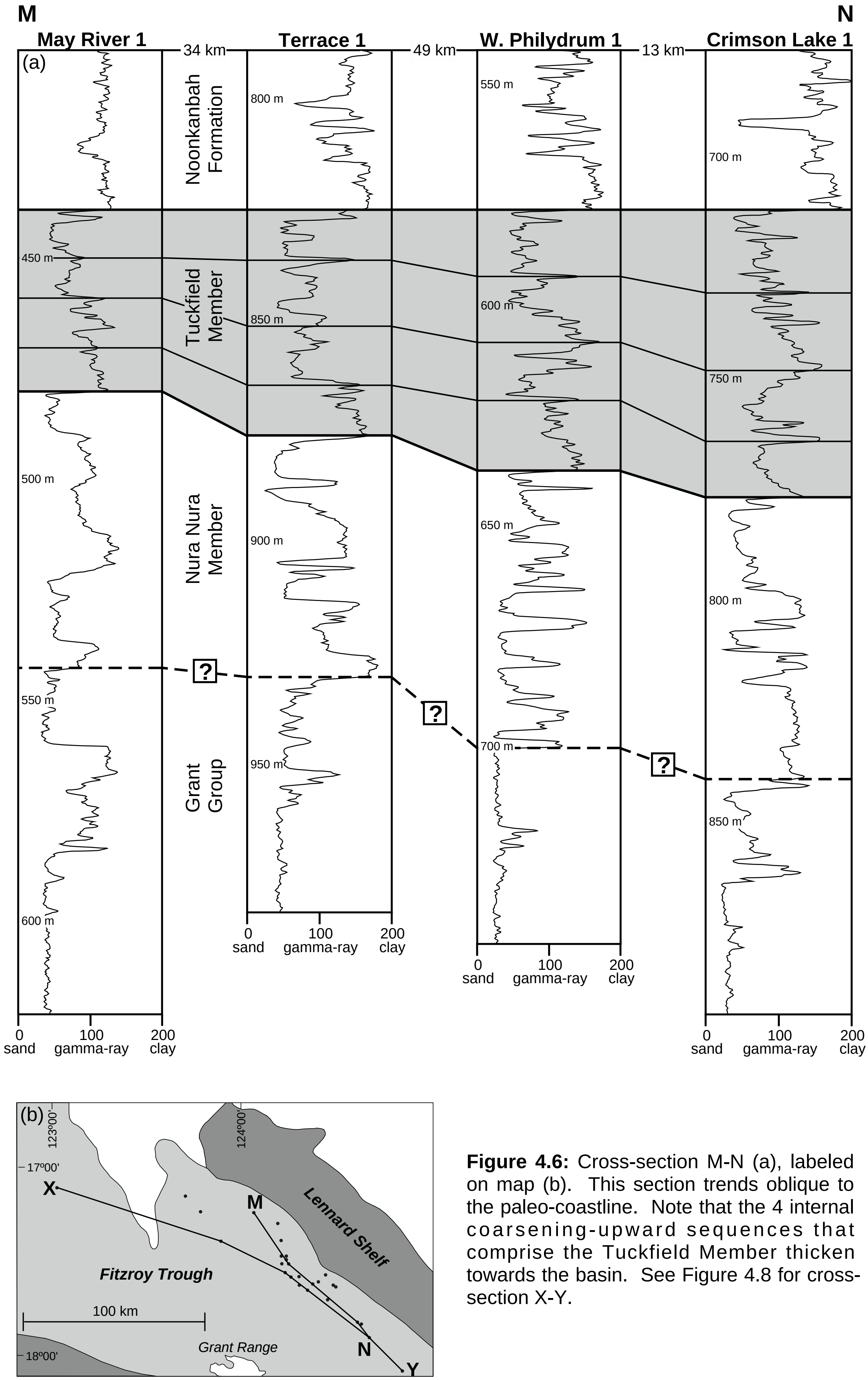

Figure 4.6: Cross-section M-N (a), labeled on map (b). This section trends oblique to the paleo-coastline. Note that the 4 internal coarsening-upward sequences that comprise the Tuckfield Member thicken towards the basin. See Figure 4.8 for cross-section X-Y.

(mud and shale) with minor amounts of coarser-grained sand and silt (Crowe and Towner, 1981). These muddy deposits result in a typically high-value gamma-ray log that is punctuated by thin, laterally discontinuous sandstone stringers that emit low gamma-ray readings (Figures 4.5 and 4.6).

Moving deeper into the stratigraphic section, the boundary between the Noonkanbah Formation and the Tuckfield Member is typically marked by a drastic downward decrease in average gamma-ray values (Figures 4.5 and 4.6). This sudden decrease marks the transition from the bottom of the muddy Noonkanbah Formation to the top of the coarser-grained Tuckfield Member. In the study area, the Tuckfield Member generally consists of one major coarsening-upward sequence that systematically ranges in thickness from 39 to 68 m (Table 4.1 and Figure 4.7). As Figure 4.7 illustrates, the Tuckfield Member gradually thickens toward the basin in a wedge that trends roughly parallel to the trough's northern paleo-coastline (northwest/southeast). Within the major coarsening-upward cycle, 4 internal coarsening-upward cycles of relatively equal thickness can also be identified (Figures 4.5 and 4.6). These internal coarsening-upward cycles thicken basinward (Figure 4.6). Parallel to the paleo-coastline, these internal coarsening-upward cycles maintain a relatively constant thickness and can be traced along strike for more than 200 km (Figure 4.8).

The contact between the Tuckfield Member and the underlying Nura Nura Member is also typically marked by a drastic downward decrease in average gamma-ray values (Figures 4.5, 4.6, and 4.8). This gamma-ray decrease indicates a sudden coarsening of grainsize from the base of the Tuckfield Member to the top of the Nura Nura Member. Similar to the Tuckfield deposits, the Nura Nura deposits display a coarsening-upward trend at some locations (e.g. Terrace 1 and Crimson Lake 1 in Figure 4.6). Unlike the Tuckfield deposits, this coarsening-upward trend is not laterally continuous throughout the study area (e.g. West Philydrum 1 in Figure 4.6). The lateral variability of this unit, combined with the unconformable relationship between the Nura Nura Member and the underlying heterogeneous Grant Group, makes it difficult to identify the lower bounding surface of the Poole Sandstone with absolute certainty.

CYCLICITY AND SPECTRAL ANALYSES

To gain a better understanding of cyclicity recorded within the Poole Sandstone, spectral analyses were performed on gamma-ray data from the Terrace 1 well (Table 1;

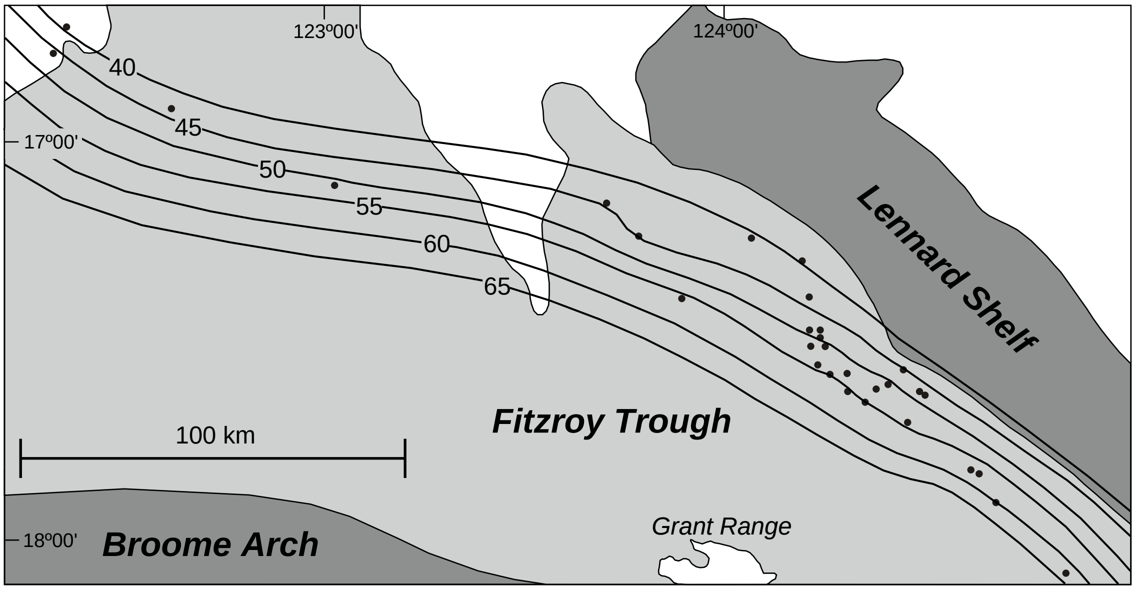

Figure 4.7: Isopach map of the Tuckfield Member (in meters). In this area, the unit systematically thickens towards the basin, perpendicular to the Early Permian paleo-coastline.

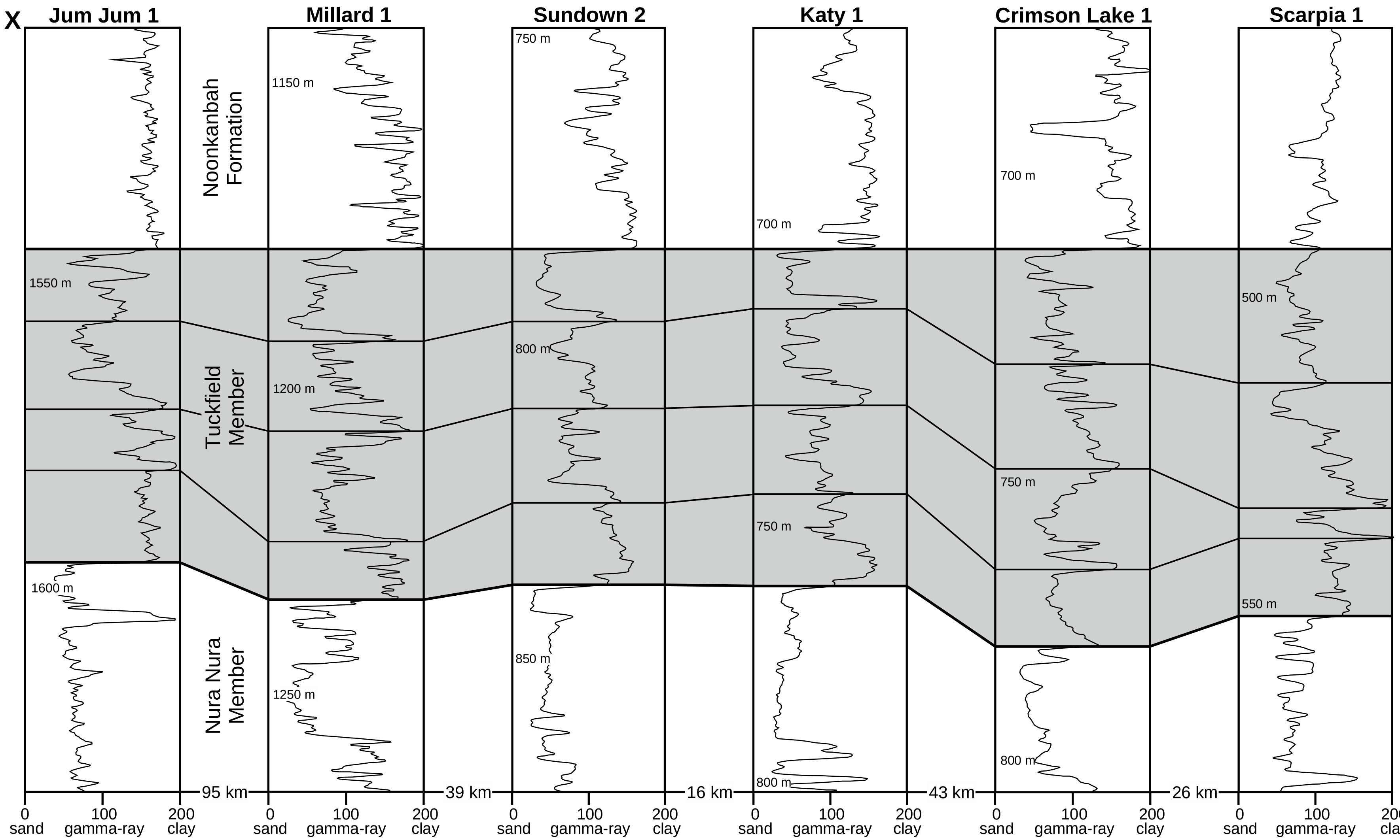

Figure 4.8: Cross-section X-Y. This section trends approximately parallel to the paleo-coastline. Note that the 4 internal coarsening-upward sequences that comprise the Tuckfield Member are approximately equal in thickness. See Figure 4.6b for the location of line X-Y.

Appendix 12). The results of these analyses are presented in Figure 4.9. In this figure, the upper spectral plot (Figure 4.9a) was generated using the "Timeseries" program, whereas the lower spectral plot (Figure 4.9b) was generated using the "AnalySeries 1.1" program. Spectral peaks in both plots (Figures 4.9a and 4.9b) represent cycles recorded in the rock record. The reciprocal of the frequency for each peak is equal to the average period of that cycle in meters (shown in rectangles above spectral peaks). The spectral peaks generated by the two programs were compared, averaged, and used to determine the periodicities of all significant cycles recorded at that location (Figure 4.9c). According to these analyses, cycles with average periodicities of 69.5 m, 28.6 m, 15.4 m, 10.3 m, 6.9 m, 5.3 m, 3.0 m, and 2.6 m were detected.

STRATIGRAPHIC EVOLUTION

The Poole Sandstone was deposited in a shallow-marine (less than 20 m of water) to non-marine depositional environment throughout the Fitzroy Trough (Crowe and Towner, 1981; Brakel and Totterdell, 1993). Although there are no outcrop exposures of the Poole Sandstone in the northern Fitzroy Trough/Lennard Shelf area, sub-surface gamma-ray logs can be used to further constrain the depositional environment of the unit in this region. The gamma-ray signature of the lower Nura Nura Member is highly variable throughout the study area. In places, the Nura Nura Member consists of a coarsening-upward package of sediments (e.g. Terrace 1 log in Figure 4.6). In other places, this member consists of an irregular package of sediments with no apparent coarsening- or fining-upward trend (e.g. West Philydrum log in Figure 4.6). The lateral variability displayed by this unit indicates that it was probably deposited in a wide variety of near-shore (possibly shallow-marine and non-marine) environments.

In contrast, the gamma-ray signature of the overlying Tuckfield Member is relatively consistent throughout the study area. This unit occurs as one thick (39 to 68 m) coarsening-upward sequence. Four internal coarsening-upward cycles of approximately equal thickness can also be identified and traced throughout the area. The coarsening-upward nature and lateral consistency of the Tuckfield Member in this region suggests that these deposits may be analogous to the laterally extensive, shallow-marine Tuckfield Member deposits of the Poole Range.

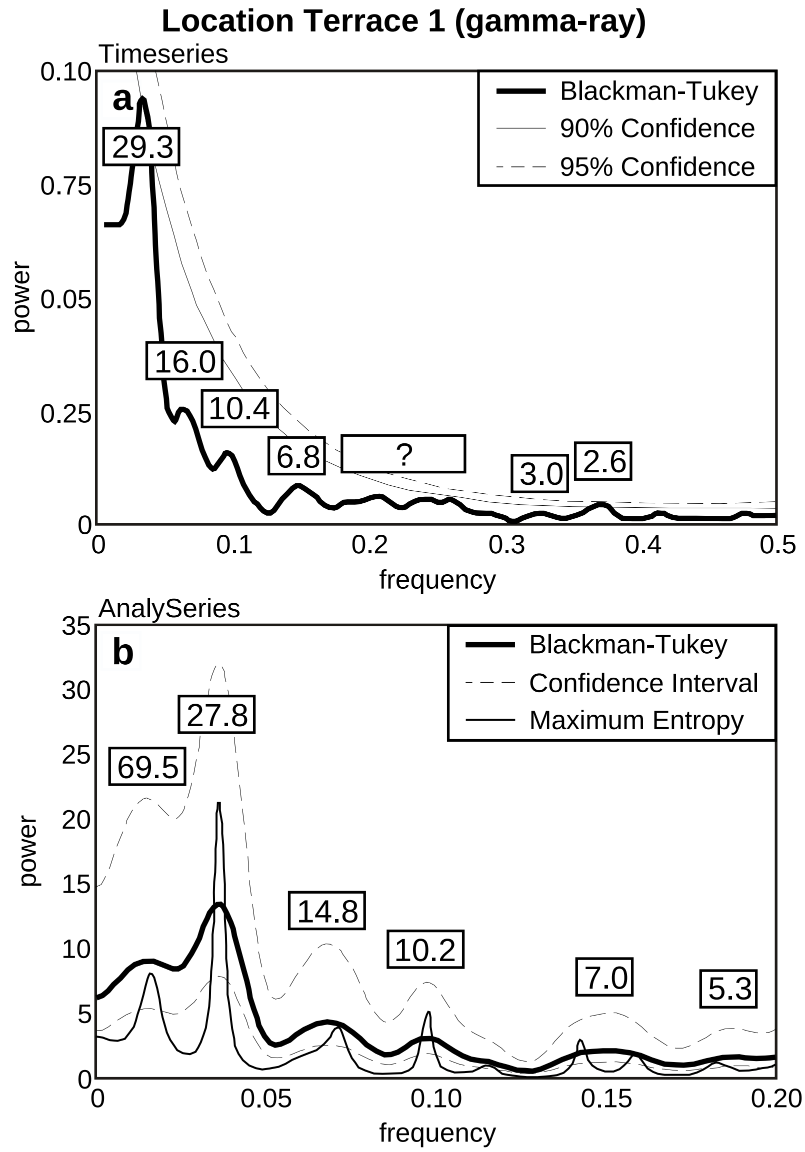

c

Cycle Thickness	Terrace 1 Ratios	Periodicities (years) & Order of Sea-level Fluctuation
69.5 meters	10.1:1	1,000,000 (3rd order)
28.6 meters	4.1:1	410,000 (4th order)
15.4 meters	2.2:1	220,000
10.3 meters	1.5:1	150,000
6.9 meters	1	100,000 (5th order)
5.3 meters	1:1.3	77,000
3.0 meters	1:2.3	43,500 (6th order)
2.6 meters	1:2.7	37,000 (6th order)

Figure 4.9: Spectral analyses of gamma-ray data from the Terrace 1 well. Data were analyzed using two spectral programs as a cross-check on results. (a) displays spectrum (calculated using the Blackman-Tukey method) with 90% and 95% confidence lines. Results produced by "Timeseries" program. (b) displays two spectra (one with associated confidence interval, calculated using the Blackman-Tukey method; the second calculated using the maximum entropy method). Results produced by "AnalySeries 1.1" program. In (a) and (b), peaks in the spectra mark cycles. Average cycle periods are listed in rectangles above spectral peaks. (c) lists dominant cycles detected by the spectral analyses, their conversion into ratios relative to the 6.9 m cycle, and the interpreted periodicities of the cycles (given in years).

To verify that the Tuckfield Member sediments in the Poole Range are indeed analogous to the Tuckfield Member sediments in this study, gamma-ray logs from the two areas were compared. In Figure 4.3, a lithology log with associated gamma-ray data from the Poole Range (Location P-1, see Figure 4.1) and a gamma-ray log (Terrace 1) from the Lennard Shelf are juxtaposed. The Terrace 1 log was initially chosen because it displays well-developed cyclicity, and more importantly, the Tuckfield Member at this location is of a similar thickness to the Tuckfield Member in the Poole Range. When the gamma-ray logs from the two distant areas (more than 200 km apart) are placed side by side, it becomes apparent that there is a cycle for cycle positive correlation between the two datasets. Therefore, it can be assumed that the Tuckfield Member in the northern Fitzroy Trough/Lennard Shelf area consists of shallow-marine clastic sediments that are similar in nature to those observed in the Poole Range.

Although the tectonic versus eustatic origin of cycle development remains controversial (Miall, 1997), identified Tuckfield Member cycles from the Poole Range have been attributed to orbitally controlled fluctuations in sea-level (Chapter 2, this volume). This suggests that the genetically similar deposits located in the northern Fitzroy Trough/Lennard Shelf region may record the same astronomical cycles. During the mid-Permian, these astronomical perturbations are retrodicted to have had periodicities of 17,600 and 21,000 years (precession); 44,000 and 35,000 years (obliquity), 100,000 years (eccentricity), and 410,000 years (elongated eccentricity) (Berger and Loutre, 1994). These parameters were converted into ratios by setting the 100,000 year cycle equal to one. For example, the number of 44,000 year cycles in each 100,000 year cycle is equal to 2.3 (100,000 ÷ 44,000 = 2.3). So, the ratio used for the 44,000 year cycle is 1:2.3. Therefore, expected Milankovitch ratios relative to the 100,000 year eccentricity cycle are: 4.1:1 (elongated eccentricity: 410,000 years); 1:2.3 (obliquity: 44,000 years); 1:2.9 (obliquity: 35,000 years); 1:4.8 (precession: 21,000 years); and 1:5.7 (precession: 17,800 years).

Spectral analyses of the Terrace 1 gamma-ray log identified several orders of cyclicity with average periodicities of 69.5 m, 28.6 m, 15.4, m, 10.3 m, 6.9 m, 5.3 m, 3.0 m, and 2.6 m. At Location P-1 in the Poole Range, cycles averaging 6.2 m thick were attributed to 100,000 year changes in Earth's eccentric orbit (Chapter 2, this volume). By assuming that the 6.9 m cycle identified on the Terrace 1 log is equivalent to the 100,000 year eccentricity cycle from the Poole Range, average periodicities can be calculated (in years) for all identified Terrace 1 cycles. Figure 4.9c summarizes this conversion (periodicities in meters to periodicities in years). Based upon these analyses, several orders of Milankovitch-band cycles are recorded on the Terrace 1 log. In addition to the eccentricity cycle (100,000 year/6.9 m), this log records an elongated eccentricity cycle (410,000 year/28.6 m) and both components of mid-Permian obliquity (43,500 year/3.0 m and 37,000 year/2.6 m).

In addition to Milankovitch-band cyclicity, other cycles were also identified on the Terrace 1 log. Although the 10.3 m (150,000 year) cycle and the 5.3 m (77,000 year) cycle do not correspond to known astronomical periodicities, they do roughly correspond to “extra” non-Milankovitch-band cycles that were recorded within the Poole Range deposits (Chapter 2, this volume). These “extra” cycles have been attributed to tectonism and/or short- to long-term changes in sediment supply (Chapter 2, this volume). The 15.4 m cycle identified on the Terrace 1 log may represent the apparent 200,000 year cycle that was described by Hinnov (2000). And finally, the 69.5 m (1,000,000 year) cycle identified on the Terrace 1 log may record the global 3rd order type of cyclicity that was initially described by Vail et al. (1977) and later modified by Haq et al. (1987).

Although the identified cycles do not correspond exactly to the observed Tuckfield Member cycles on the Terrace 1 log, it is important to remember that the data analyzed were drawn from the upper Grant Group to the lower Noonkanbah Formation, not just the Tuckfield Member. Therefore, cycle values reported in Figure 4.9 are averages from the entire sequence, and do not provide specific information concerning the Tuckfield Member. Nonetheless, they can be used as a general guideline.

In summary, the Tuckfield Member and possibly the Nura Nura Member of the Poole Sandstone record a 3rd order global sea-level cycle. This cyclicity may be attributed to large-scale tectonic events and/or global sea-level fluctuation associated with the break-up of Gondwanan ice-sheets. Superimposed upon the 3rd order cyclicity (in the Tuckfield Member and perhaps in the Nura Nura Member) are higher-frequency Milankovitch-band cycles that record glacio-eustatic sea-level fluctuation related to the waxing and waning of Gondwanan ice-sheets. Since much of the Fitzroy Trough was covered by a shallow-sea during the Early Permian, cyclicity related to sea-level fluctuation is laterally extensive throughout the basin.

PETROLEUM POTENTIAL

Although to date the unit remains non-productive, the Early Permian Poole Sandstone has long been identified as a potential petroleum reservoir (e.g. Jackson et al., 1994; Apak and Carlsen, 1996). In the northern Fitzroy Trough/Lennard Shelf region, the Poole Sandstone (particularly the Tuckfield Member) consists of a series of laterally extensive, coarsening-upward sequences of near-shore, shallow-marine clastic sediments. Although the reported porosity and permeability values for this unit are limited, the data that does exist is extremely favorable. Porosities up to 42% (Havord et al., 1997; Adkins, 2003; Chapter 1, this volume) and permeability values of up to 1700 md (Havord et al., 1997) have been reported for the Poole Sandstone. Residual oil and fluorescence in wells located on the lower Lennard Shelf (e.g. Terrace 1) indicate that hydrocarbons have previously passed through this unit (Havord et al., 1997). Unfortunately, most of the wells that have been drilled in the Lennard Shelf area are concentrated around the Beagle Bay and Pinnacle Fault Systems, suggesting that hydrocarbon exploration has historically focused on potential structural traps. However, offsets associated with the faults are greatest at depth and at a minimum higher in the section (where the Poole Sandstone is located). Therefore, if hydrocarbons do remain in the Poole Sandstone, they are probably located higher on the Lennard Shelf, in an up-dip location. Hence, exploration of the Poole Sandstone should focus on exploiting up-dip stratigraphic traps instead of structural traps around the Beagle Bay and Pinnacle Fault Systems.

CONCLUSIONS

This study is the first detailed investigation into the sub-surface stratigraphic evolution of the Early Permian Poole Sandstone. In the northern Fitzroy Trough/Lennard Shelf region, the Poole Sandstone consists of two distinct depositional units: the lower Nura Nura Member and the upper Tuckfield Member. In the study area, the Tuckfield Member and possibly the Nura Nura Member consist of a 3rd order package of predominantly shallow-marine clastic sediments. Internal cyclicity has been noted on gamma-ray logs and identified by spectral analyses. These internal cycles are laterally extensive and have been attributed to Milankovitch-band glacio-eustatic sea-level fluctuations.

Chapter 5

Shallow-marine sedimentary rhythms from the southern Sydney Basin, New South Wales, Australia: a mid-Permian record of glacio-eustacy

ACKNOWLEDGMENT

Chapter 5 resulted from a joint project with Helen Lever. Helen assisted with the collection of data, preliminary interpretations, and editing of the manuscript. Other than Helen's valuable editorial comments, all text and figures presented in this chapter are my work.

ABSTRACT

Glacially influenced marine sediments of the Permian Pebbley Beach Formation (Shoalhaven Group) are exposed along the coast of the southern Sydney Basin, New South Wales, Australia. These sediments outcrop as a repetitive series of coarsening-upward cycles that record deposition in an inner shelf to shoreface environment. At the outcrop scale, a typical Pebbley Beach cycle consists of a 5 to 10 m thick vertical succession of mudstone, interbedded mudstone and siltstone, and sandstone. Superimposed upon the deposition of the repetitive, coarsening-upward cycles is the occurrence of lonestones and diamictites, probably dropped from passing icebergs.

Although depositional cyclicity has been previously recognized in the Shoalhaven Group, the mechanism of formation for the cycles remains poorly understood. In this study, gamma-ray measurements were collected from outcrop exposures of the Pebbley Beach Formation. Spectral analyses were performed on the gamma-ray data to better define cyclicity. Results of the spectral analyses indicate that the Pebbley Beach deposits record several orders of meter- to decameter-scale cycles. These cycles correlate strongly with the known mid-Permian orbital periodicities of eccentricity, obliquity, and precession. This positive correlation indicates that Milankovitch-forcing and glacio-eustacy played a significant role in the formation of the Pebbley Beach cycles. The recognition of Milankovitch-band cyclicity within the Pebbley Beach Formation provides evidence that Permo-Carboniferous glaciation extended into at least the Ufimian stage of the Late Permian.

Key Words: glacio-eustacy, late Paleozoic glaciation, Milankovitch cyclicity, Pebbley Beach Formation, Permian, Shoalhaven Group, Sydney Basin

INTRODUCTION

Earth's climate during the latter part of the Permian (post-Sakmarian) has long been the subject of much scientific speculation and debate. During the 1960's and 1970's, Crowell and Frakes investigated the late Paleozoic climate and paleogeography of Gondwana (e.g. Frakes, 1969; Crowell, 1975). Based upon the occurrence of direct glacial deposits and the recognition of worldwide glacio-eustatic cyclothems, Crowell (1978) concluded that Permo-Carboniferous glaciation began during the Visean (Early Carboniferous) and ended during the Kazanian (Late Permian).

Since the 1970's, various studies have attempted to expand and refine Crowell and Frakes' early work (e.g. Veevers and Powell, 1987; Visser, 1993b; Visser, 1989; Crowell, 1995). Many of these studies suggest that glaciers persisted on parts of Gondwana up to at least the Triassic boundary (e.g. Veevers et al., 1994a; Veevers, 2000a). However, others indicate that Gondwanan deglaciation and the onset of global greenhouse conditions occurred by the end of the Early Permian (e.g. Visser, 1993a; Visser, 1996; Santos et al., 1996). Some studies even argue that Gondwanan deglaciation may have occurred as early as the late Sakmarian (e.g. Dickens, 1985, 1996; Scotese et al., 1999). Many of these investigations were based upon the sometimes ambiguous occurrence of direct glacial deposits (striated clasts, tillites, etc.). In contrast, this study evaluates the likelihood of post-Sakmarian glaciation by testing high frequency sedimentary cycles for a glacio-eustatic driving mechanism.

The Sydney Basin, New South Wales, Australia (Figure 5.1) contains a thick succession of shallow-marine Permian strata (Gostin and Herbert, 1973; Tye et al., 1996). In the southern extremities of the basin, the mid-Permian Pebbley Beach Formation (Shoalhaven Group) records broad-scale cyclic changes in the depositional environment. These cyclic changes have been attributed to sea-level fluctuations caused by glacio-eustacy, changing sediment supply, and/or basin tectonics (Eyles et al., 1998).

Although the Pebbley Beach Formation has been extensively studied, the mechanisms of formation for the depositional cyclicity have yet to be fully addressed. This paper examines the role that glacio-eustacy played in the formation of these cycles. Although tectonism and sediment supply certainly affected Permian sedimentation in the Sydney Basin, this paper demonstrates that glacio-eustacy contributed significantly to the formation of depositional cyclicity in the Pebbley Beach Formation.

REGIONAL SETTING

The Sydney Basin forms the southern part of the larger north/south-trending Sydney-Bowen Basin (Figure 5.1). During the Late Carboniferous to Early Permian, the Sydney-Bowen Basin developed by extension (Veevers, 2000a) possibly in a back-arc environment (Scheibner, 1974; Battersby, 1981; Tye et al., 1996) along the eastern margin of Australia (Veevers et al., 1994b, Veevers, 2000a). By the mid-Permian, the basin had evolved into a 2000 km long foreland basin located between the Lachlan-Thomson Fold Belt to the west and the New England Fold Belt to the east (Scheibner and Basden, 1998; Veevers, 2000a) (Figure 5.1).

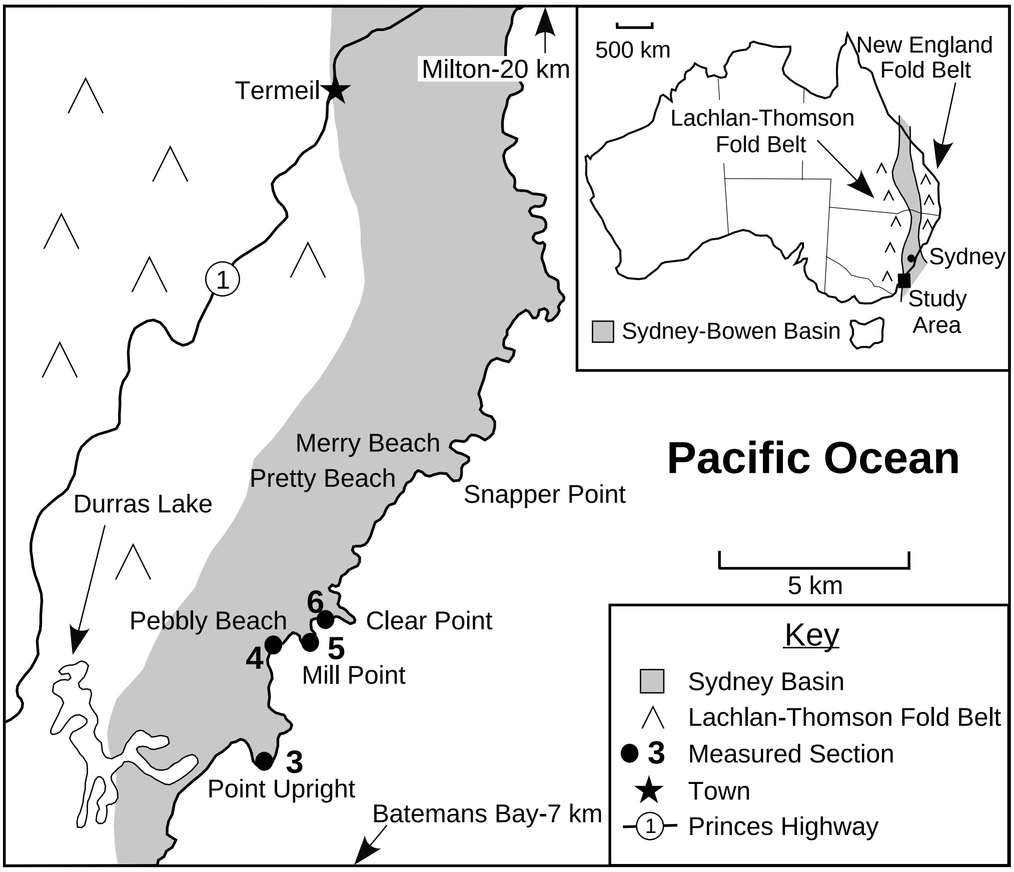

Figure 5.1: Simplified map of the southern Sydney Basin. For the measured sections presented in this chapter, location numbers on the map correspond with figure numbers in the text (e.g. data from Location 3 is presented in Figure 5.3).

A thick package of Permo-Triassic sediments fills the southern extremities of the basin (Figure 5.2). These deposits sit unconformably on highly deformed Ordovician, Silurian, and Devonian rocks of the Lachlan-Thomson Fold Belt (Gostin and Herbert, 1973; Carey, 1978). Apart from minor faulting and slight warping, sediments filling the basin have remained relatively undisturbed since their deposition (Gostin and Herbert, 1973).

During the Early Permian when much of its sediments were deposited, the Sydney Basin lay at high paleolatitudes along the southeastern margin of Gondwana (Veevers and Powell, 1987; Veevers, 2000c). Southern Australia was positioned proximal to a large ice sheet centered over east Antarctica and much of continental Australia was covered by terrestrial ice-caps (Crowell and Frakes, 1971; Crowell, 1978, 1995). Although the cessation of Permian glaciation is not well constrained, sediments in the southern Sydney Basin provide a detailed record of glacial influence into the Late Permian. Glaciofluvial conglomerates and tillites of the Talaterang and Shoalhaven Groups are exposed along the western margin of the basin (Herbert, 1980a; Tye et al., 1996). To the east, correlative glacially-influenced marine deposits (Talaterang and Shoalhaven Groups) are exposed along the coast between Milton and Batemans Bay (Tye et al., 1996; Eyles et al., 1997, 1998) (Figures 5.1 and 5.2). This study focuses on the Pebbley Beach Formation of the Shoalhaven Group where it outcrops between Point Upright and Clear Point (Figure 5.1).

AGE OF THE SHOALHAVEN GROUP

Prior to 1997, the Talaterang and Shoalhaven deposits were classified as Early Permian (Gostin and Herbert, 1973; Tye et al., 1996) without further division into international stages. To better constrain the chronostratigraphy of the Talaterang and Shoalhaven deposits, Eyles et al. (1997, 1998) used absolute ages of 277 Ma for the base of the Wasp Head Formation (Talaterang Group) (Veevers et al., 1994b) and 260 Ma for tephra in the Wandrawandian Siltstone (Shoalhaven Group) (Runnegar, 1980). The two dates were placed upon a Phanerozoic timescale that was developed specifically for eastern Australia (Veevers et al., 1994b). Accordingly, the Wasp Head Formation (Talaterang Group) was inferred to be Sakmarian, the Pebbley Beach Formation (Shoalhaven Group) was inferred to be Sakmarian to Artinskian, and the Snapper Point Formation and Wandrawandian Siltstone (Shoalhaven Group) were inferred to be Kungurian.

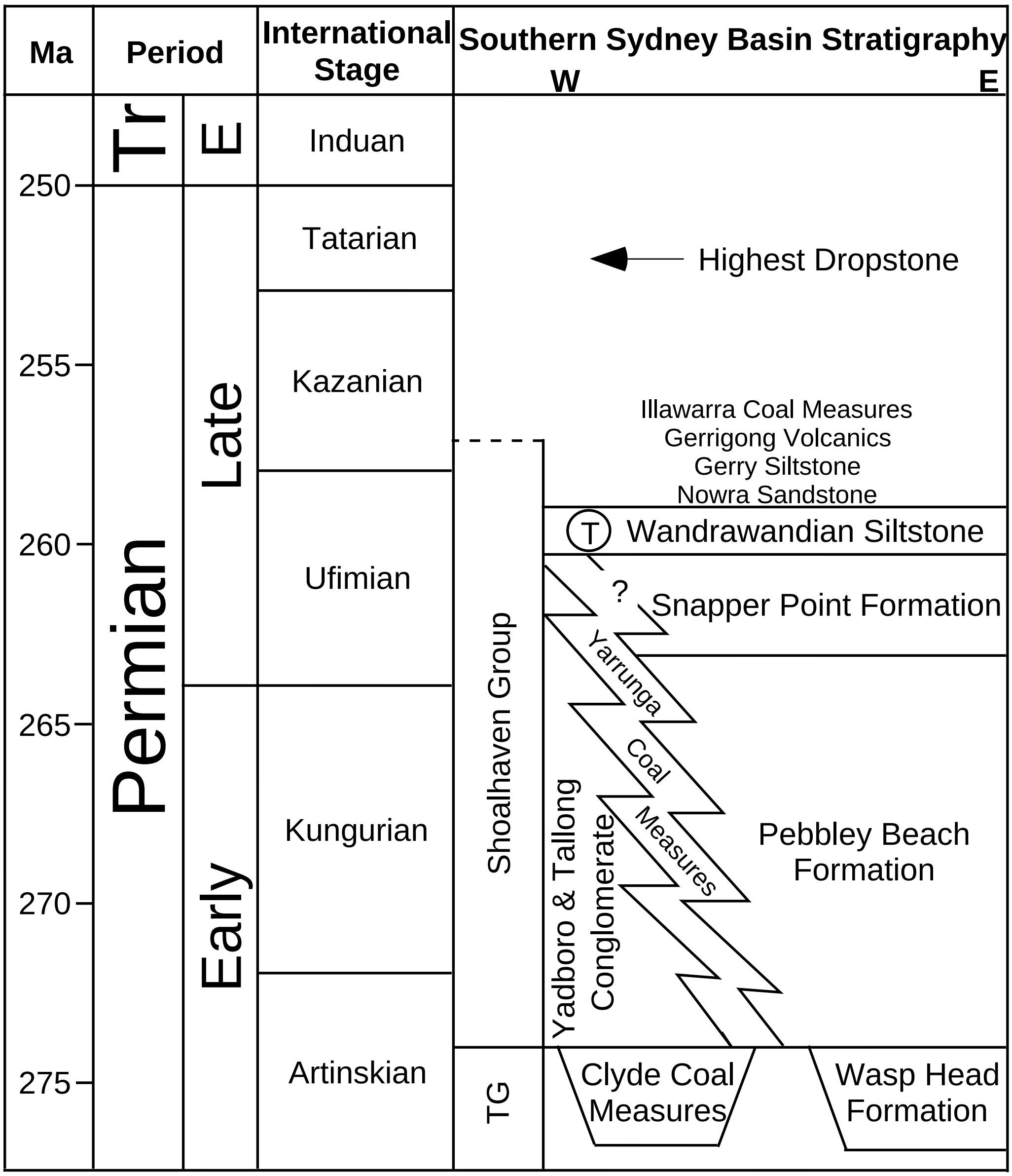

Figure 5.2: Stratigraphic units of the southern Sydney Basin (adapted from Eyles et al., 1998 after Tye et al., 1996). Period and stage dates are from Veevers (2000b) after Roberts et al. (1996). The base of the Wasp Head Formation has been dated at 277 Ma (Runnegar, 1980; Eyles et al., 1998). A tephra (marked by T) in the middle of the Wandrawandian Siltstone has been dated at 260 Ma (Veevers et al., 1994b; Eyles et al., 1998). All other formation boundaries are provisional.

Recently, this timescale was updated (Veevers, 2000b). The revisions are based upon SHRIMP zircon dating of the Permian System of eastern Australia (Bowen and Sydney Basins) (Roberts et al., 1996). When the absolute dates of 277 Ma and 260 Ma are considered in reference to the updated timescale, the ages of the Talaterang and Shoalhaven Groups correspond to younger stages than previously believed. According to the updated timescale, the Wasp Head Formation is Artinskian, the Pebbley Beach Formation is Artinskian to Ufimian, and the Snapper Point Formation and Wandrawandian Siltstone are Ufimian (Figure 5.2). The comparison of these ages with known palynomorph stages has yet to be fully addressed.

METHODS

Four sections from the Pebbley Beach Formation, ranging in thickness from 8 to 25 m, were logged on a bed-by-bed basis for lithology, fossils (trace and body), sedimentary structures, and vertical and lateral facies changes. Sections were correlated, giving a total stratigraphic column of approximately 45 m.

Gamma-ray measurements were collected from each outcrop at a 0.25 m spacing (Appendix 13) and plotted against the associated lithological log. Spectral analyses were performed on the composite gamma-ray dataset to characterize cyclicity in a quantitative fashion. As a cross-check on the results, two spectral analysis programs ("Timeseries" and "AnalySeries") were used. To determine the role that Milankovitch-forcing played in the formation of depositional cyclicity, results from the spectral analyses were compared with known mid-Permian orbital periodicities.

FACIES ASSOCIATIONS

For this study, deposits of the Pebbley Beach Formation were divided into three major facies associations. Short but highly detailed sedimentological logs with associated gamma-ray data are shown in Figures 5.3-5.6. The four measured sections were correlated (Figure 5.7), resulting in a total stratigraphic column of approximately 45 m (Figure 5.8).

Facies Association 1 (swaley and trough-cross-stratified sandstone)

Facies Association 1 (FA 1) is composed predominantly of swaley and trough cross-stratified sandstone (Figure 5.9a). These sandstones often contain a mixed pelycypod-bryozoa-brachiopod fauna, including the epifaunal suspension-feeder

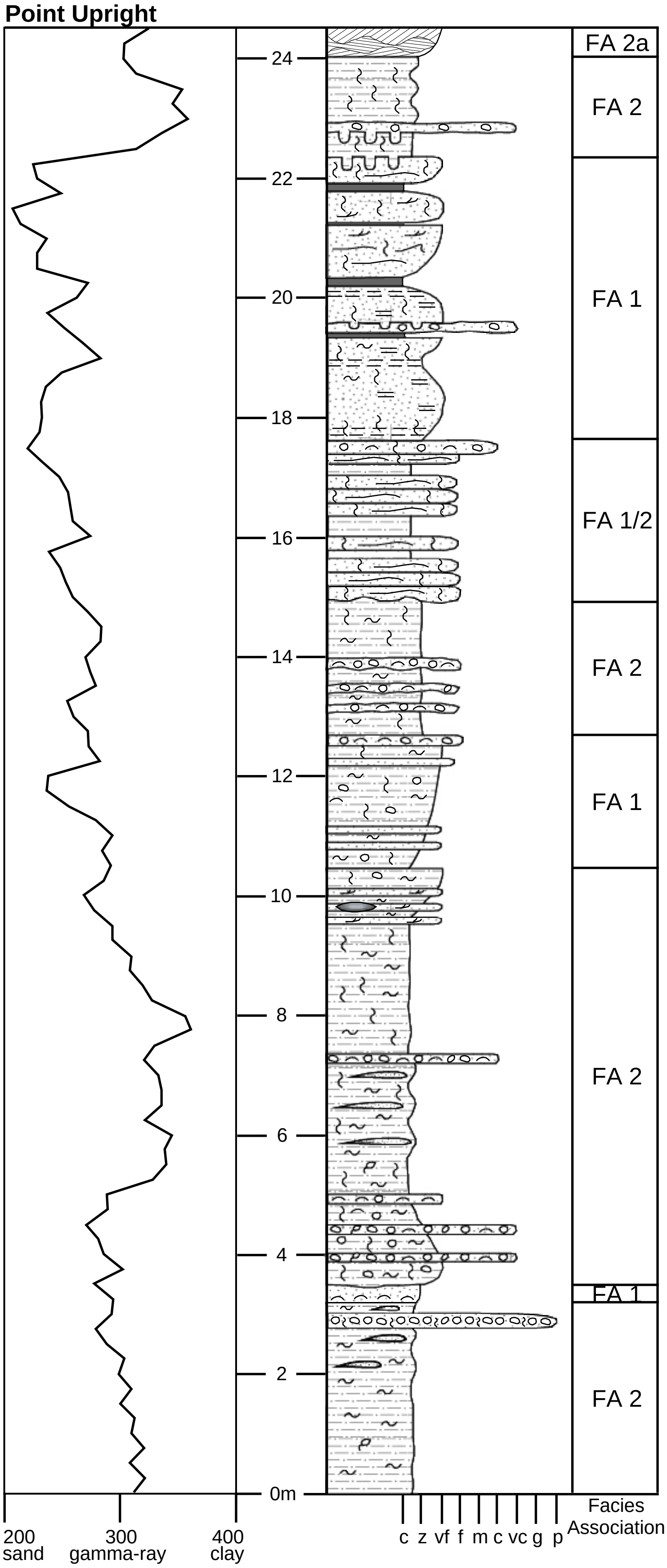

Figure 5.3a: Lithology log with associated gamma-ray data and environmental interpretations (facies associations) from Point Upright (Location 3 on Figure 5.1). The base of the measured section is located at 56H 0257462/UTM 6052561 (using the Australian Geodetic Datum 1966 coordinates). Grainsize increments listed from left to right on x-axis of lithology log are as follows: c (clay/mud); z (silt); vf (very fine sand); f (fine sand); m (medium sand); c (coarse sand); vc (very coarse sand); g (gravel); p (pebble). See Figure 5.3b for key.

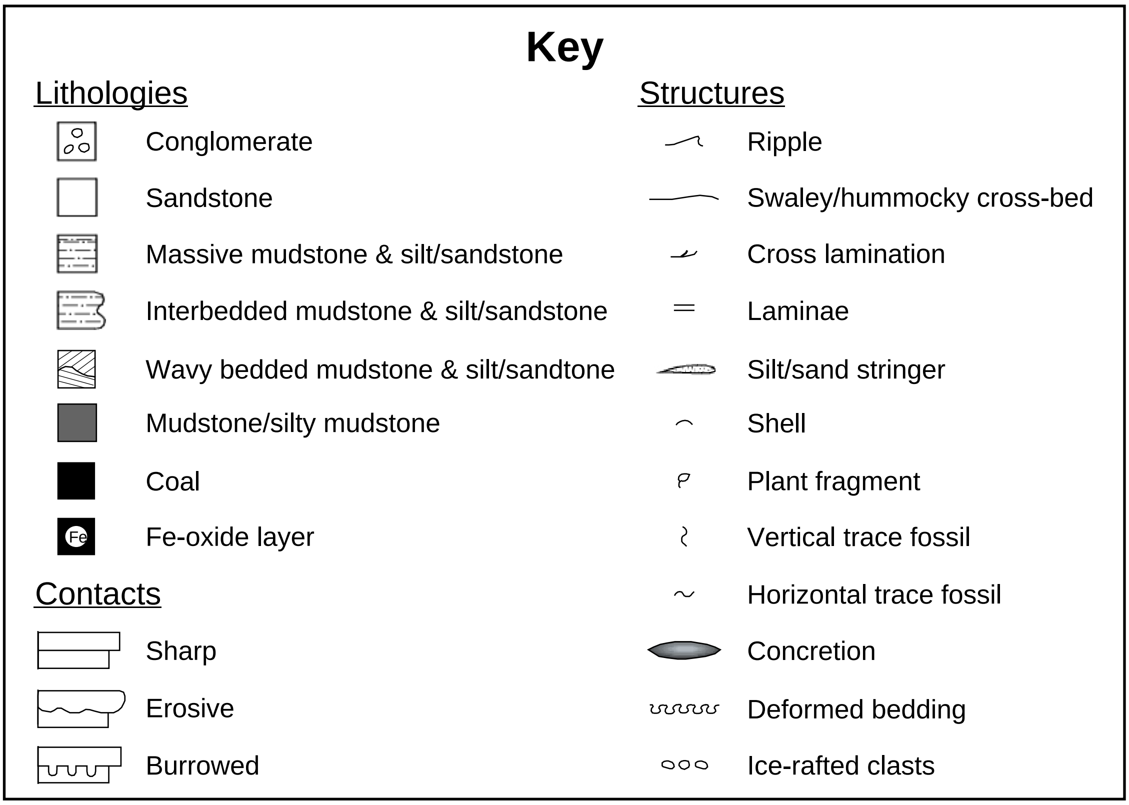

Figure 5.3b: Key for all measured sections in Chapter 5.

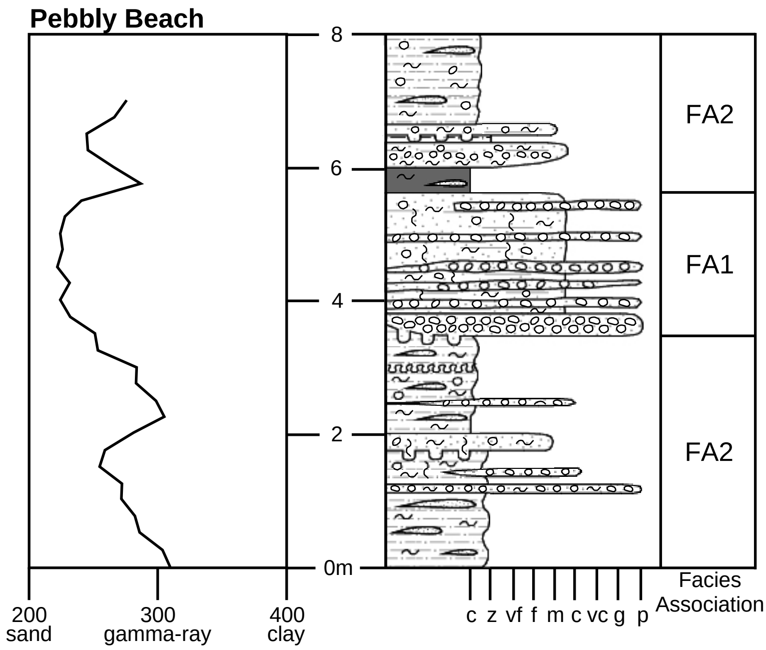

Figure 5.4: Lithology log with associated gamma-ray data and environmental interpretations (facies associations) from south of Pebbly Beach (Location 4 on Figure 5.1). The base of the measured section is located at 56H 0257527/UTM 6055617 (using the Australian Geodetic Datum 1966 coordinates). Key as in Figure 5.3b.

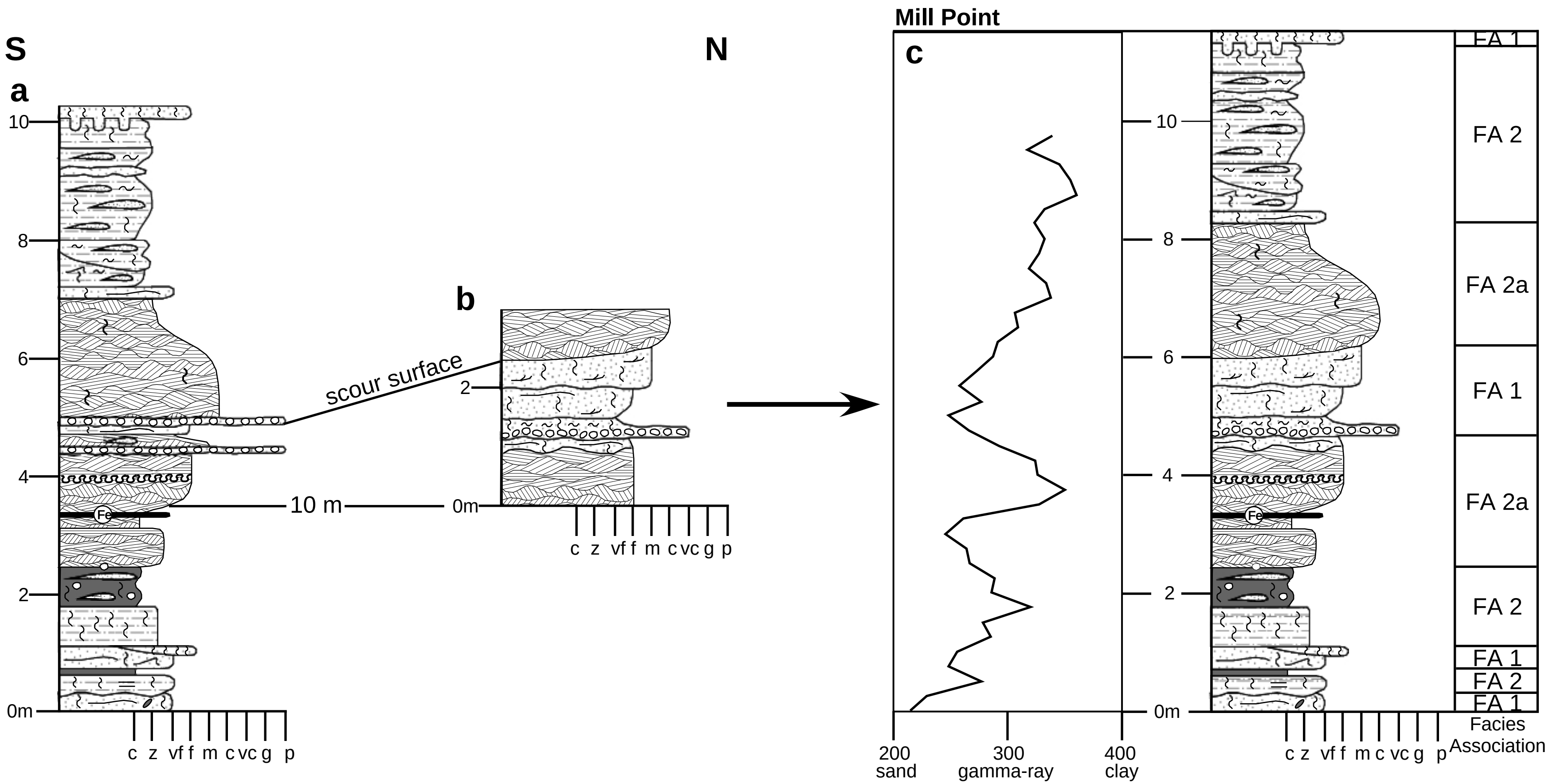

Figure 5.5: Lithology log with associated gamma-ray data and environmental interpretations (facies associations) from Mill Point (Location 5 on Figure 5.1). The base of section (a) is located at 56H 0258351/UTM 6055867 (using the Australian Geodetic Datum 1966 coordinates). A major scour event removed part of the original sediments at the 5 m mark in section (a). At the tip of Mill Point (section b), the scour occurs at a higher stratigraphic level, revealing a more complete record of deposition. Section (c) is the composite log that resulted from the combination of sections (a) and (b). Key as in Figure 5.3b.

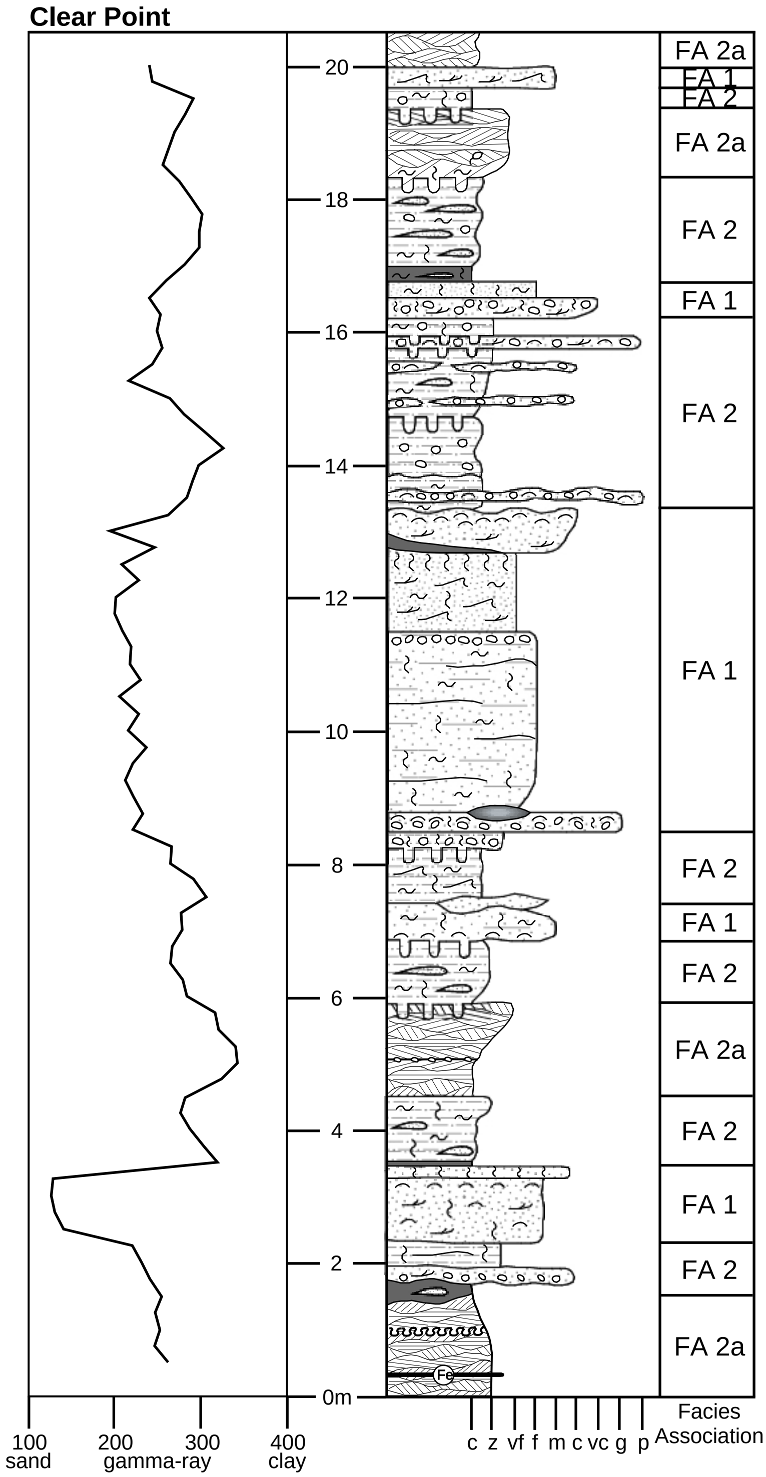

Figure 5.6: Lithology log with associated gamma-ray data and environmental interpretations (facies associations) from Clear Point (Location 6 on Figure 5.1). The base of the measured section is located at 56H 0258658/UTM 6056430 (using the Australian Geodetic Datum 1966 coordinates). Key as in Figure 5.3b.

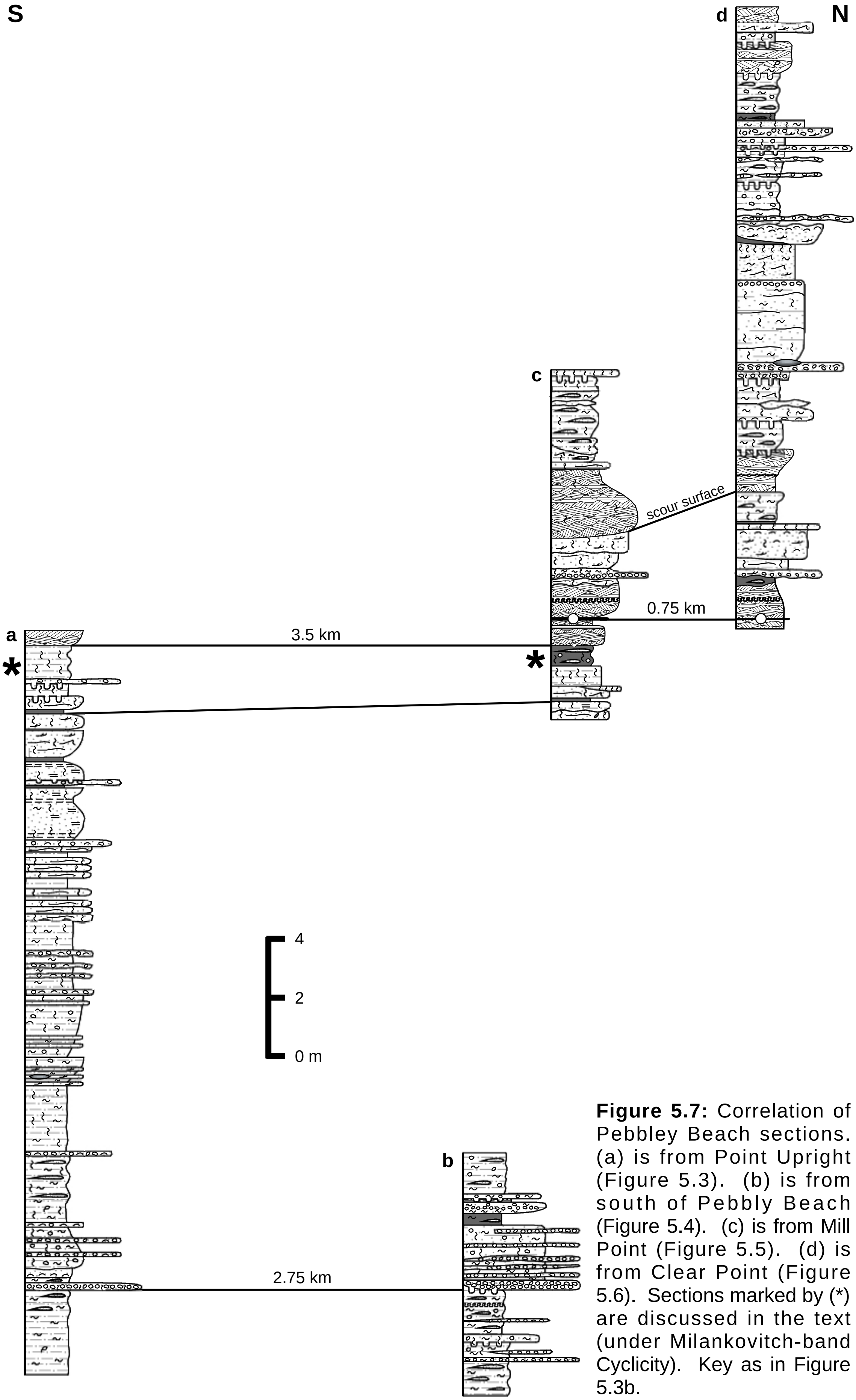

Figure 5.7: Correlation of Pebbley Beach sections. (a) is from Point Upright (Figure 5.3). (b) is from south of Pebbly Beach (Figure 5.4). (c) is from Mill Point (Figure 5.5). (d) is from Clear Point (Figure 5.6). Sections marked by (*) are discussed in the text (under Milankovitch-band Cyclicity). Key as in Figure 5.3b.

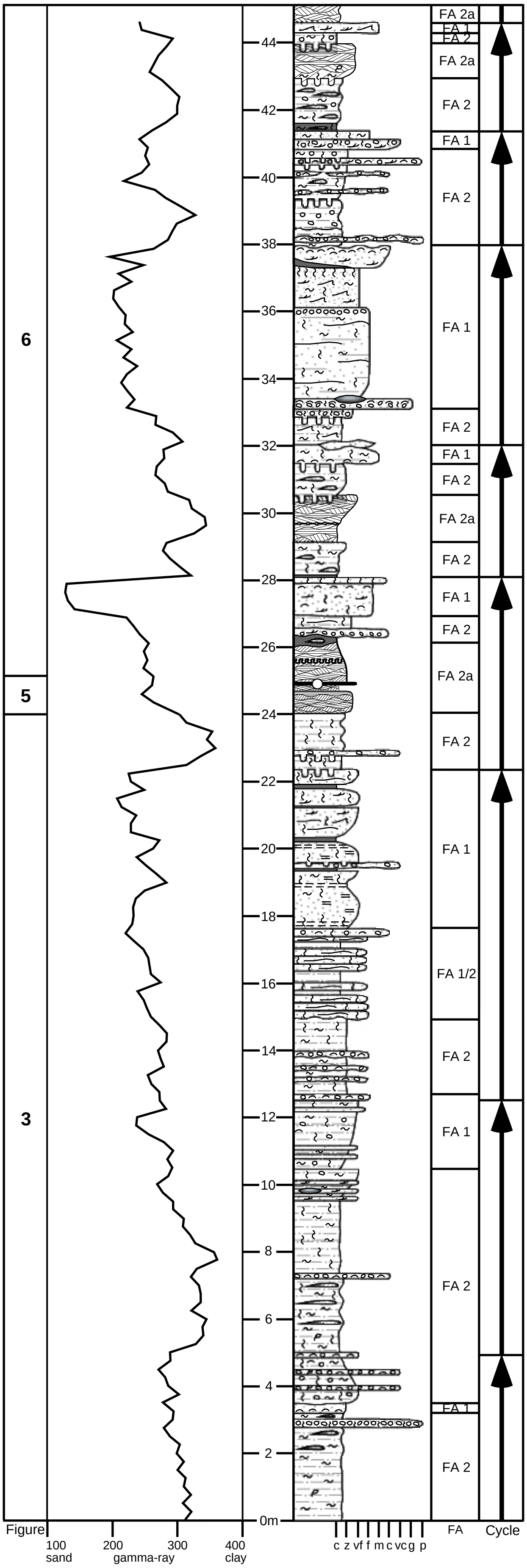

Figure 5.8: Composite Pebbley Beach lithological log with associated gamma-ray data and environmental interpretations (facies associations). The left-hand column, labeled "Figure," denotes the location/figure from which that part of the column is derived. The right-hand column, labeled "Cycle," marks a series of shallowing- and coarsening-upward cycles that are based upon the combined lithology and gamma-ray data. Key as in Figure 5.3b.

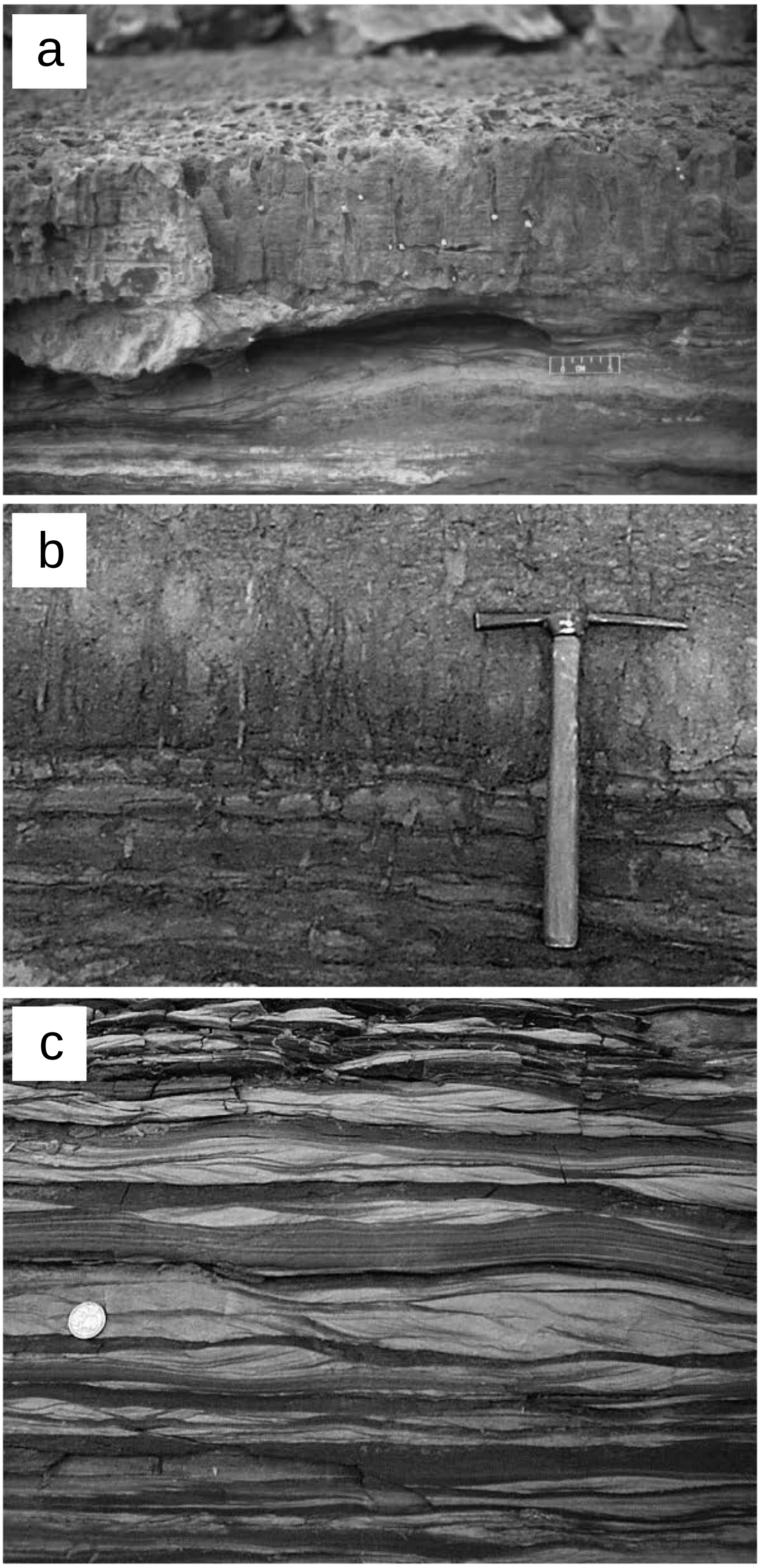

Figure 5.9: Dominant facies of the Pebbley Beach Formation. (a) is a typical swaley cross-stratified sandstone of Facies Association 1 from the Mill Point section (Figure 5.5/Location 5): 56H 0258351/UTM 6055867 (using the Australian Geodetic Datum 1966 coordinates). Note the *Skolithos* ichnofacies. Scale is 5 cm. (b) is a typical bioturbated muddy siltstone of Facies Association 2 from the Pebbly Beach section (Figure 5.3/Location 3): 56H 0257462/UTM 6052561 (using the Australian Geodetic Datum 1966 coordinates). Note that the *Cruziana* ichnofacies has nearly destroyed all traces of bedding. (c) is a typical wavy-bedded muddy sandstone of Facies Association 2a from the Mill Point section (Figure 5.5/Location 5): 56H 0258351/UTM 6055867 (using the Australian Geodetic Datum 1966 coordinates).

Eurydesma. Both in-situ life assemblages and death assemblages are present. Bed tops are sparsely to commonly bioturbated by a *Skolithos* ichnofacies. These sands are interbedded with wave-rippled sandstone, hummocky cross-stratified sandstone, and minor mudstone. Lonestones and diamictites are common (see description below).

Facies Association 2 (bioturbated muddy siltstone and sandstone)

Facies Association 2 (FA 2) includes muddy siltstone/sandstone, silty mudstone, and finely laminated black mudstone (Figure 5.9b). This association is often bioturbated by a *Cruziana* ichnofacies. Typically, all original sedimentary structures in the muddy silt/sandstone are destroyed by bioturbation, leaving a mottled appearance. Where bioturbation has not completely obliterated bedding, a crude textural banding is apparent. This banding consists of cm-scale beds of light colored, hummocky cross-stratified sand-rich units and bioturbated, dark colored mud-rich units. Fine sandstone laminae and glendonites occur in the laminated mudstone. Lonestones and diamictites are common (see description below).

Facies Association 2a (wavy-bedded muddy sandstone)

Facies Association 2a (FA 2a) consists of wavy-bedded muddy silt/sandstone with more-massive silty mudstone and minor coal stringers (Figure 5.9c). This association is sparsely bioturbated by a *Cruziana* ichnofacies and contains coalified wood fragments. The wavy-bedded muddy silt/sandstones record apparent bi-directional paleocurrents preserved by trough cross-stratification. These deposits locally fill large U-shaped scour channels that are discussed in more detail below (Major Erosional Surfaces). Lonestones and diamictites are rare.

Lonestones and diamictites

Lonestones and diamictites (Figure 5.10) occur throughout most facies of the Pebbley Beach Formation. These outsized clasts vary in size from sand particles to boulders measuring several meters in diameter. They range from well-rounded to angular and are composed of local and extra-basinal lithologies such as gneiss, granite, phyllite, quartzite, rhyolite, schist, and slate. Larger clasts deform underlying facies and they are draped by overlying strata. Rare striated clasts are present.

Diamictites occur as small clusters and laterally continuous layers. They range in thickness from a few centimeters (single clast) to over 1 m. Some beds and clusters

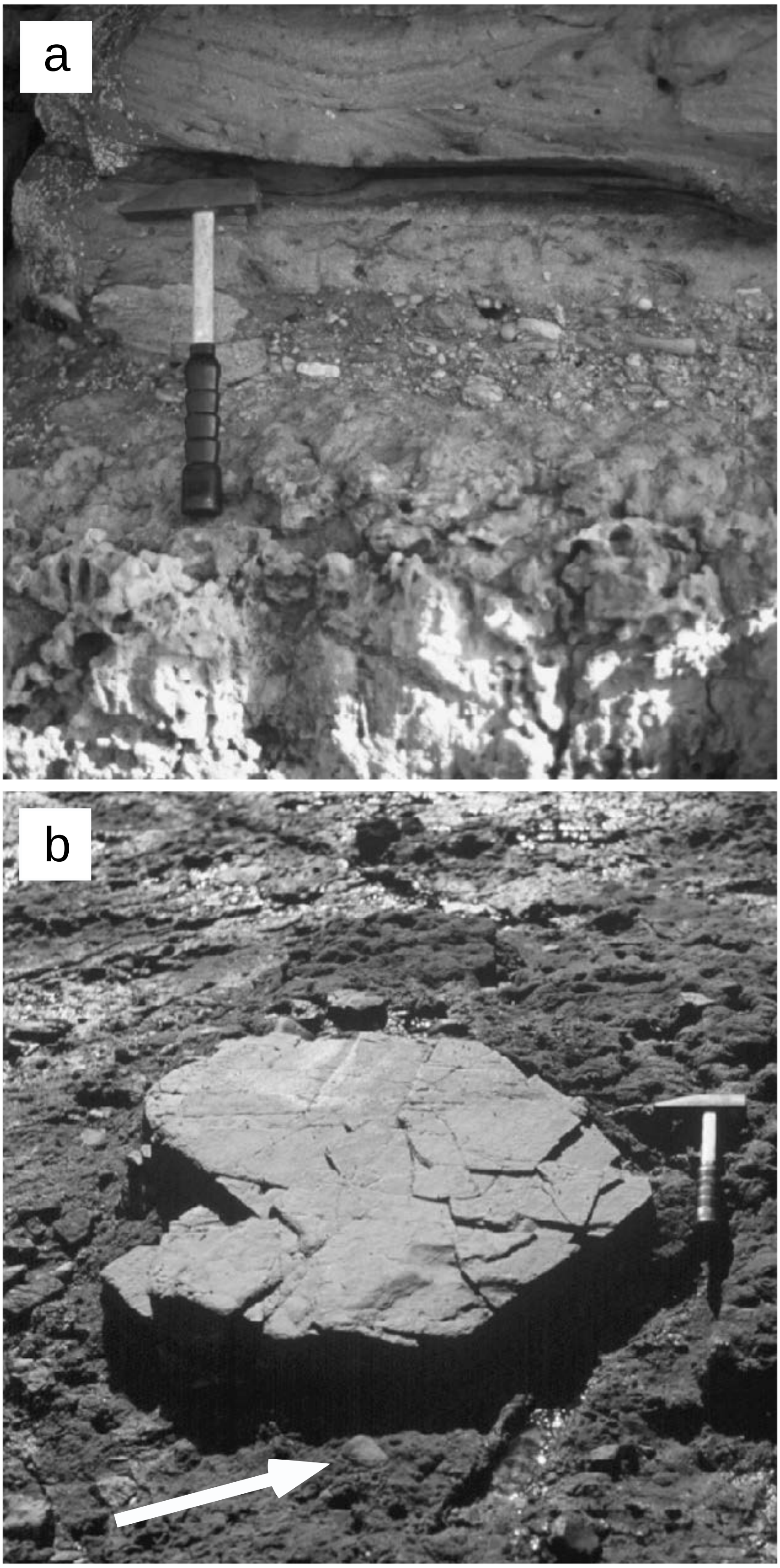

Figure 5.10: Ice-rafted debris occurs throughout the Pebbley Beach Formation as lonestones and diamictites. (a) shows a typical diamictite below a trough cross-stratified sandstone. Photograph taken at 56H 0271321/UTM 6087697 (using the Australian Geodetic Datum 1966 coordinates). (b) illustrates the diverse range of clast size: sand and gravel (marked by arrow) alongside a larger clast measuring 0.5 m in diameter. Photograph taken at 56H 0257527/UTM 6055617 (using the Australian Geodetic Datum 1966 coordinates).

contain disarticulated bivalve shells. Beds and clusters tend to have sharp bases and highly irregular upper surfaces that are often bioturbated from above.

MAJOR EROSIONAL SURFACES

Major erosional surfaces with relief up to 4 m occur locally in the Shoalhaven Group (Eyles et al., 1997, 1998). In outcrop, these surfaces have broad U-shaped cross-sections (up to tens of meters wide) and are often veneered by outsized clasts. One of these erosional surfaces occurs in the measured section at Mill Point (Figures 5.5 and 5.11). This undulatory surface truncates an underlying sequence of coarsening-upward sediments. The "scour" is filled with a series of thin (up to 2 m) erosionally-based packages of FA 2a (wavy-bedded muddy sandstone). In places, the wavy-bedded muddy sandstone units (FA 2a) above the "scour" sit unconformably on bioturbated swaley and trough cross-stratified sandstones (FA 1) below the "scour." In other places, the erosional surface cuts more deeply into the underlying sequence placing the upper wavy-bedded muddy sandstone units (FA 2a) unconformably on older wavy-bedded muddy sandstone units (FA 2a). Underlying this erosional surface, a zone of soft-sediment deformation is apparent in some areas. This deformed zone consists of a series of concave-upward sand pillows separated by near-vertical pipes of mud (Figure 5.11b).

DEPOSITIONAL INTERPRETATION

The three facies associations identified in the Pebbley Beach Formation record a variety of depositional settings ranging from shoreface to inner shelf. Environmental interpretations are shown on the sedimentological logs (Figures 5.3-5.6 and 5.8).

Facies Association 1

FA 1 (Figure 5.9a) accumulated in a storm-dominated shoreface setting. The presence of *Eurydesma* indicates a cold depositional environment (Runnegar, 1979). Coarse debris was deposited from floating ice.

Facies Association 2

FA 2 (Figure 5.9b) records sedimentation in a storm and ice influenced, muddy, inner shelf environment. Laminated mudstone represents the deepest depositional

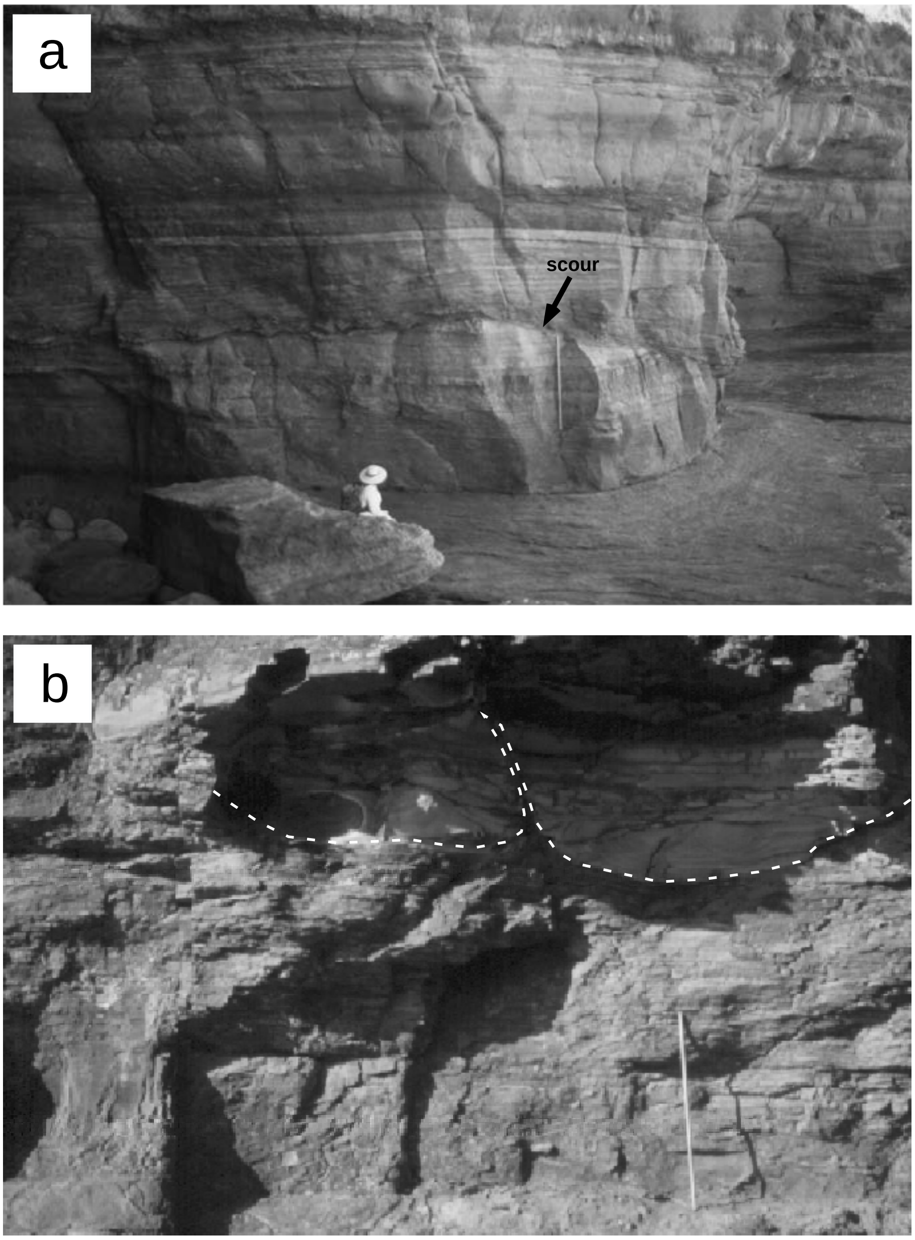

Figure 5.11: Major erosional surface at Mill Point (Figure 5.5/Location 5): 56H 0258351/UTM 6055867 (using the Australian Geodetic Datum 1966 coordinates). This scour may record an episode of iceberg grounding. (a) shows the erosional surface cutting into underlying sediments of a coarsening-upward sequence. (b) shows a zone of deformation underlying the scour surface. Note the concave-upward sand pillows separated by a near-vertical pipe of mud. The scale in both photographs is 1.5 m.

facies. Glendonites indicate deposition in a near freezing, still water environment (Suess et al., 1985; Carr et al., 1989).

Facies Association 2a

FA 2a (Figure 5.9c) includes the most enigmatic deposits of the Pebbley Beach Formation. Gostin and Herbert (1973) and Tye et al. (1996) interpreted the wavy-bedded muddy sandstones of FA 2a to be tidal-flat deposits. However, Eyles et al. (1998) preferred a deeper marine setting for these sediments. They suggest that the muddy sands are the result of oscillatory, wave-driven currents close to storm wave base. This would make the sediments of FA 2a some of the deepest deposits in the Pebbley Beach Formation. Eyles et al. (1998) based their interpretation upon the lateral extent and continuity of the depositional units combined with the absence of other shallow-water features (e.g. narrow incised tidal channels, mud intraclasts, desiccation cracks, fluvial and/or coastal plain deposits).

Based upon the above arguments and the stratigraphic relationship of facies (FA 2a typically occurs between an upper and lower package of FA 2: Figure 5.8), it is here agreed that these sediments are unlikely to be tidal-flat deposits. However, it is equally unlikely that these sediments record deposition in a significantly more shore-distal environment than the sediments of FA 2. Based upon gamma-ray emissions (Figure 5.8), the deposits of FA 2a appear to be lithologically similar to the deposits of FA 2. Additionally, it is doubtful that the wavy-bedded muddy sandstones could have been deposited on an open shelf near storm-wave base. If that was the case, high-angle erosional surfaces would be expected. Instead, the sediments tend to be laterally continuous. This evidence suggests that the wavy-bedded muddy sandstones of FA 2a were probably deposited in a similar shelfal position to the sediments of FA 2. However, the wavy-bedded muddy sandstones may record deposition in a more protected environment than the sediments of FA 2. Such an environment would have allowed the influence of tides to be dominant over the influence of waves, thereby providing a mechanism of formation for the observed bi-directional sedimentary structures.

Lonestones and Diamictites

Lonestones and diamictites of the Pebbley Beach Formation (Figure 5.10) have been previously interpreted as ice-rafted debris (Gostin and Herbert, 1973; Tye et al.,

1996) deposited from icebergs (Crowell and Frakes, 1971; Herbert, 1980b; Eyles et al., 1998).

Major Erosional Surfaces

Eyles et al. (1998) suggested that the major erosional surface at Mill Point (Figure 5.11) was created by wave and current scour in relatively shallow water. It is also possible that the scour resulted from shoreface erosion during sea level rise. However, Eyles et al. (1997) interpreted a similar erosional surface in the Snapper Point Formation (at Snapper Point: Figures 5.1 and 5.2) to be the result of the grounding of floating ice on the sea floor. The scour at Snapper Point is similar to the scour at Mill Point in that it truncates underlying deposits, is veneered by coarser-grained sediments, and has an underlying zone of deformation. Unlike the erosional surface at Mill Point, the erosional surface at Snapper Point is of low relief. However, this does not exclude the possibility that the Mill Point scour may have been formed by iceberg grounding. Eden and Eyles (2001) report that iceberg scours are typically 1-2 m deep but can be up to 30 m deep in exceptional cases. Therefore, it is suggested that the scour at Mill Point may represent an episode of iceberg grounding.

DEPOSITIONAL CYCLICITY

Sedimentation in the Pebbley Beach Formation is dominated by the deposition of repetitive, coarsening-upward cycles (Figure 5.12). In its most complete state, a typical Pebbley Beach cycle (Figure 5.13) is marked by a thin mudstone to silty mudstone unit at its base (FA 2). This unit coarsens upward into interbedded muds and silts that are usually bioturbated by a *Cruziana* ichnofacies (FA 2). Above the interbedded muds and silts, a package of wavy-bedded muddy silt/sandstone (FA 2a) often occurs. This package typically grades upward into another unit of bioturbated, interbedded muds and silts (FA 2). Cycles are usually capped by swaley and trough cross-stratified sands with a *Skolithos* ichnofacies and marine fossils (FA 1).

Superimposed upon the deposition of the repetitive, coarsening-upward cycles is the occurrence of lonestones and diamictites (Figure 5.8). In the Pebbley Beach Formation, individual ice-rafted clasts and layers occur rarely to abundantly in all facies (Figure 5.13). The deposition of these lonestones and diamictites appears to be non-cyclic

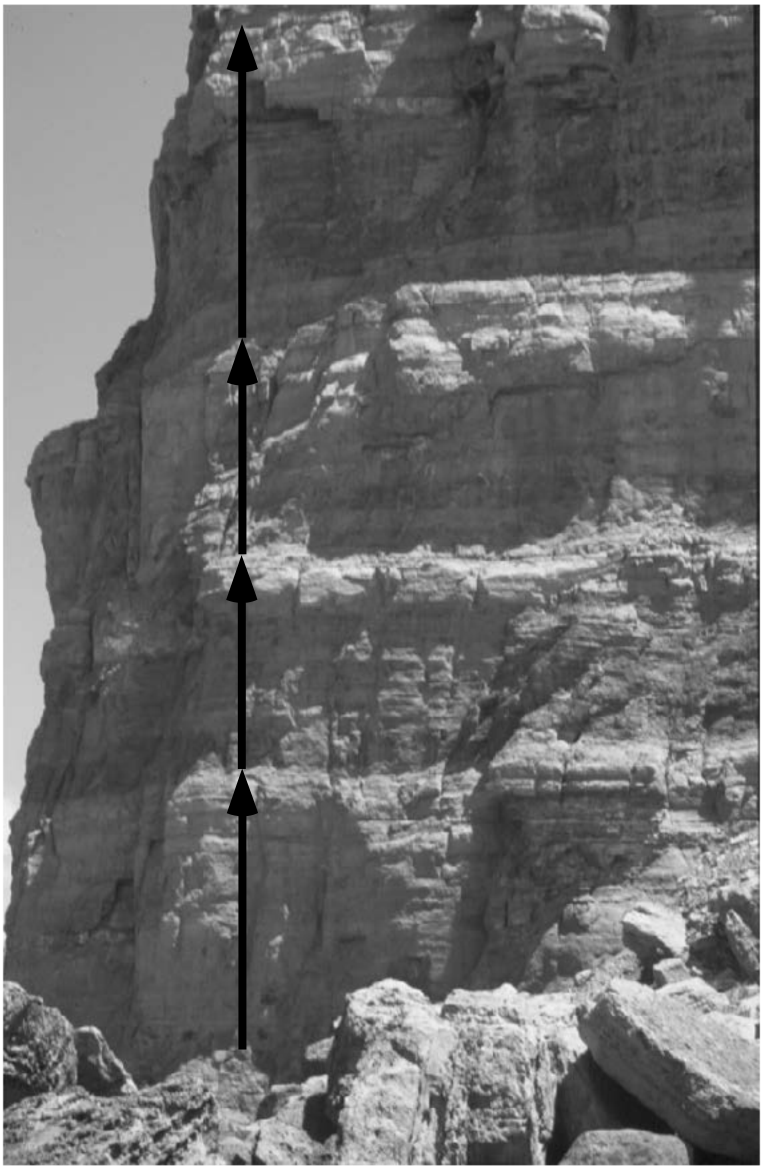

Figure 5.12: Four shallowing- and coarsening-upward cycles from Point Upright (Figure 5.3/Location 3): 56H 0257462/UTM 6052561 (using the Australian Geodetic Datum 1966 coordinates). Each cycle, marked by an upward-pointing arrow, is approximately 7 m thick. This section is equivalent to the lower 28 m of Figure 5.8.

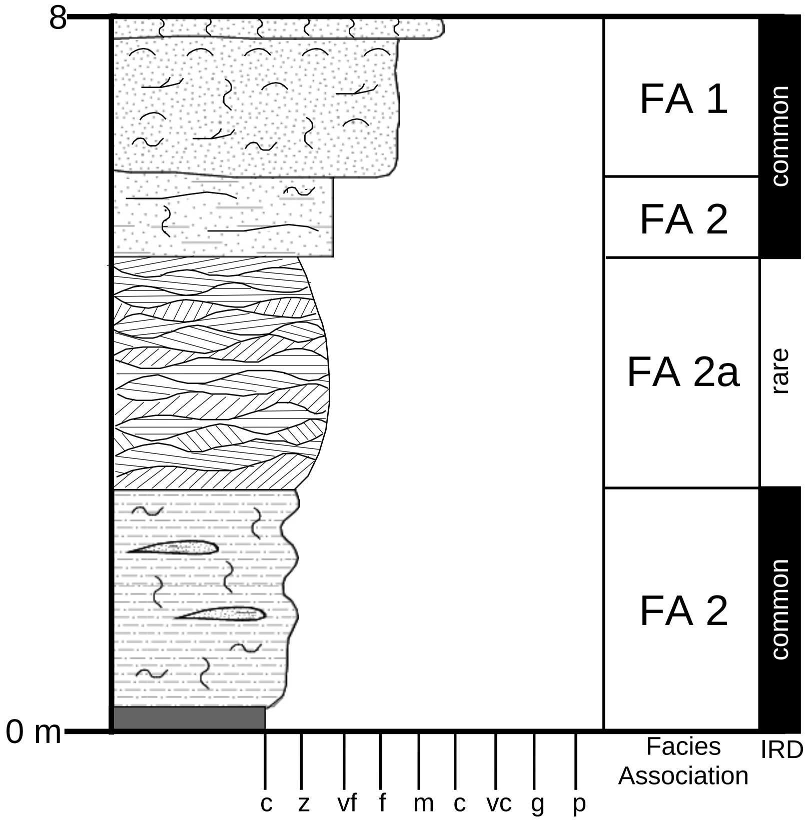

Figure 5.13: A typical Pebbley Beach cycle with associated environmental interpretations (facies associations). The likely occurrence of ice-rafted debris (IRD) is marked for each Facies Association (FA). Key as in Figure 5.3.

Figure 5.8 demonstrates the repetitive nature of Pebbley Beach cycles. Inner shelf deposits of FA 2 and 2a repeatedly shallow and coarsen upward to the shoreface deposits of FA 1. This same trend can be seen on the composite gamma-ray log (Figure 5.8). Upward-pointing arrows in Figure 5.8 denote eight successive coarsening-upward cycles. Complete cycles occur in the upper half of the composite section (Figure 5.8). In the lower half, FA 2a is absent indicating that an open-shelf environment prevailed during this time. Cycle boundaries are based upon the combined lithological and gamma-ray data. These boundaries are often marked by an abrupt drowning event that places muddy inner shelf deposits with higher gamma-ray values on top of sandy shoreface deposits with lower gamma-ray values. The lower 28 m of Figure 5.8 are approximately equivalent to the four cycles shown in Figure 5.12.

SPECTRAL ANALYSIS

Spectral analysis is an objective, statistical method for detecting cyclicity in a dataset. It is particularly useful because it is able to differentiate regular cycles from random events. The composite gamma-ray log from the Pebbley Beach Formation (Figure 5.8) was analyzed for cyclicity using two spectral analysis programs (Figure 5.14). Results generated by "Timeseries" (Weedon and Read, 1995) are shown in Figure 5.14a. Results generated by "AnalySeries 1.1" (Paillard et al., 1996), are shown in Figure 5.14b. Peaks in the spectra (Figures 5.14a and 5.14b) represent cycles recorded in the rock record. The reciprocal of the frequency for each peak is equal to its average cycle period in meters. Spectral peaks generated by the two programs were compared, averaged, and used to determine the periodicities of all significant cycles (Figure 5.14c). For example, the 9.0 m cycle in Figure 5.14a was averaged with the 8.0 m cycle in Figure 5.14b to obtain an average cycle thickness of 8.5 m (Figure 5.14c). According to these analyses, several orders of cyclicity with average periods of 19.7 m, 8.5 m, 4.9 m, 3.2 m, 1.8 m and 1.3 m are recorded in the Pebbley Beach deposits.

MILANKOVITCH CYCLICITY

Milankovitch cycle is a term used to describe any cycle that is caused by changes in Earth's orbital elements. Milankovitch-scale cyclicity is often recorded in the rock record as high-frequency sedimentary cycles (i.e. cyclothems: Abbott and Carter, 1994). This is possible because cyclic changes in Earth's orbit cause climatic fluctuations that affect the distribution of radiation reaching Earth's atmosphere. These

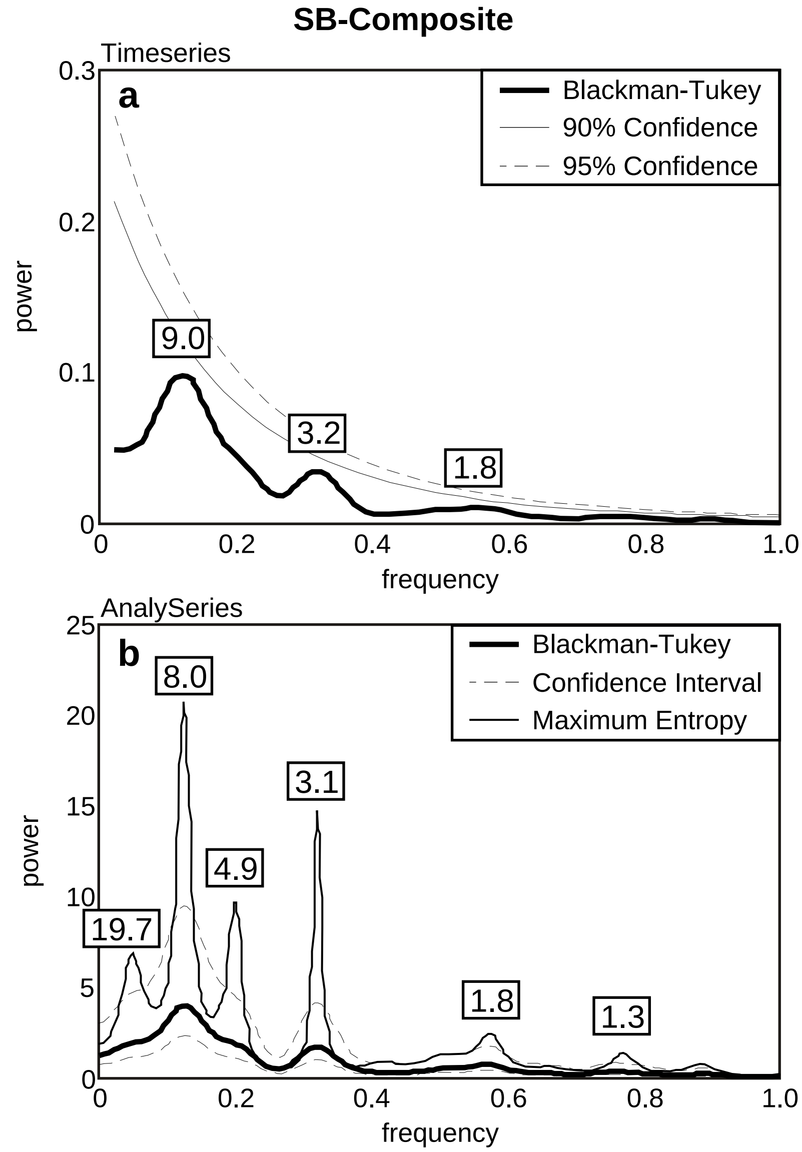

c

Cycle Thickness	SB-Composite Ratios
19.7 meters	2.3:1
8.5 meters	1
4.9 meters	1:1.7
3.2 meters	1:2.7
1.8 meters	1:4.7
1.3 meters	1:6.5

Figure 5.14: Spectral analyses of gamma-ray data from the composite Pebbley Beach section. Data were analyzed using two spectral programs as a cross-check on results. (a) displays spectrum (calculated using the Blackman-Tukey method) with 90% and 95% confidence lines. Results produced by "Timeseries" program. (b) displays two spectra (one with associated confidence interval, calculated using the Blackman-Tukey method; the second calculated using the maximum entropy method). Results produced by "AnalySeries 1.1" program. In (a) and (b), peaks in the spectra mark cycles. Average cycle periods are listed in rectangles above spectral peaks. (c) lists dominant cycles detected by the spectral analyses and their conversion into ratios relative to the 8.5 m cycle.

fluctuations can be directly linked to the waxing and waning of glaciers (Berger and Loutre, 1994). The total volume of Earth's glacial ice varies inversely with global sea-level. As global sea-level fluctuates, coarsening- or fining-upward cycles can be deposited in any given location.

Modern orbital parameters are well established with periodicities of approximately 410,000 years (elongated eccentricity), 100,000 years (eccentricity), 41,000 years (obliquity), and 19,000 to 23,000 years (precession) (Berger, 1988; DeBoer and Smith, 1994). However, the values for obliquity and precession have slowly changed throughout geologic time because the Earth-Moon-Sun rotational system is not static. During the mid-Permian, obliquity is retrodicted to have had a periodicity with dual components of 44,000 and 35,000 years. Precession is retrodicted to have had a periodicity with dual components of 21,000 and 17,600 years. The periodicities for eccentricity (100,000 years) and elongated eccentricity (410,000 years) have remained relatively constant (Berger and Loutre, 1994).

Since the periodicities of the Pebbley Beach cycles are spatial (given in meters) and the periodicities of the mid-Permian orbital parameters are temporal (given in years), they cannot be directly compared. To effectively compare the two sets of numbers, each must first be converted into ratios. For the Pebbley Beach cycles, this conversion is shown in Figure 5.14c. For example, if the 8.5 m cycle is assumed to equal one, the number of 4.9 m cycles in each 8.5 m cycle is 1.7 (8.5 ÷ 4.9 = 1.7). The mid-Permian orbital periodicities were converted into ratios by assuming that the 100,000 year cycle is equal to one. For example, the number of 44,000 year cycles in each 100,000 year cycle is equal to 2.3 (100,000 ÷ 44,000 = 2.3). The complete listing of the mid-Permian Milankovitch ratios is given in the second line of Table 5.1.

In addition to listing the mid-Permian orbital periodicities and their associated ratios, Table 5.1 also lists the ratios for the Pebbley Beach Formation (originally given in Figure 5.14c). Clearly, the Pebbley Beach cycles compare favorably to the Milankovitch periodicities, especially for obliquity and precession. In fact, the only spectral peak that does not correspond with the expected orbital ratio is the one listed under elongated eccentricity. It is possible that this peak may record an apparent 200,000 year cycle (Hinnov, 2000). However, it is more likely that this peak is erroneous due to the short total thickness of the composite measured section (45 m). Since spectral programs search for repetitive cycles, they do not accurately detect periodicities greater than about half the total length of the section.

Periodicities	Elongated	Eccentricity	Obliquity		Precession	
	410,000	100,000	44,000	35,000	21,000	17,600
Expected Milankovitch Ratios	4.1:1	1	1:2.3	1:2.9	1:4.8	1:5.7
Pebbley Beach Ratios	2.3:1	1	1:1.7	1:2.7	1:4.7	1:6.5

Table 5.1: Results of spectral analyses. Line 1 lists Milankovitch orbital parameters with their associated periodicities. Line 2 lists Milankovitch parameters in ratios relative to the 100,000 year cycle. Line 3 lists the ratios of the Pebbley Beach composite gamma-ray data. Note the favorable comparison between the Milankovitch ratios and the Pebbley Beach ratios.

Additionally, the spectral analyses may have been influenced by variations in lithology. For example, in Figure 5.7 the top of column A (marked by *) is siltier than its correlative in column C (also marked by *). Not only are these two intervals lithologically different, they also have distinctly different gamma-ray readings. Therefore, the spectral results could vary depending on how the individual gamma-ray logs (Figures 5.3-5.6) are pieced together to form the composite gamma-ray log (Figure 5.8).

Another consideration is incomplete preservation of the original deposits. Major scour surfaces occur throughout the Shoalhaven Group. As has been discussed, one of these erosional surfaces occurs in the measured section of the Pebbley Beach Formation. Regardless of the mechanism of formation for this scour, it most certainly removed some of the original sediments. Although efforts have been made to present the most complete composite section possible (Figure 5.8), it is likely that some original deposits are missing.

Fortunately, it would be expected that the above factors would mask cyclicity, not enhance it. Therefore, the results of the spectral analyses, combined with the sediments' shallow-marine depositional setting, support the theory that an orbitally-forced, glacio-eustatic driving mechanism is largely responsible for the formation of cyclicity in the Pebbley Beach Formation.

CLIMATIC SIGNIFICANCE

This paper demonstrates that the Pebbley Beach Formation not only contains sediments deposited by floating ice, but also records glacio-eustatic sea-level fluctuations. Based upon paleocurrent data, Eyles et al. (1997, 1998) proposed that the icebergs in the Permian Sydney Basin probably calved from unstable ice margins in Antarctica. If this interpretation is correct and the ages used in Veevers' timescale (2000b) are accurate, Gondwanan glaciation must have persisted into at least the Ufimian stage of the Late Permian.

CONCLUSIONS

Excellent coastal exposures have allowed for detailed measurements and facies interpretations of the Pebbley Beach Formation. Eight vertically stacked, coarsening- and shallowing-upward cycles have been identified in outcrop. Spectral analysis has been used to better define cyclicity in the Pebbley Beach Formation. Identified cycles are consistent with known mid-Permian orbital periodicities. Although depositional cyclicity has been previously recognized in the Shoalhaven Group, this is the first study to demonstrate a quantitative correlation between this cyclicity and the known mid-Permian orbital parameters.

A recently published timescale based upon SHRIMP zircon dating from the eastern coast of Australia (Veevers, 2000b) was used to date these deposits. This timescale indicates that the Pebbley Beach Formation may be slightly younger than previously believed. If the proposed ages are correct, the Shoalhaven Group provides evidence that Permo-Carboniferous glaciation extended into the Late Permian. Therefore, these deposits may record some of the final stages of Gondwanan glaciation.

Concluding Remarks

MAJOR CONCLUSIONS

The purpose of this project was to test for mid- to Late Permian (post-Sakmarian) glacio-eustatic cyclothem development within Australia. This study focuses on the largely unstudied Artinskian Tuckfield Member of the Poole Sandstone (Fitzroy Trough, onshore Canning Basin). Data presented in this thesis demonstrate that the cyclicity which occurs in both shallow-marine and non-marine Tuckfield Member sequences compares favorably with the known mid-Permian earth orbital periodicities of elongated eccentricity, eccentricity, obliquity, and precession (Chapters 2 and 3). This study also demonstrates that the Tuckfield Member cycles (i) are laterally extensive and (ii) compare favorably with correlative shallow-marine cycles from eastern Australia (Artinskian to Ufimian Pebbley Beach Formation, southern Sydney Basin, New South Wales) (Chapters 2 and 5) and elsewhere in the world (Chapter 2). The laterally extensive nature of the Tuckfield Member cycles, combined with their strong correlation to the orbital periodicities and other correlative shallow-marine cycles, indicate that glacio-eustatic sea-level fluctuation probably controlled the formation of depositional cyclicity in the Fitzroy Trough during the Artinskian. Therefore, glaciers must have persisted on Gondwana, or elsewhere, into at least the Artinskian stage of the Early Permian, and probably into the Ufimian stage of the Late Permian as indicated by the New South Wales deposits.

FUTURE WORK

This manuscript provides a comprehensive summary of Artinskian cyclothem development in the onshore Canning Basin, Western Australia. It also provides a brief summary of correlative Artinskian to Ufimian cyclothem development in the southern Sydney Basin, New South Wales. However, it is important to remember that the work discussed in this thesis is only a part of the larger, Australia-wide study initiated by Dr. Steve Abbott. Similar work completed in the Carnarvon Basin has been summarized in several manuscripts (Lever, 2002, 2003a, 2003b) and in an unpublished Ph.D. thesis (Lever 2003c). Similar work in the Tasmanian Basin is currently in progress.

Once research from the Tasmanian Basin is complete, data from all four areas (Canning, Carnarvon, Sydney, and Tasmanian Basins) can be compared and synthesized into one comprehensive dataset. From this Australia-wide data, it may be possible to develop an estimated eustatic sea-level curve for the Permian system of Australia. This localized curve will add further support for the still contentious theory of global sea-level fluctuation. In additon, it may help refine existing Late Paleozoic 3rd-order sea-level charts (e.g. Ross and Ross, 1985, 1987). This data could be significant because the present Permian eustacy charts are predominantly based upon stable cratonic successions in North America (Ross and Ross, 1995). Ross and Ross (1995) themselves recognized the importance of the Permian successions in Australia when they wrote: "…Australia has marine and glacial-marine depositional sequences that may eventually help tie sea-level events in high and middle latitudes of Gondwana with those of low latitudes of cratonic North America and the Tethys."

In addition to refining global sea-level charts, the comprehensive dataset may also be used to track the waxing and waning of glaciers and the presence of high-latitude continental ice throughout the Permian. Since much uncertainty still surrounds the timing of glaciation(s) and the frequency of interglacial episodes during the Permo-Carboniferous, this could be a significant scientific contribution. Crowell (1995) suggested that the Carboniferous and earliest Permian was marked by at least 3 distinct episodes of glaciation. Similarly, Dickens (1996) provides convincing evidence that the mid- to Late Permian (post-Sakmarian) was marked by alternating phases of warmer and colder climate. Although Dickens (1996) suggests that glaciation had completely ceased by the end of the Sakmarian, some earlier studies indicate that glaciation may have persisted past this point (e.g. Crowell, 1995; Read, 1995). Work in the Canning Basin suggests that glaciation did indeed continue into the Artinskian stage of the Early Permian. Likewise, work in the Carnarvon Basin suggests that glaciers were present, at least at high-latitudes, during the Kungurian to Ufimian stages (Lever, 2003a). However, neither independent study can alone answer the question of whether or not glacioeustacy consistently affected sedimentation from the Artinskian through the Ufimian and beyond. Therefore, the major questions that remain to be answered are: (i) Did glaciation continuously drive high-frequency, Milankovitch-band, sea-level fluctuation throughout the Permian or are glacio-eustatic sea-level fluctuations confined to the colder climatic periods defined by Dickens? (ii) In either case, do Milankovitch-band, glacio-eustatic sea-level fluctuations persist up to the Triassic boundary and beyond or do they end sometime during the Late Permian? By comparing cyclothem development in the four temporally overlapping successions studied in this Australia-wide project, it may be possible to answer these questions in the near future.

References

REFERENCES

Abbott, S.T. and Carter, R.M. (1994) The sequence architecture of mid-Pleistocene (*c*.1.1-0.4 Ma) cyclothems from New Zealand: facies development during a period of orbital control on sea-level cyclicity. In: *Orbital Forcing and Cyclic Sequences* (Eds. P.L. de Boer and D.G. Smith), *Special Publication of the International Association of Sedimentologist*, 19, 367-394.

Adkins, R.M. (2003) Regressive systems tract cyclicity in shore-zone deposits: sedimentology and stratigraphy of the Lower Permian Tuckfield Member (Poole Sandstone), onshore Canning Basin, Western Australia. *Australian Journal of Earth Sciences,* 50, in press.

Algeo, T.J. and Wilkinson, B.H. (1988) Periodicity of mesoscale Phanerozoic sedimentary cycles and the role of Milankovitch orbital modulation. *Journal of Geology,* 96, 313-322.

Allen, J.R.L. (1964) Studies in fluviatile sedimentation: six cyclothems from the Lower Old Red Sandstone, Anglo-Welsh Basin. *Sedimentology,* 3, 163-198.

Apak, S.N. (1996) Depositional history of the Lower Permian Carolyn Formation and Poole Sandstone in the northern Canning Basin: implications for hydrocarbon potential. *Geological Survey of Western Australia Record* 1996/8.

Apak, S.N. and Backhouse, J. (1998) Redefinition of the Grant Group and reinterpretation of the Permo-Carboniferous Succession, Canning Basin, Western Australia. In: *The Sedimentary Basins of Western Australia: Proceedings of the Petroleum Exploration Society of Australia Symposium* (Eds. P.G. Purcell and R.R. Purcell), 683-694.

Apak, S.N. and Carlsen, G.M. (1996) A compilation and review of data pertaining to the hydrocarbon prospectivity in the Canning Basin. *Western Australia Geological Survey Record* 1996/10.

Astin, T.R. (1990) The Devonian lacustrine sediments of Orkney, Scotland: implications for climate cyclicity, basin structure and maturation history. *Journal of the Geological Society of London*, 147, 141-151.

Barrell, J. (1913) The Upper Devonian delta of the Appalachian geocyncline. *American Journal of Science,* 36, p. 429-472.

Battersby, D.G. (1981) New Discoveries in the Surat/Bowen Basin. *The APEA Journal,* 21, 39-44.

Bentley, J. (1984) Petroleum geology of the central Broome Platform. In: *The Canning Basin W.A.: Proceedings of the Geological Society of Australia/Petroleum Exploration Society of Australia Symposium* (Ed. P.G. Purcell), 157-168.

Berger, A. (1977) Long-term variations of the Earth's orbital elements. *Celestial Mechanics,* 15, 53-74.

Berger, A. (1988) Milankovitch theory and climate. *Review of Geophysics,* 26, 624-657.

Berger, A. and Loutre, M.F. (1994) Astronomical forcing through geological time. In: *Orbital Forcing and Cyclic Sequences* (Eds. P.L. de Boer and D.G. Smith), *Special Publication of the International Association of Sedimentologists,* 19, 15-24.

Blackman, R.B. and Tukey, J.W. (1958) *The measurement of power spectra from the point of view of communication engineering,* Dover Publications, New York, 190 pp.

Boardman, D.R. and Heckel, P.H. (1989) Glacial-eustatic sea-level curve for early Late Pennsylvanian sequence in north-central Texas and biostratigraphic correlation with curve for midcontinent North America. *Geology,* 17, 802-805.

Borer, J.M. and Harris, P.M. (1991) Lithofacies and cyclicity of the Yates Formation, Permian Basin: Implications for Reservoir Heterogeneity. *American Association of Petroleum Geologists Bulletin,* 75(4), 726-779.

Botten, P. (1984) Uranium exploration in the Canning Basin: A case study. In: *The Canning Basin W.A.: Proceedings of the Geological Society of Australia/Petroleum Exploration Society of Australia Symposium* (Ed. P.G. Purcell), 485-501.

Brakel, A.T. and Totterdell, J.M. (1993) The Sakmarian-Kungurian palaeogeography of Australia. In: *Gondwana Eight: Assembly, Evolution, and Dispersal* (Eds. R.H. Findlay, R. Unrug, M.R. Banks, and J.J. Veevers), *Proceedings of the eighth Gondwana symposium,* pp. 385-396. Balkema, Rotterdam.

Brown, S.A., Boserio, I.M., Jackson, K.S., and Spence, K.W. (1984) The geological evolution of the Canning Basin-Implications for petroleum exploration. In: *The Sedimentary Basins of Western Australia: Proceedings of the Petroleum Exploration Society of Australia Symposium* (Eds. P.G. Purcell and R.R. Purcell), 85-96.

Brown, D.A., Cambell, K.S.W., and Crook, K.A. (1968) *The Geological Evolution of Australia and New Zealand.* Pergamon Press, Oxford, 409 pp.

Bush, R.M.Q. and Rollins, H.B. (1984) Correlation of Carboniferous strata using a hierarchy of transgressive-regressive units. *Geology,* 12, 471-474.

Cant, D.J. (1992) Subsurface facies analysis. In: *Facies Models: Response to Sea Level Change* (Eds. R.G. Walker and N.P. James), pp. 27-45. Geological Association of Canada, St. Johns, Newfoundland.

Carey, J. (1978) Sedimentary environments and trace fossils of the Permian Snapper Point Formation, southern Sydney Basin. *Journal of the Geologocal Society of Australia,* 25, 433-458.

Carr, P.F., Jones, B.G., and Middleton, R.G. (1989) Precursor and formation of glendonites in the Sydney Basin. *Australian Mineralogist*, 4, 3-12.

Carter, R.M., Abbott, S.T. and Naish, T.R. (1999) Plio-Pleistocene cyclothems from Wanganui Basin, New Zealand: type locality for an astrochronologic time-scale, or template for recognizing ancient glacio-eustacy? *Philosophical Transactions of the Royal Society, London,* 357, 1861-1872.

Carter, R.M. and Naish, T.R. (1998) A review of Wanganui Basin New Zealand: global reference section for shallow marine, Plio-Pleistocene (2.5-0 Ma) cyclostratigraphy. *Sedimentary Geology,* 122, 37-52.

Clemmensen, L.B., Øxnevad, I.E.I., and De Boer, P.L. (1994) Climatic controls on ancient desert sedimentation: some late Palaeozoic and Mesozoic examples from NW Europe and the Western Interior of the USA. In: *Orbital Forcing and Cyclic Sequences* (Eds. P.L. de Boer and D.G. Smith), *Special Publication of the International Association of Sedimentologist,* 19, 439-457.

Connolly, W.M. and Stanton, R.J. (1992) Interbasinal cyclostratigraphic correlation of Milankovitch band transgressive-regressive cycles: Correlation of Desmoinesian-Missourian strata between southeastern Arizona and the midcontinent of North America. *Geology,* 20, 999-1002.

Crowe, R.W.A. and Towner, R.R. (1976a) Permian stratigraphic nomenclature, Noonkanbah 1:250,000 sheet. *Geological Survey of Western Australia, Annual Report for 1975*, 56-58.

Crowe, R.W.A. and Towner, R.R. (1976b) Environmental interpretation of the Permian Nura Nura Member of the Poole Sandstone, Noonkanbah Sheet Area, Canning Basin: A gradation between fluviatile and shallow-water marine facies. *Geological Survey of Western Australia, Annual Report for 1975,* 59-62.

Crowe, R.W.A. and Towner, R.R. (1977) Definitions of some new and revised rock units in the Canning Basin. *Geological Survey of Western Australia*, *Record* 1976/24.

Crowe, R.W.A. and Towner, R.R. (1981) Noonkanbah, Western Australia: 1:250,000 Geological Series-Explanatory Notes. Australian Government Publishing Service, Canberra.

Crowell, J.C. (1975) The Late Paleozoic glaciation. In: *Gondwana Geology* (Ed. K.S.W. Campbell), pp. 313-331. Australian National University Press, Canberra.

Crowell, J.C. (1978) Gondwanan glaciation, cyclothems, continental positioning, and climate change. *American Journal of Science,* 278, 1345-1372.

Crowell, J.C. (1995) The ending of the Late Paleozoic Ice Age during the Permian Period. In: *The Permian of Northern Pangea, v. 1, Paleogeography, Paleoclimates, Stratigraphy* (Eds. P.A. Scholle, T.M. Peryt and D.S. Ulmer-Scholle), pp. 62-74. Springer-Verlag, Berlin.

Crowell, J.C. and Frakes, L.A. (1971) Late Paleozoic Glaciation: Part IV, Australia. *Geological Society of America Bulletin,* 82, 2515-2540.

De Boer, P.L. and Smith, D.G. (1994) Orbital forcing and cyclic sequences. In: *Orbital Forcing and Cyclic Sequences* (Eds. P.L. de Boer and D.G. Smith), *Special Publication of the International Association of Sedimentologists,* 19, 1-14.

Dickens, J.M. (1985) Late Palaeozoic glaciation. *BMR Journal of Australian Geology and Geophysics,* 9, 163-169.

Dickens, J.M. (1996) Problems of a Late Palaeozoic glaciation in Australia and subsequent climate in the Permian. *Palaeogeography, Palaeoclimatology, Palaeoecology,* 125, 185-197.

Eden, D.J. and Eyles, N. (2001) Description and numerical model of Pleistocene iceberg scours and ice-keel turbated facies at Toronto, Canada. *Sedimentology,* 48, 1079-1102.

Ellyard, E.J. (1984) Oil migration in the northern Canning Basin-A regional review. In: *The Canning Basin W.A.: Proceedings of the Geological Society of Australia/Petroleum Exploration Society of Australia Symposium* (Ed. P.G. Purcell), 359-376.

Eyles, C.H. and Eyles, N. (2000) Subaqueous mass flow origin for Lower Permian diamictites and associated facies of the Grant Group, Barbwire Terrace, Canning Basin, Western Australia. *Sedimentology,* 47, 343-356.

Eyles, C.H., Eyles, N., and Gostin, V.A., (1998) Facies and allostratigraphy of high latitude, glacially influenced marine strata of the Early Permian southern Sydney Basin, Australia. *Sedimentology,* 45, 121-161.

Eyles, C.H., Mory, A.J., and Eyles, N. (2003) Carboniferous-Permian facies and tectonostratigraphic successions of the glacially influenced and rifted Carnarvon Basin, western Australia. *Sedimentary Geology,* 155, 63-86.

Eyles, N., Eyles, C.H., Apak, S.N., and Carlsen, G.M. (2001) Permian-Carboniferous tectono-stratigraphic evolution and petroleum potential of the northern Canning Basin, Western Australia. *American Association of Petroleum Geologists Bulletin,* 85(6), 989-1006.

Eyles, N., Eyles, C.H., and Gostin, V.A. (1997) Iceberg rafting and scouring in the Early Permian Shoalhaven Group of New South Wales, Australia: Evidence of Heinrich-like events? *Palaeogeography, Palaeoclimatology, Palaeoecology,* 136, 1-17.

Eyles, N., Mory, A.J., and Backhouse, J. (2002) Carboniferous-Permian palynostratigraphy of west Australian marine rift basins: resolving tectonic and eustatic controls during Gondwanan glaciations. *Palaeogeography, Palaeoclimatology, Palaeoecology,* 184, 305-319.

Fielding, C.R. and Webb, J.A. (1996) Facies and cyclicity of the Late Permian Bainmedart Coal Measures in the northern Prince Charles Mountains, MacRobertson Land, Antarctica. *Sedimentology*, 43, 295-322.

Frakes, L.A. (1969) Late Paleozoic glaciation: pt 1: South America. *Geological Society of America Bulletin,* 80, 1007-1042.

Galloway, W.E. and Hobday, D.K. (1996) *Terrigenous Clastic Depositional Systems: Applications to Fossil Fuel and Groundwater Resources, 2nd edition,* Springer, Berlin, 489 pp.

Gibson, D. L. (1983) Pender, Western Australia: 1:250,000 Geological Series-Explanatory Notes. Australian Government Publishing Service, Canberra.

Gibson, D.L. and Crowe, R.W.A. (1982) Mount Anderson (2nd edition), Western Australia: 1:250,000 Geological Series-Explanatory Notes. Australian Government Publishing Service, Canberra.

Goldhammer, R.K., Oswald, E.J., and Dunn, P.A. (1994) High-frequency glacio-eustatic cyclicity in the Middle Pennsylvanian of the Paradox Basin: an evaluation of Milankovitch forcing. In: *Orbital Forcing and Cyclic Sequences* (Eds. P.L. de Boer and D.G. Smith), *Special Publication of the International Association of Sedimentologists,* 19, 243-283.

Goldstein, B.A. (1989) Waxings and wanings in stratigraphy, play concepts, and prospectivity in the Canning Basin. *The APEA Journal,* 29(1), 466-508

Gonzalez-Bonorino, G. and Eyles, N. (1995) Inverse relationship between ice extent and the late Paleozoic glacial record of Gondwana. *Geology*, 23, 1015-1018.

Gostin, V.A. and Herbert, C. (1973) Stratigraphy of the Upper Carboniferous and Lower Permian sequence, southern Sydney Basin. *Journal of the Geological Society of Australia*, 20, 49-70.

Griffin, T.J., Tyler, I.M., and Playford, P.E. (1993) Lennard River (3rd Edition), Western Australia: 1:250,000 Geological Series-Explanatory Notes. Perth.

Guppy, D.J., Lindner, A.W., Rattigan, J.J., and Casey, J.N. (1952) The stratigraphy of the Mesozoic and Permian sediments of the Desert Basin, Western Australia. *19th International Geological Congress (Gondwana Symposium) Algeria,* 101-114.

Guppy, D.J., Lindner, A.W., Rattigan, J.J., and Casey, J.N. (1958) The geology of the Fitzroy Basin, Western Australia. *Bureau of Mineral Resources, Australia, Bulletin* 36.

Hambrey, M.J. and Harland, W.B. (1981) *Earth's pre-Pleistocene glacial record,* Cambridge University Press, Cambridge, 1004 pp.

Haq, B.U., Hardenbol, J., and Vail, P.R. (1987) Chronology of fluctuating sea levels since the Triassic. *Science*, 235, 1156-1167.

Havord, P., Apak, S.N., and Carlsen, G.M. (1997) Permo-Carboniferous petroleum reservoir data, selected wells, Canning Basin, Western Australia. *Geological Survey of Western Australia Record* 1996/11.

Haykin, S. (1983) *Nonlinear methods of spectral analysis,* 2^{nd} edition, Springer-Verlag, Berlin.

Hays, J.D., Imbrie, J., and Shackleton, N.J. (1976) Variations in the Earth's orbit: Pacemaker of the ice ages. *Science*, 194, 1121-1132.

Heckel, P.H. (1977) Origin of phosphatic black shale facies in Pennsylvanian cyclothems of mid-continent North America. *American Association of Petroleum Geologists Bulletin,* 61, 1045-1068.

Heckel, P.H. (1986) Sea-level curve for Pennsylvanian eustatic marine transgressive-regressive depositional cycles along midcontinent outcrop belt, North America. *Geology,* 14, 330-334.

Herbert, C. (1980a) Southwestern Sydney Basin. *Geological Survey of New South Wales Bulletin*, 26, 10-52.

Herbert, C. (1980b) Evidence for Glaciation in the Sydney Basin and Tamworth synclinorial zone. *Geological Survey of New South Wales Bulletin,* 26, 274-293.

Hinnov, L.A. (2000) New Perspectives on Orbitally Forced Stratigraphy. *Annual Review of Earth and Planetary Sciences,* 28, 419-475.

Hocking, R., Mory, A.J., and Williams, I.R. (1994) An atlas of Neoproterozoic and Phanerozoic Basins of Western Australia. In: *The Sedimentary Basins of Western Australia: Proceedings of thePetroleum Exploration Society of Australia Symposium* (Eds. P.G. Purcell and R.R. Purcell), 21-43.

Horstman, E.L. (1984) Source rocks in the Canning Basin: A review. In: *The Canning Basin W.A.: Proceedings of the Geological Society of Australia/Petroleum Exploration Society of Australia Symposium* (Ed. P.G. Purcell), 345-352.

House, M.R. (1995) Orbital forcing timescales: an introduction. In: *Orbital Forcing Timescales and Cyclostratigraphy* (Eds. M.R. House and A.S. Gale), Geological Society Special Publication, 85, 1-18.

Hunt, D. and Tucker, M.E. (1992) Stranded parasequences and the forced regressive wedge systems tract: deposition during base-level fall. *Sedimentary Geology,* 81, 1-9.

Imbrie, J. (1985) A theoretical framework for the Pleistocene ice ages. *Journal of the Geological Society, London,* 142, 417-432.

Imbrie, J. and Imbrie, K.P. (1979) *Ice Ages: Solving the Mystery*. Enslow Publishing, Short Hills, NJ.

Jackson, M.J., Kennard, J.M., Romine, K., Southgate, P.N., Jones, P.J., Nicoll, R., Young, G., and Zeilinger, I. (1994) Petroleum systems in the Canning Basin. *The APEA Journal*, 34(1), 142-155.

Kennard, J.M., Jackson, M.J., Romine, K.K., Shaw, R.D., and Southgate, P.N. (1994) Depositional sequences and associated petroleum systems of the Canning Basin, WA. In: *The Sedimentary Basins of Western Australia: Proceedings of thePetroleum Exploration Society of Australia Symposium* (Eds. P.G. Purcell and R.R. Purcell), 657-676.

Klein, G. deV. and Willard, D.A. (1989) Origin of the Pennsylvanian coal-bearing cyclothems of North America. *Geology,* 17, 152-155.

Lambeck, K (1980) *The Earth's Variable Rotation: its Origin, History, and Physical Constitution (*6th edition). Cambridge University Press, Cambridge.

Lever, H. (2002) Stratigraphy of the Upper Permian Kennedy Group of the onshore Carnarvon Basin (Merlinleigh Sub-basin), Western Australia. *Australian Journal of Earth Sciences,* 49 (3), 539-550.

Lever, H. (2003a) Cyclic sedimentation in the shallow marine Late Permian Kennedy Group, Carnarvon Basin, Western Australia. Submitted to *Sedimentary Geology*.

Lever, H. (2003b) Climatic belts in the mid-Late Permian: evidence from the Kennedy Group, onshore Carnarvon Basin, Western Australia. Submitted to *Gondwana 11*.

Lever, H. (2003c) *Cyclicity in the Late Permian Kennedy Group, Carnarvon Basin, Western Australia: causes of cyclic sedimentation in a shallow marine sea*. Unpublished Ph.D. thesis. James Cook University, Townsville.

Miall, A.D. (1997) *The Geology of Stratigraphic Sequences.* Springer-Verlag, Berlin and Heidelberg, 433 pp.

Michaelsen, P. and Henderson, R.A. (2000) Facies relationships and cyclicity of high latitude, Late Permian coal measures, Bowen Basin, Australia. *International Journal of Coal Geology,* 44, 19-48.

Middleton, M.F. (1992) Seismic Stratigraphy, Structural Analysis, and Tectonic Evolution of the Northern Canning Basin, Western Australia. *Geological Survey of Western Australia Record* 1991/5.

Miller, D.J. and Eriksson, K.A. (2000) Sequence stratigraphy of Upper Mississippian strata in the central Appalachians: A record of glacioeustasy and tectonoeustasy in a foreland basin setting. *American Association of Petroleum Geologists Bulletin,* 84, 210-233.

Naish, T., Beu, A.G., Carter, R.M., Edwards, A.R., Kamp, P.J.J., Pilans, B., Saul, G., and Wolf, K. (1998) Astronomical calibration of a Southern Hemisphere Plio-Pleistocene reference section, Wanganui Basin, New Zealand. *Quaternary Science Review*, 17, 695-710.

Naish, T. and Kamp, P.J.J. (1997) Sequence stratigraphy of sixth-order (41 k.y.) Pliocene Pleistocene cyclothems, Wanganui Basin, New Zealand: A case for the regressive systems tract. *Geological Society of America Bulletin,* 109(8), 978-999.

Nicoll, R.S. (1984) Conodont studies in the Canning Basin-A review and update. In: *The Canning Basin W.A.: Proceedings of the Geological Society of Australia/Petroleum Exploration Society of Australia Symposium* (Ed. P.G. Purcell), 439-444.

O'Brien, P.E., Lindsey, J.F., Knauer, K., and Sexton, M.J. (1998) Sequence stratigraphy of a sandstone-rich Permian glacial succession, Fitzroy Trough, Canning Basin, Western Australia. *Australian Journal of Earth Sciences,* 45, 533-545.

Olsen, H. (1990) Astronomical forcing of meandering river behavior: Milankovitch cycles in Devonian of East Greenland. *Palaeogeography, Palaeoclimatology, Palaeoecology,* 79, 99-115.

Olsen, H. (1994) Orbital forcing on continental depositional systems–lacustrine and fluvial cyclicity in the Devonian of East Greenland. In: *Orbital Forcing and Cyclic Sequences* (Eds. P.L. de Boer and D.G. Smith), *Special Publication of the International Association of Sedimentologist,* 19, 429-438.

Olsen, P.E. (1986) A 40-million-year lake record of early Mosozoic orbital climatic forcing. *Science,* 234, 842-848.

Olsen, P.E. and Kent, D.V. (1999) Long-period Milankovitch cycles from the Late Triassic and Early Jurassic of eastern North America and their implications for the calibration of the Early Mesozoic time-scale and the long-term behavior of the planets. *Philosophical Transactions of the Royal Society, London,* 357, 1761-1786.

Paillard, D., Labeyrie, L., and Yiou, P. (1996) Macintosh Program Performs Time-Series Analysis. *www.agu.org/eos_elec.*

Payton, C. E. (Ed.) (1977) Seismic Stratigraphy – Applications to Hydrocarbon Exploration. *American Association of Petroleum Geologists, Memoir 26*, 516 p.

Playford, P.E. (1984) Platform-margin and marginal-slope relationships in Devonian reef complexes of the Canning Basin. In: *The Canning Basin W.A.: Proceedings of the Geological Society of Australia/Petroleum Exploration Society of Australia Symposium* (Ed. P.G. Purcell), 189-214.

Plint, A.G. (1988) Global eustacy and the Eocene sequence in the Hampshire Basin, England. *Basin Research*, 1, 11-22.

Posamentier, H.W., Allen, G.P., James, D.P., Tesson, M. (1992) Forced regressions in a sequence stratigraphic framework: concepts, examples, and exploration significance. *Bulletin of the American Association of Petroleum Geologists*, 76, 1687-1709.

Purcell, P.G. (1984) The Canning Basin, W.A. - An Introduction. In: *The Canning Basin WA: Proceedings of the Geological Society of Australia/Petroleum Exploration Society of Australia Symposium* (Ed. P.G. Purcell), 3-19.

Purcell, P.G. and Poll, J. (1984) The Seismic Definition of the Main Structural Elements of the Canning Basin. In: *The Canning Basin WA: Proceedings of the Geological Society of Australia/Petroleum Exploration Society of Australia Symposium* (Ed. P.G. Purcell), 73-84.

Purcell, P.G. and Purcell, R.R. (1994) *The Sedimentary Basins of Western Australia: Proceedings of the Petroleum Exploration Society of Australia Symposium*.

Rampino, M.R., Prokoph, A., and Adler, A. (2000) Tempo of the end-Permian event: High resolution cyclostratigraphy at the Permian-Triassic boundary. *Geology*, 28, 643-646.

Ramsbottom, W.H.C. (1979) Rates of transgression and regression in the Carboniferous of NW Europe. *Journal of the Geological Society, London*, 136, 147-153.

Read, J.F. (1995) Overview of carbonate platform sequences, cycle stratigraphy and reservoirs in greenhouse and ice-house worlds. In: *Milankovitch Sea Level Changes, Cycles and Reservoirs on Carbonate Platforms in Greenhouse and Ice-house Worlds* (Eds. J.F. Read, C. Kerans, and L.J. Weber) *SEPM Short Course Notes*, 35, Part 1, 102 pp.

Redfern, J. and Millward, E. (1994) A review of the sedimentology and stratigraphy of the Permo Carboniferous Grant Group, Canning Basin, Western Australia. In: *The Sedimentary Basins of Western Australia: Proceedings of the Petroleum Exploration Society of Australia Symposium* (Eds. P.G. Purcell and R.R. Purcell), 753-756.

Reijmer, J.J.G., Sprenger, A., Ten Kate, W.G.H.Z., Schlager, W., and Krystyn, L. (1994) Periodicities in the composition of Late Triassic calciturbidites (Eastern Alps, Austria). In: *Orbital Forcing and Cyclic Sequences* (Eds. P.L. de Boer and D.G. Smith), *Special Publication of the International Association of Sedimentologists*, 19, 323-343.

Roberts, J., Claoue-Long, J., and Foster, C.B. (1996) SHRIMP zircon dating of the Permian System of eastern Australia. *Australian Journal of Earth Sciences*, 43, 401-421.

Ross, C.A. and Ross, J.R.P. (1985) Late Paleozoic depositional sequences are synchronous and worldwide. *Geology*, 13, 194-197.

Ross, C.A. and Ross, J.R.P. (1988) Late Paleozoic trangressive-regressive deposition. In: *Sea-level changes: An intergrated approach: Society of Economic Paleontologists and Mineralogists Special Publication 42* (Eds. C.K. Wilgus, B.S. Hastings, C.G. St. C. Kendall, H.W. Posamentier, C.A. Ross, and J.C. Van Wagoner), 228-247.

Ross, C.A. and Ross, J.R.P. (1987) Late Paleozoic sea levels and depositional sequences. In: *Timing and Depositional History of Eustatic Sequences: Constraints of Seismic Stratigraphy* (Eds. C.A. Ross and D. Haman), *Special Publication 124*, pp 137-149. Cushman Foundation for Foraminiferal Research, Ithaca.

Ross, C.A. and Ross, J.R.P. (1995) Permian Sequence Stratigraphy. In: *The Permian of Northern Pangea, v. 1, Paleogeography, Paleoclimates, Stratigraphy* (Eds. P.A. Scholle, T.M. Peryt and D.S. Ulmer-Scholle), pp. 98-123. Springer-Verlag, Berlin.

Runnegar, B.N. (1979) Ecology of *Eurydesma* and the *Eurydesma* fauna, Permian of eastern Australia. *Alcheringa*, 3, 261-285.

Runnegar, B.N. (1980) Excursion Guide, Day 7, Stop 3, Montague Roadstead, Jervis Bay (Early Permian Shoalhaven Group), *New South Wales Geological Survey Bulletin*, 26, 523-530.

Santos, P.R. dos, Rocha-Compos, A.C., and Canuto, J.R. (1996) Patterns of late Paleozoic deglaciation in the Parana Basin, Brazil. *Palaeogeography, Palaeoclimatology, Palaeoecology*, 125, 941-163.

Saul, G., Naish, T.R., Abbott, S.T., and Carter, R.M. (1999) Sedimentary cyclicity in the marine Plio-Pleistocene of the Wanganui basin (New Zealand): Sequence stratigraphic motifs characteristic of the past 2.5 m.y. *Geological Society of America Bulletin*, 111(4), 524-537.

Scheibner, E. (1974) A plate tectonic model of the Paleozoic tectonic history of New South Wales. *Journal of the Geologcial Society of Australia*, 20, 405-426.

Scheibner, E. and Basden, H. (1998) Geology of New South Wales-Synthesis. Volume 2 Geological Evolution. *New South Wales Geological Survey Memoirs*, 13, 666 pp.

Schwarzacher, W. (1993) *Cyclostratigraphy and the Milankovitch Theory, Developments in Sedimentology 52*, Elsevier, Amsterdam, 225 pp.

Scotese, C.R., Boucot, A.J., and McKerrow, W.S. (1999) Gondwanan palaeogeography and palaeoclimatology. *Journal of African Earth Sciences* 28(1), 99-114.

Shackleton, N.J. and Opdyke, N.D. (1973) Oxygen isotope and palaeo-magnetic stratigraphy of Pacific core V28-238: oxygen isotope temperatures and ice volumes in a 10^5 and 10^6 year scale. *Quaternary Research*, 3, 39-55.

Shaw, R.D., Tyler, I.M., Griffin, T.J., and Webb, A. (1992a) New K-Ar constraints on the onset of subsidence in the Canning Basin, Western Australia. *Journal of Australian Geology and Geophysics,* 13, 31-35.

Shaw, R.D., Zeitler, P.K., McDougall, I., and Tingate, P.R. (1992b) The Palaeozoic history of an unusual intracratonic thrust belt in central Australia based on ^{40}Ar-^{39}Ar, K-Ar and fission track dating. *Journal of the Geological Society, London,* 149, 937-954.

Sierro, F.J., Ledesma, S., Flores, J.A., Torrescusa, S., and Martinez del Olmo, W. (2000) Sonic and gamma-ray astrochronology: Cycle to cycle calibration of Atlantic climatic records to Mediterranean sapropels and astronomical oscillations. Geology, 28 (8), 695-698.

Smith, A.G., Hurley, A.M., and Briden, J.C. (1981) *Phanerozoic Paleocontinental World Maps,* Cambridge University Press, London, 102 pp.

Smith, N.D. and Ashley, G. (1985) Proglacial lacustrine environment. In: *Glacial sedimentary environments* (Eds. G.M. Ashley, J. Shaw, and N.D. Smith), *Society of Economic Paleontologists and Mineralogists Short Course,* 16, 135-216.

Spaulding, W.G. (1991) Pluvial climatic episodes in North America and North Africa: types and correlation with global climate. *Palaeogeography, Palaeoclimatology, Palaeoecology,* 84, 217-227.

Suess, E., Balzer, W., Hess, E.K.F., Muller, P.J., and Wefer, G. (1985) Calcium carbonate hexahydrate from organic-rich sediments of the Antarctic shelf: Precursor of glendonites. *Science,* 1216, 1128-1131.

Talbot, M.R. (1985) Major bounding surfaces in eolian sandstones-a climatic model. *Sedimentology,* 32, 257-265.

Tankard, A.J. (1986) Depostional response to foreland deformation in the Carboniferous of eastern Kentucky. *American Association of Petroleum Geologists Bulletin,* 70, 853-868.

Tiedemann, R., Sarnthein, M., Shackleton, N.J. (1994) Astromomical timescale for the Pliocene Atlantic d^{18}O and dust flux records of Ocean Drilling Program site 659. *Paleoceanography,* 9, 619-638.

Towner, R.R. (1981) Derby (2nd Edition), Western Australia: 1:250,000 Geological Series-Explanatory Notes. Australian Geovernment Publishing Services, Canberra.

Tye, S.C., Fielding, C.R., and Jones, B.G. (1996) Stratigraphy and sedimentology of the Permian Talaterang and Shoalhaven Groups in the southernmost Sydney Basin, New South Wales. *Australian Journal of Earth Sciences,* 43, 57-69.

Udden, J.A. (1912) Geology and mineral resources of the Peoria quadrangle, Illinois. *U.S. Geological Survey Bulletin 506,* 47-50.

Vail, P.R., Audemard, F., Bowman, S.A., Eisner, P.N., Perez-Cruz, C. (1991) The stratigraphic signatures of tectonics, eustasy and sedimentology – an overview. In: *Cycles and Events in Stratigraphy*, (Eds. G. Einsele, W. Ricken, and A. Seilacher), 617-659.

Vail, P.R., Mitchum, R.M., and Thompson, S. (1977) Seismic stratigraphy and global changes of sea level, part 4: global cycles of relative changes of sea level. *American Association of Petroleum Geologist, Memior 26,* 83-97.

Veevers, J.J. (2000a) Permian-Triassic Pangean basins and foldbelts along the Panthalassan margin of Gondwanaland. In: *Billion-year earth history of Australia and neighbours in Gondwanaland* (Ed. J.J. Veevers), pp. 292-308, Gemoc Press, Sydney.

Veevers, J.J. (2000b) Time Scale. *In: Billion-year earth history of Australia and neighbours in Gondwanaland* (Ed. J.J. Veevers), pp. 3-8, Gemoc Press, Sydney.

Veevers, J.J. (2000c) Australia in Pangea and Gondwanaland. In: *Billion-year earth history of Australia and neighbours in Gondwanaland* (Ed. J.J. Veevers), pp. 9-11, Gemoc Press, Sydney.

Veevers, J.J., Conaghan, P.J. and Powell, C.McA. (1994b) Eastern Australia. In: *Permian Triassic basins and foldbelts along the Panthalassan margin of Gondwanaland* (Eds. J.J. Veevers and C.McA. Powell), *Geological Society of America Memoirs,* 184, 11-171.

Veevers, J.J. and Powell, C.McA. (1987) Late Paleozoic glacial episodes in Gondwanaland reflected in transgressive-regressive depositional sequences in Euramerica. *Geological Society of America Bulletin,* 98, 475-487.

Veevers, J.J., Powell, C.McA., Collinson, J.W., and Lopez-Gamundi, O.R. (1994a) Synthesis. In: *Permian-Triassic basins and foldbelts along the Panthalassan margin of Gondwanaland* (Eds. J.J. Veevers and C.McA. Powell), *Geological Society of America Memoirs,* 184, 331-353.

Visser, J.N.J. (1993a) Sea-level changes in a back-arc-foreland transition: the late Carboniferous-Permian Karoo Basin of South Afric. *Sedimentary Geology,* 83, 115-131.

Visser, J.N.J. (1993b) A reconstruction of the late Palaeozoic ice sheet on southwestern Gondwana. In: *Gondwana Eight: Assembly, Evolution, and Dispersal* (Eds. R.H. Findlay, R. Unrug, M.R. Banks, and J.J. Veevers), *Proceedings of the eighth Gondwana symposium*, pp. 449-458. Balkema, Rotterdam.

Visser, J.N.J. (1989) The Permo-Carboniferous Dwyka Formation of southern Africa: deposition by a predominantly subpolar marine ice sheet. *Palaeogeography, Palaeoclimatology, Palaeoecology*, 70, 377-391.

Visser, J.N.J. (1996) Controls on Early Permian Shelf deglaciation in the Karoo Basin of South Africa. *Palaeogeography, Palaeoclimatology, Palaeoecology*, 125, 129-139.

Von Brun, V, (1996) The Dwyka Group in the nothern part of the Kwazulu/Natal, South Africa: sedimentation during Late Paleaeozoic deglaciation. *Palaeogeography, Palaeoclimatology, Palaeoecology*, 125, 941-163.

Wanless, H.R. and Shephard, F.P. (1936) Sea level and climatic changes related to Late Paleozoic cycles. *Geological Society of America Bulletin*, 47, 1177-1206.

Weedon, G.P. (1991) The spectral analysis of stratigraphic time series. In: *Cycles and Events in Stratigraphy* (Eds. G. Einsele, W. Ricken, and A. Seilacher), pp. 840-854, Springer-Verlag, Berlin, Germany.

Weedon, G.P., Jenkyns, H.C., Coe, A.L., and Hesselbo, S.P. (1999) Astronomical calibration of the Jurassic time-scale from cyclostratigraphy in Britsih mudrock formations. *Philosophical Transactions of the Royal Society, London*, 357, 1787-1813.

Weedon, G.P. and Read, W.A. (1995) Orbital-climatic forcing of Namurian cyclic sedimentation from spectral analysis of the Limestone Coal Formation, Central Scotland. In: *Orbital-forcing, Timescales, and Cyclostratigraphy* (Eds. M.R. House and A.S. Gale), *Geological Society of London Special Publication*, 85, 51-66.

Weller, J.M. (1931) The conception of cyclical sedimentation during the Pennsylvanian period. *Illinois State Geological Survey Bulletin 60*, 163-177.

Wood, R. (2000) Novel paleoecology of a postextinction reef: Famennian (Late Devonian) of the Canning Basin, northwestern Australia. *Geology*, 28(11), 987-990.

Yeates, A.N., Crowe, R.W.A., Towner, R.R., Wyborn, L.A.I., and Passmore, V.L. (1975) Notes on the geology of the Gregory Sub-basin and adjacent areas of the Canning Basin, Western Australia. *Bureau of Mineral Resoureces, Australia, Record* 1975/77.

Yeates , A.N., Gibson, D.L., Towner, R.R., and Crowe, R.W.A. (1984) Regional Geology of the Onshore Canning Basin, W.A. In: *The Canning Basin W.A.: Proceedings of the Geological Society of Australia/Petroleum Exploration Society of Australia Symposium* (Ed. P.G. Purcell), 23-55.

Zachos, J.C., Flower, B.P., and Paul, H. (1997) Orbitally placed climate oscillations across the Oligocene/Miocene boundary. *Nature*, 388, 567-570.

Zachos, J., Pagani, M, Sloan, L., Thomas, E., and Billups, K. (2001) Trends, Rhythms, and Aberrations in Global Climate 65 Ma to Present. *Science,* 292, 686-693.